DIAGNOSIS AND RECOVERY OF HARDWARE FAULTS ENCOUNTERED DURING OPERATION OF MOBILE ROBOTS

A Thesis Submitted to
the Graduate School of
İzmir Institute of Technology
in Partial Fulfillment of the Requirements for the Degree of

DOCTOR OF PHILOSOPHY

in Mechanical Engineering

by
Osman Nuri Şahin

December 2020
İZMİR

ACKNOWLEDGMENTS

I would like to express my deep and sincere gratitude to my supervisor Dr. Can DEDE for giving me the opportunity to work together, for the valuable knowledge he shared during my time in IzTech Robotics Laboratory and for providing invaluable guidance, support, and patience throughout the dissertation studies. Similarly, I would like to express my endless gratitude to the co-supervisor, Prof. Serhan ÖZDEMİR, for his contribution to the dissertation and for his kindly attitude to me throughout the dissertation studies. I would like to thank the rest of my thesis committee: Prof. Enver TATLICIOĞLU, Dr. Gökhan KİPER, Dr. Levent ÇETİN, and Dr. Kerem ALTUN for their insightful comments and encouragement.

I would like to say a special thanks to my labmates, Emre UZUNOĞLU, Barış TANER, Mert KANIK, Çağhan KİRİŞCİ, Omar MAAROOF, Murat DEMİREL, Gizem ATEŞ, Egecan TÜRK, İbrahimcan GÖRGÜLÜ, Uğur NALBANT, Orhan AYİT, Onur ÇELİK, Halil TETİK, Cevahir KARAGÖZ, Furkan KÜÇÜKOĞLU, Mert YILMAZ, Merve ÖZKAHYA, Emir MOBEDİ, Oğulcan IŞITMAN, Elvan DOĞAN KUMTEPE, Erkan PAKSOY, and Hazal EMET for their support and friendship.

I am grateful to my family Mehmet Sena ŞAHİN, Sönmez ŞAHİN, Selçuk ŞAHİN, Gülhan SABANCI ŞAHİN and Zeynep Ece ŞAHİN for their endless support not only during this period but also whole my life.

ABSTRACT

DIAGNOSIS AND RECOVERY OF HARDWARE FAULTS ENCOUNTERED DURING OPERATION OF MOBILE ROBOTS

Mobile robots are used in many critical tasks. In such tasks, it is of great importance to tolerate the faults that the robot may encounter during the operation in order to complete the task successfully. This dissertation focuses on tolerating the faults that occur in the hardware of the mobile robots. To tolerate these faults, it is necessary to be prepared for the faults that the robot may encounter during the operation and to determine an appropriate fault toleration strategy. The mobile robot considered in this dissertation has holonomic motion ability in the plane thanks to its omnidirectional wheels. The types of faults focused on are the slippage of one of the wheels of this mobile robot and the performance degradation in the motor that actuates one of the wheels. To tolerate these two faults, an active fault tolerant control method is developed. A model-based fault diagnosis algorithm is developed for fault diagnosis algorithm, which is one of the two main parts of active fault tolerant control. To obtain the dynamic model of the mobile robot that is used in this algorithm, firstly, the friction between the wheel and the ground used is modeled. The parameters of the friction model are identified via the developed test setup. As a result of the tests performed for fault diagnosis, it is seen that these two types of faults occurring in the holonomic mobile robot can be diagnosed with developed fault diagnosis algorithm. In order to tolerate these faults, two different fault recovery algorithms which make use of kinematic redundancy of the mobile robot are developed, and the developed algorithms are tested. As a result of the fault recovery tests performed for the motor performance degradation, it is observed that the motion performance of the mobile robot improved despite the presence of the fault. Thanks to the developed recovery algorithm in the recovery tests for wheel slippage, it is observed that there is a significant decrease in the amount of slippage occurring on the faulty wheel and accordingly the mobile robot performs the desired motion more accurately.

ÖZET

GEZİCİ ROBOTLARIN İŞLETİMLERİ SIRASINDA KARŞILAŞILAN DONANIMSAL HATALARIN TEŞHİSİ VE GİDERİLMESİ

Bu tezde gezici (mobil) robotların donanımlarında ortaya çıkan hataların giderilmesi konusuna odaklanılmıştır. Mobil robotlar birçok kritik görevde kullanılmaktadır. Bu tip görevlerde, robotun görev sırasında karşılaşabileceği hataların giderilmesi görevin başarı ile tamamlanabilmesi açısından büyük önem arz etmektedir. Bu hataların giderilmesi için robotun görev sırasında karşılaşabileceği hatalar için hazırlıklı olunmalı ve bir hata giderme stratejisinin belirlenmesi gerekmektedir. Tezde kullanılan mobil robot bünyesinde bulundurduğu çok yönlü tekerlekler sayesinde düzlemde holonomik olarak hareket edebilen bir gezici robottur. Tez sırasında odaklanılan hatalar, bu mobil robotun tekerleklerinden birinde meydana gelebilecek kayma ve tekerleklerden birini tahrik eden eyleyicilerden birinde ortaya çıkabilecek performans düşüşüdür. Bu iki tip hatanın telafi edilmesi için aktif olarak hatayı giderebilecek bir denetim yöntemi geliştirilmiştir. Aktif hata giderilmesinin iki ana unsurundan biri olan hatanın teşhisi için model tabanlı bir hata teşhis algoritması geliştirilmiştir. Bu algoritmada kullanılan mobil robotun dinamik modelinin elde edilebilmesi için öncelikle mobil robotta kullanılan tekerlek ile zemin arasındaki sürtünme modellenmiştir. Kullanılan sürtünme modelinden bulunan parametreler geliştirilen test düzeneği ile bulunmuştur. Geliştirilen hata teşhis algoritması için gerçekleştirilen testler sonucunda robotta ortaya çıkan hatanın bu iki hata türünden hangisi olduğunun teşhis edilebildiği görülmüştür. Bu hataların giderilmesi için tezde iki farklı hata telafi algoritması geliştirilmiş ve geliştirilen algoritmalar test edilmiştir. Motor hatası için gerçekleştirilen hata telafi testleri sonucunda hatanın varlığına rağmen robotun hareketinde iyileşme olduğu görülmüştür. Tekerlek kayması için yapılan telafi testlerine geliştirilen telafi algoritması sayesinden hatalı tekerlekte meydana gelen kayma miktarında önemli ölçüde bir düşüş gerçekleştiği ve buna bağlı olarak mobil robotun istenen hareketi daha doğru olarak yapabildiği görülmüştür.

I dedicate this dissertation to my parents; Mehmet Sena Şahin and Sönmez Şahin.

TABLE OF CONTENTS

LIST OF FIGURES

Figure **Page**

Figure **Page**

Figure **Page**

LIST OF TABLES

CHAPTER 1

INTRODUCTION

Today, use of robots is increasing in many industrial, military, and civil fields. In the industrial field, robots can work independently in various jobs, or they can be used in common working areas with human workers. Faults that may arise in this type of robots can cause both production disruptions and situations that may endanger the safety of the workers that these robots interact with. With the widespread use of robots, faults that may occur in robots can also bring various safety concerns. Apart from these, robots perform various critical operational activities in difficult conditions such as robots used in search and rescue missions. A fault that occurs in the robot during the operation may cause the operation to be interrupted or to completely fail.

Robots, which consist of software and mechanical/electronics hardware, have different designs according to their usage areas. They are equipped with various sensors to improve the interaction of the robot with its environment. Faults that occur in the fundamental components such as the motors and sensors of the robots can cause these robots to degrade or even lose its functions. Although these fundamental components are similar, due to structural differences in a wide range of robot types, fault types in each robot can be different from each other. This dissertation focuses on tolerating faults encountered in mobile robots.

Mobile robots are primarily classified according to the environment in which they work, including air, land, and water, as well as according to the locomotion systems that enable them to move in working environments. The locomotion systems that are used in terrestrial robots are legs, wheels, and tracks. The wide variety of robots means that different types of faults will arise specifically for each robot. However, as in other land vehicles, the most widely used locomotion system in terrestrial robots is the wheels that provide the most effective movement.

Mobile robots are robots that do not have a limited workspace unlike robotic arm manipulators, and they can perform given tasks by freely moving in an unlimited workspace thanks to their locomotion systems. Mobile robots can be teleoperated, autonomous or semi-autonomous. Autonomous mobile robots perform the given task

with high degree of autonomy. They are equipped with various sensor which gain information about surrounding of the robot for increasing localization ability as well as autonomous mobility. They can adapt changing conditions of their surroundings according to their sensory information. Also, autonomous mobile robots can work without any human assistance. Otherwise, teleoperated mobile robots are controlled by human operator from a distance. Mobile robots are used in many civil and military applications at various environments. They perform number of life-threatening tasks where they are carried out by people or places that are difficult to reach by human beings. Some of these missions can be listed as bomb disposal, nuclear missile reactors under investigation and exploration, space missions and underwater missions. Also, some robots are designed to facilitate many activities in everyday life like cleaning robots or accelerate production in industrial applications such as lifting robots.

In tasks achieved with mobile robots, the task success depends on the operator's skill (if the robot is controlled by a human operator), the movement ability of the robot in the environment, and having the appropriate equipment for the mission. Faults that may arise from the hardware and/or software of the robot during the execution of the task can affect the completion of the task. It is very important in terms of time and cost to continue executing the task despite such faults encountered in robots operating in difficult to reach places like space missions. For this reason, robots that perform critical tasks in difficult conditions should have a fault-tolerant control (FTC) algorithm in the case of experiencing faults that may occur during the mission. In the diagnosis part, which is the first of the two main parts of this type of control method, information about the presence of the fault, the faulty component/subsystem, and the size of the fault should be diagnosed. After that, in the second part, which is named as the recovery, an appropriate toleration strategy should be applied, and the robot should be able to fulfill the task despite the fault. The fault-tolerant control is not specifically developed only for mobile robots but also it can be employed for a wide range of applications. In fact, works have been carried out by using various methodologies for the diagnosis and recovery of the faults in many applications like aircrafts, nuclear reactors, and industrial applications (Li et al., 2020, Wang et al., 2017, Yu et al., 2018). Some of the previously developed fault detection and recovery methods are also used for tolerating the faults encountered in mobile robots.

Mobile robots work mostly in distant and sometimes in unknown environments and thus, being prepared for possible faults becomes a critical part in the developments

of the mobile robots. Mobile robots have some unique systems like locomotion systems and many kinds of sensors for localization and perception of the changing environment. These are some differences of mobile robots from the industrial robot arms. Therefore, comparing the possible faults in industrial robot arms and mobile robots, there can be several faults which are specific to mobile robots.

1.1. Aim of the Dissertation

The type of fault that may occur in mobile robots is one of the factors that determine the magnitude of the negative impact on the mobile robot. These faults can take effect for a certain period of time during the operation of the robot and disappear in time, as well as during the entire motion after the fault occurs. For this reason, whether the fault is temporary or permanent has an important role in determining the method to be used in tolerating the fault. Mobile robots are designed in a very different structure according to their usage areas, and accordingly, the faults that occur in mobile robots also vary. This dissertation focuses on a temporary fault and a permanent fault that may occur in wheeled indoor mobile robots. This dissertation aims to diagnose and recover two of the most common faults that a wheeled mobile robot may encounter during its mission, namely the motor fault and the wheel slippage, with a model-based fault diagnosis algorithm without interrupting the task. The mobile robot used in the dissertation is a mechanically and electronically improved version of the mobile robot (Çelik, 2016) that was previously developed in IzTech Robotics Laboratory. It has holonomic motion ability thanks to its omnidirectional wheels.

Since the wheels are in continuous contact with the ground, they can be affected by environmental conditions and wear over time. Due to this abrasion or unpredictable situations on the ground, the grip between the wheel and the ground is reduced and slippage may occur. The slippage that may occur on one of the wheels of the robot may cause the robot to fail to perform the desired motion. One of the topics targeted by this dissertation is the diagnosis of slippage and the toleration of the involuntary movement caused as a result of it. To apply a model-based fault diagnosis for wheel slippage, the friction between the ground and the wheel should be modeled. Therefore, the first part of the dissertation focuses on the modeling of the friction characteristic between the omnidirectional wheel used in the holonomic mobile robot and the ground on which the robot moves. Modeling of this friction, more precisely, finding the parameters of the

friction model, is difficult with the tests performed on the mobile robot. Therefore, a test setup suitable for the structural condition of the omnidirectional wheel is constructed. With this test setup, it is aimed to identify and verify model parameters.

Various actuators are used to actuate the joints in the locomotion systems of mobile robots. One of the most used of these actuators is DC motors. Mobile robots operate in various harsh conditions and motors operating under these conditions may experience performance degradation over time. The performance degradation that occurs in these motors that enable the movement of the mobile robot can make it difficult to control the robot. Another type of fault focused on in the dissertation is the performance degradation that may occur in one of the motors used in the robot. In the diagnosis of this fault, it is aimed to use model-based fault diagnosis algorithm, which also includes the motor model, and to develop a recovery algorithm that adjusts the weight distribution of the wheels according to the fault situation.

By a suitable investigation of the robot's performance, when a fault in the robot occurs, symptoms called residuals are calculated by the model-based fault diagnosis algorithm. With the help of these symptoms, the information about the fault in the system can be obtained. For the recovery part, a recovery strategy specific to the type of fault should be determined. For this reason, it is important to know which component is prone to having faults. Therefore, in the second part of the dissertation, it is aimed to create a fault diagnosis algorithm in which the dynamic model of the robot is used to give not only information about a fault in the robot but also information about which component of the system is faulty.

After obtaining the robot model and developing a fault diagnosis algorithm which makes use of kinematic redundancy of the mobile robot for both fault types, it is aimed to develop a recovery strategy as the last part of the dissertation. In this way, the robot can perform the desired movement despite these two faults. Since the slippage fault due to external factors is a temporary fault and motor fault is considered as a permanent fault, two different recovery strategies are needed for these types of faults.

As a result, the dissertation objectives are listed as:

1. Making a holonomic mobile robot more suitable for fault toleration with mechanical and hardware improvements,

2. Modeling the friction characteristic between the wheel and the ground,

3. Development of the entire holonomic mobile robot system model,

4. Diagnosing wheel slippage and motor performance degradation fault with model-based method,

5. Developing two different recovery strategies for both types of faults.

1.2. Contributions

Friction models between the wheel and the ground, which have an important place in vehicle dynamics, are used in the modeling of many land vehicles, especially automobiles. However, when it comes to mobile robots, studies on this subject are very limited. This dissertation investigates the longitudinal friction characteristics of an omnidirectional wheel which is increasingly being used in mobile robot applications. The effect of the lateral frictional force due to the special structure of the omnidirectional wheels on the longitudinal motion is also examined in this dissertation. Although there are previous works on friction characteristics of other types of wheels in the literature, the omnidirectional wheel investigated in this work has not been considered yet. As a consequence, the generated wheel friction model can be used by the researchers and engineers that construct mobile robot controllers for their mobile robots using this type of wheels.

The second contribution of the dissertation is the diagnosis of wheel slippage and motor faults together with a model-based method. Model-based fault diagnosis is also very difficult for mobile robots since they are complicated and relatively difficult to model. In this dissertation, the friction between the mobile robot and the ground is modeled and included in the system model. In this way, it is possible to isolate the fault that occurs in the robot.

The last contribution is the development of recovery strategies that tolerate the effects of wheel slippage and motor faults. Similar motion defects may arise if one of the two faults occur in the robot. However, in the case of wheel slippage caused by substances such as oil on the ground, the fault may disappear when mobile robot moves away from that part of the ground. However, the motor fault is permanent. For this reason, two different recovery strategies have been developed in the dissertation for both types of faults.

1.3. Dissertation Outline

The second chapter of the dissertation includes literature survey on the concept of fault-tolerant control. In this chapter, the subsystems of the fault-tolerant control system and the methods applied in these subsystems in the literature are explained. Also, the classification of faults encountered in mobile robots according to subsystems is given and fault-tolerant control methods used in the literature for these faults are explained.

The general design details, mechanical and electronic components of the four-wheeled holonomic mobile robot used in the dissertation are explained in Chapter 3. Also, kinematic, and dynamic equations of the robot are given in this chapter.

The experimental test setup developed to identify the parameters of the friction model is explained in Chapter 4. With this test setup, the friction model parameters at the longitudinal axis used in the mobile robot are identified and these parameters are verified by various validation tests. Also, the effect of the movement in the lateral axis on the movement in the longitudinal axis is investigated.

With the dynamic model of the mobile robot, which is completed with the identified parameters of the friction model, a model-based fault diagnosis algorithm is developed. The studies carried out to diagnose the slippage and motor faults in the holonomic mobile robot used in the dissertation are explained in Chapter 5. First, the studies carried out with the test setup to diagnose both faults are presented and then, fault diagnosis studies performed with the mobile robot are presented.

The holonomic mobile robot is designed as a four-wheeled structure to tolerate faults that may occur in one of the wheels. Thanks to this structure, the robot can perform the desired motion with non-faulty wheels whenever a fault occurs in one of the wheels. For this, the weights given to the wheels should be adjusted according to the type of faults. The developed recovery methods are first tested in simulation. After the tests are carried out in simulation, real robot tests are performed and recovery methods for wheel slippage and motor performance degradation are tested. In the Chapter 6 of the dissertation, recovery studies are explained.

The last chapter of the dissertation is devoted to the conclusions and discussions.

CHAPTER 2

LITERATURE REVIEW

In this chapter, firstly, an overview of the fault-tolerant control concept is presented. The fault-tolerant control methods in the literature, and the advantages and disadvantages of these methods are explained. Also, an overview of the fault types is given. Since the fault tolerance in mobile robots is considered in this dissertation, various types of hardware faults that can be encountered in mobile robots are discussed in the following section. Finally, the methods employed to tolerate the faults in mobile robot applications are discussed in the last section of this chapter.

2.1. Fault Tolerant Control

The fault-tolerant control systems (FTCS) can automatically tolerate the hardware faults occurring in the system without any external intervention (Zhang et al., 2008). However, it is necessary to state the difference between fault-tolerant systems and fail-safe systems used especially in high-risk applications such as nuclear reactors. Blanke et al. (1997) made the distinction between fail-safe systems and fault-tolerant systems as follows: “Fail-safe systems are able to withstand any single point failure without any noticeable change in their functionality or performance. Fault-tolerant systems may degrade performance when a fault occurs, but a fault will not develop into a failure at the system level if this could be prevented through proper action in the programmable parts of a control loop.” The faults that occur in the fail-safe systems are mostly tolerated by hardware redundancy. On the other hand, the effects of the faults that occur in fault tolerant systems are to be tolerated at an acceptable level with the adaptations and changes made in the control algorithm. According to Blanke et al. (1997) fault-tolerant systems

- aim to prevent any fault from developing into failure at system level,
- use information redundancy to detect faults,
- use reconfiguration in programmable system components to accommodate faults,
- accept degraded performance due to a fault but keep plant availability,
- are low cost and/or requires no new hardware.

FTCS should be designed to give the most appropriate performance according to the situation where the fault occurs. In the case of a fault in the system, the system behaviors vary considerably according to the size of the faults compared to the non-faulty situation. In this case, FTCS should ensure the operation of the system at an acceptable performance level to ensure the continuity of the system's operation. FTC can be divided into two main categories as passive fault-tolerant control (PTFC) and active fault-tolerant control (AFTC) (Eterno, 1985). This classification of the FTC is represented in Figure 2.1.

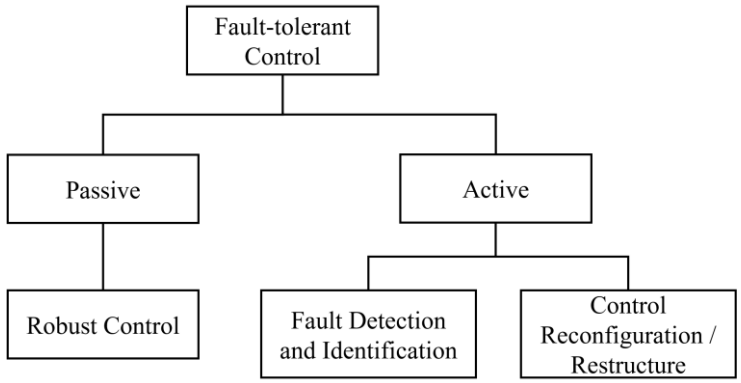

Figure 2.1. Classification of the fault-tolerant control (Source: Eterno, 1985)

The PFTC systems are built to be robust and fixed to maintain performance against faults and uncertainty. The main goal of the PFTC is to compensate for the effect of the fault in the system and ensure the stability of the system with acceptable performance losses (Frank, 2004). The PFTC systems do not have a reconfigurable controller and do not need any fault detection and isolation/identification (FDI) algorithm, but their fault-tolerant capability is limited. A structure of a general PFTC system is represented in Figure 2.2.

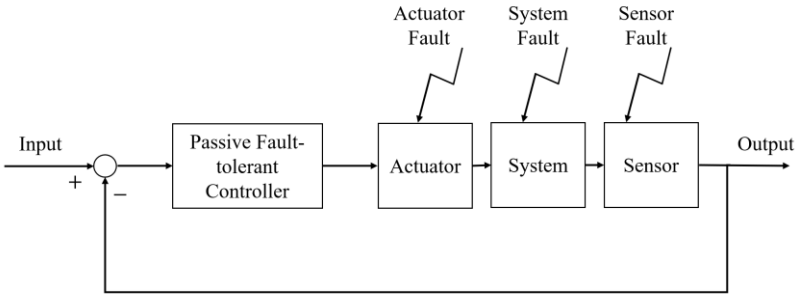

Figure 2.2. A structure of the PFTC system (Source: Jiang et al., 2012)

On the other hand, in AFTC systems, the control method is reconfigured with a reconfiguration mechanism to maintain the system with acceptable performance and ensure system stability despite the faults that occur in the system (Amin et al., 2019). Frank (2004) listed the main aims of an AFTC as follows:

- to prevent local faults from developing into a system failure that can end the mission of the system
- to avoid safety hazards for human by the effect of the faulty devices
- to protect the environment.

AFTC systems should have an FDI algorithm to detect a fault in the system and determine the source of the fault, a reconfiguration mechanism, and a reconfigurable controller (Zhang et al., 2008). A general structure of an AFTC system is represented in Figure 2.3.

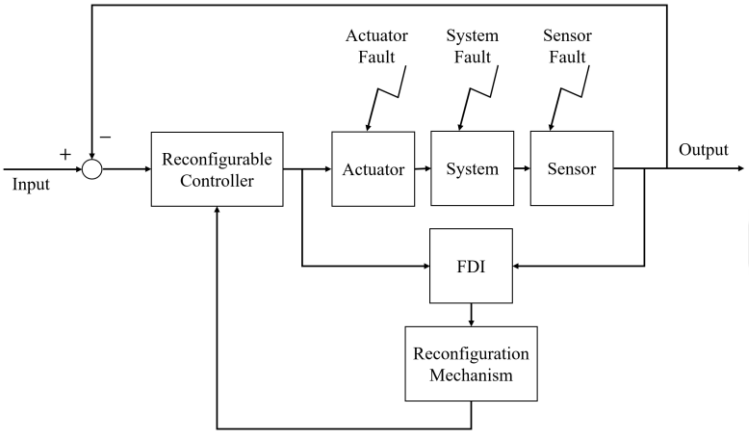

Figure 2.3. A general structure of the AFTC system (Source: Amin et al., 2012)

There are some important issues to consider when creating AFTC systems. First of all, the controller used in the system should be reconfigurable in a way that allows the faults that occur in the system to be tolerated rapidly. Since the fault that occurs in the system cause a rapid negative impact on the stability and performance of the system, there is a very low time interval for the FDI algorithm to diagnose the fault, the reconfiguration mechanism to work, and the controller to reconfigure and reduce the effect of the fault on the system. The subsystems in AFTC systems should fulfill their duties in this limited time and the system should continue to operate in stable and acceptable performance. Another important issue for AFTC systems is that the FDI algorithm should be sensitive to faults and designed in a robust structure against model uncertainty and unknown inputs (Zhang et al., 2008).

Jiang et al. (2012) compared two FTC system approaches concerning advantages and limitations, through a philosophical point of view and with a case study which uses a flight controller system for aircraft. The comparison results of the study are given in Table 2.1. According to these results, the main disadvantage of the AFTC system is that the system is very complex and difficult to implement but suitable for tolerating a different kind of faults. On the other hand, PFTC system is simple and easy to implement with respect to AFTC system but the fault-tolerant capability is limited.

Table 2.1. Comparison between active and passive FTC systems (Source: Jiang et al., 2012)

	Active FTC	Passive FTC
Potential for performance optimization	Yes	No
Dealing with beyond design basis failures	Yes	No
Immediate control action after the fault	No	Yes
Sensitive to the results of FDD	Yes	No
Guaranteed stability for the design basis faults	N/A	Yes
Switching transients	Yes	No
Smooth in operation during a fault occurrence	No	Yes
Time before control in action	Yes	No
Easy in implementation	No	Yes
Controller design time (based on optimization)	Short	Long

The ability to diagnose the faults that occur in the system quickly and accurately constitutes an essential part of AFTC systems. The diagnosis can be divided into three main parts: detection, isolation, and identification. First of all, when a fault causes unexpected behaviors on the way that the system functions, a mechanism should exist in the system to detect whether this deviation from the system's performance is due to a fault in the system. This part is called fault detection. After this part, a fault isolation algorithm is needed to determine which component of the system is faulty. The source of the deviations in system behaviors can be a fault in actuators, sensors, or other components of the system. Appropriate isolation of the source of the fault plays a key role in the tolerance of the fault. Knowing the source of the fault allows different recovery methods to be applied according to the type of the fault. After isolating which component is faulty, identifying the information about the type of fault, the amplitude, and the cause

of the fault play an important role in reconfiguring the parameters of the controller used in the AFTC system or changing the control structure.

Fault diagnosis methods can be divided into four main categories: hardware redundancy based, plausibility test, signal/data-based and model-based. In the hardware redundancy-based fault diagnosis, there is a second component with the same features that works in parallel with a component in the system. Considering that these two components are conjugate, the outputs should be the same as well. In case a fault occurs in the system component, the outputs of the system component and the redundant component will be different from each other. The difference between the two component outputs directly points to the presence of the fault. Although it is very reliable and shows the source of the fault directly, using the equivalent of every component in the system for this purpose causes the system cost to increase considerably. For this reason, it can be said that the hardware redundancy-based fault diagnosis is a suitable method to diagnose faults that may occur in components such as sensors, where critical measurements are made in the system.

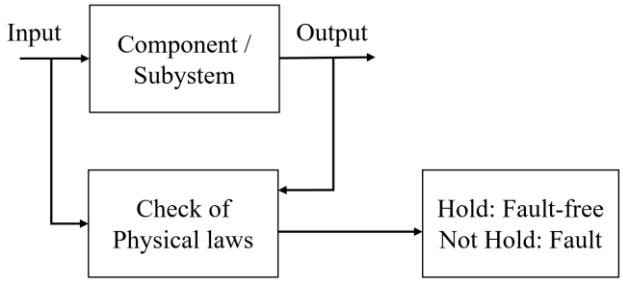

Figure 2.4. Plausibility test scheme (Source: Ding, 2008)

The behavior of the components of the system can be expressed with various physical rules. In the fault diagnosis method with plausibility test, fault diagnosis is made by checking the plausibility of the operation of the component within the framework of these rules. When there is a fault in the component, there is a change in its behavior, and it loses plausibility with respect to the physical rules expressing the non-faulty condition (Figure 2.4). Many current studies focus on fault diagnosis using either signal-based or model-based methods. Measurements are taken by various sensors during the operation of the system and the signals obtained are used at various stages in the operation of the system. The signals obtained from the system process contain information about the system behaviors as well as the fault that occur in the system. This information is

transformed into symptoms that allow more precise diagnosis of the fault by applying various signal processing methods. These symptoms can be in the form of time domain functions (arithmetic mean, magnitude, root mean square, standard deviation, trends limit values, etc.) or frequency domain functions (spectrum, frequency spectral line, etc.) according to applied symptom generation method (Gao et al., 2015). A schematic description of the signal-based fault diagnosis is represented in Figure 2.5.

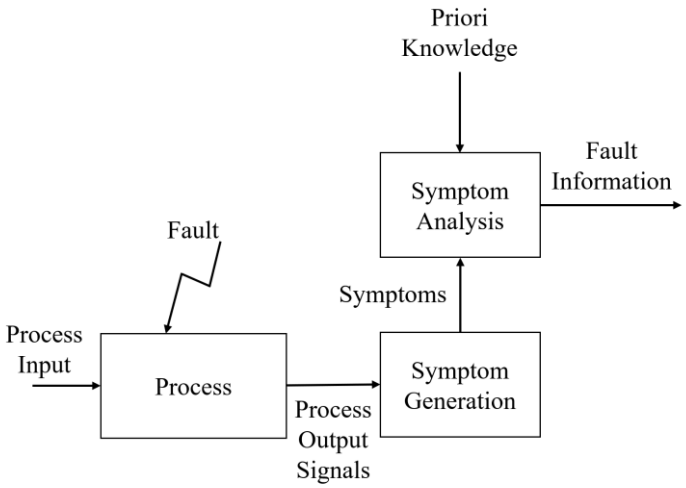

Figure 2.5. Signal-based fault diagnosis scheme (Source: Goa et al., 2015)

In the model-based fault diagnosis method, there is a system model, which is also called software redundancy, modeled by qualitative or quantitative methods that work in parallel with the actual system. This model should be created with the most appropriate method that can describe the dynamic behavior of the system. Although, the outputs of the system components are compared with the redundant ones in the hardware redundancy method, fault diagnosis is done by comparing the measured system variables with predicted variables by the model in model-based fault diagnosis. This prediction is made by sending the input of the real system to the model of the system simultaneously. The model of the system is created according to the case where there is no fault in the system. Therefore, in the case of a fault in the system, there is a difference between the measured values and the outputs of the model of the system. By interpreting these differences, which are called residuals, it is possible to get information about the faults that occurred in the system. The schematic description of the model-based fault diagnosis is represented in Figure 2.6.

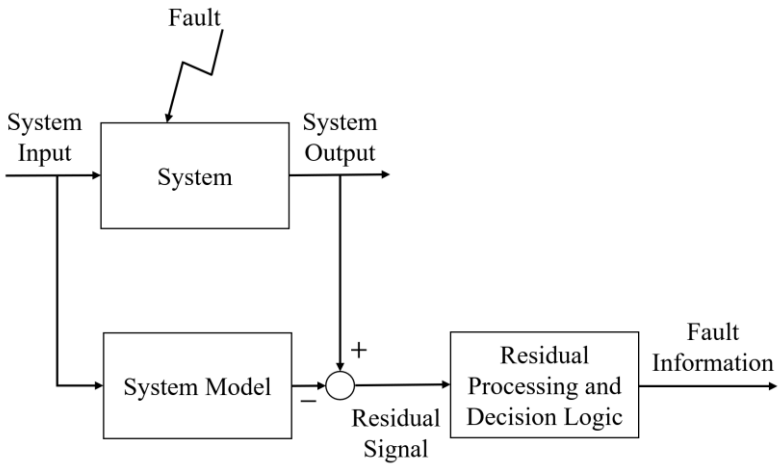

Figure 2.6. Model-based fault diagnosis scheme (Source: Ding, 2008)

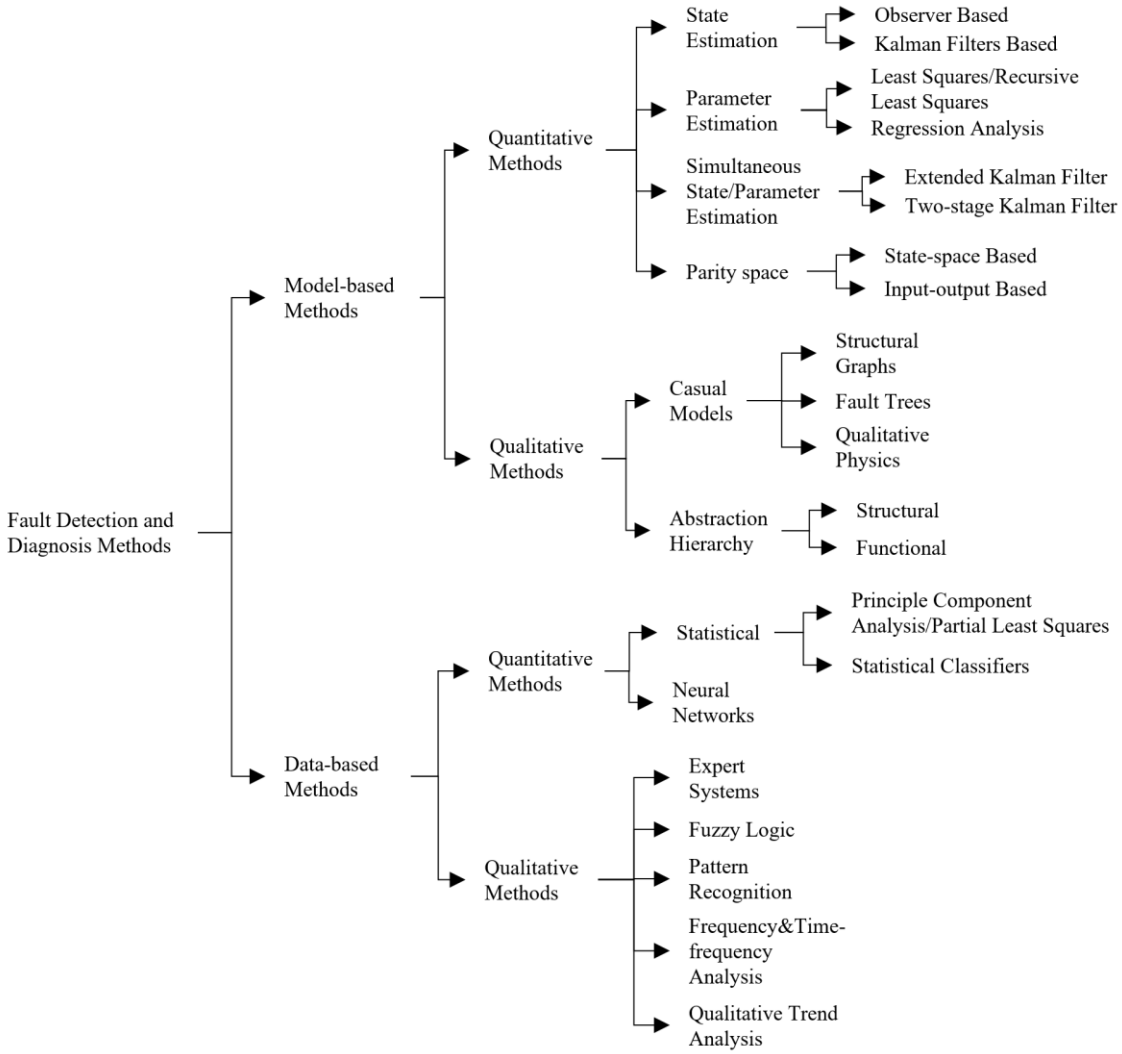

Figure 2.7. Classification of model-based and signal/data-based fault diagnosis methods (Source: Zhang et al., 2008)

There are many review papers and books in the literature about the methods used in both signal-based and model-based fault diagnosis (Gao et al., 2015; Zhang et al., 2008; Ding, 2008; Frank, 2004; Patton, 1997; Isermann 2011). The classification of the signal and model-based methods with respect to being qualitative or quantitative models is made by Venkatasubramanian et al. (2013). The refined version of this classification by Zhang et al. (2008) is represented in Figure 2.7. While in quantitative models, the system behavior is described by static and dynamic relations among system variables and parameters by using quantitative mathematical terms, in qualitative models, this relation is made with qualitative terms like if-then rules or causalities (Iserman et al., 1997).

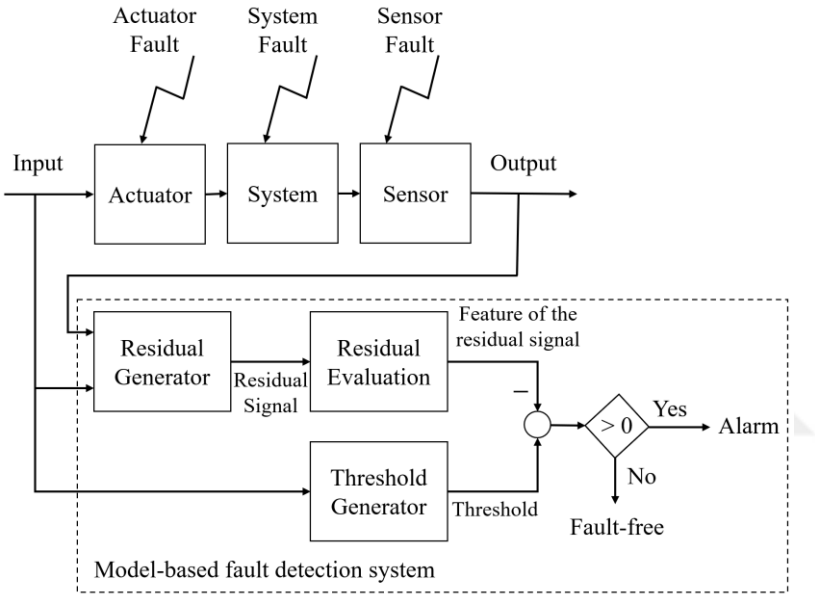

Figure 2.8. Model-based fault detection system (Source: Ding, 2008)

Model-based fault detection consists of three main parts: residual generator, residual evaluation, and threshold generator (Figure 2.8). The residual generation part contains the model of the system and where residual signals are obtained by comparing the measured values with the predicted values by the model. Zhang et al. (2008) listed qualitative methods used in the residual generation part as represented in Figure 2.9. Residual signals obtained by the system model contain fault information however, these signals are affected by disturbance and model uncertainties. For this reason, it is necessary to transform the residual signal into a form in which the effect of the fault can be seen more clearly by extracting the effects of disturbance and uncertainty. Thanks to this transformation performed in the residual evaluation part, it is possible to reduce false alarms that may arise due to disturbance and uncertainty and to facilitate the making of

decisions about the presence of faults. Although methods are applied to reduce the effects of these two factors on the residual signal, in case of no fault it is possible that there is a difference between the model outputs and the actual measurements due to these factors. For this reason, the threshold values of the residual signal should be determined according to the non-faulty condition. In this way, the presence of the fault can be easily detected according to whether the residual signal exceeds the threshold value.

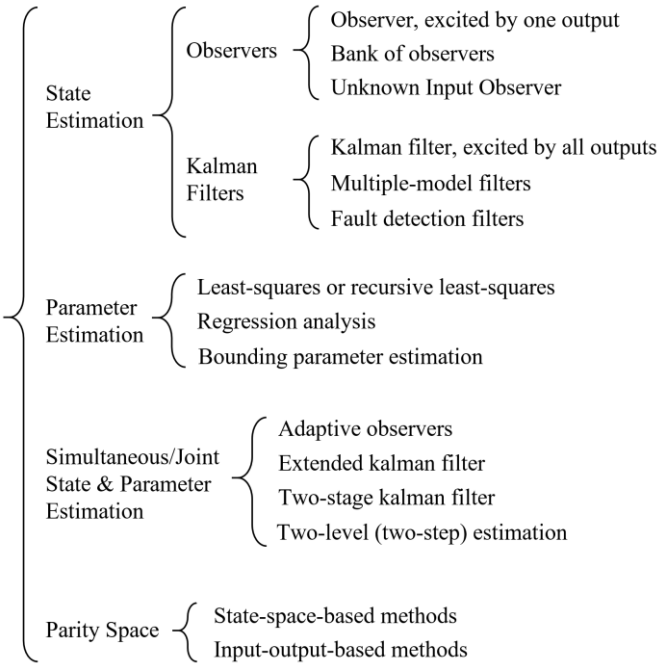

Figure 2.9. Classification of the quantitative residual generation methods (Source: Zhang et al., 2008)

2.2. Fault Types

Before mentioning the types of faults, it is necessary to define the fault. In a study of Isermann et al. (1997) the definitions revealed by IFAC Safe Process Technical Committee are released in order to avoid confusion about differences between faults, failures, and malfunction. IFAC Safe Process Technical Committee defines fault, failure, and malfunction as follows:

"**Fault:** An unpermitted deviation of at least one characteristic property or parameter of the system from the acceptable/usual/standard condition.

Failure: A permanent interruption of a system's ability to perform a required function under specified operating conditions.

Malfunction: An intermittent irregularity in the fulfillment of a system's desired function."

Isermann (2011) also listed distinguished properties of these three terms as given in Table 2.2.

Table 2.2. The distinguished properties of fault, failure, and malfunction (Source: Isermann, 2011)

Fault	**Failure**	**Malfunction**
State in the system	Failure is an event	Malfunction is an event
Can cause failure or malfunction	Caused by one or more faults	Caused by one or more faults
Fault can occur when system is working or not working	Failure can appear right after system start or abruptly due to increased stress	Malfunction can appear right after system start or abruptly due to increased stress
Difficult to detect		Temporary interruptions in the system functions
Faults occurred abruptly, incipiently or can be intermittent		

When a fault occurs in any part of the system, the system can work but some performance problems can be revealed. On the other hand, failures and malfunctions are more important problems which affect the performance of the system. If a failure occurs in any part of the system, the system can become totally unusable (Alwi et al., 2011).

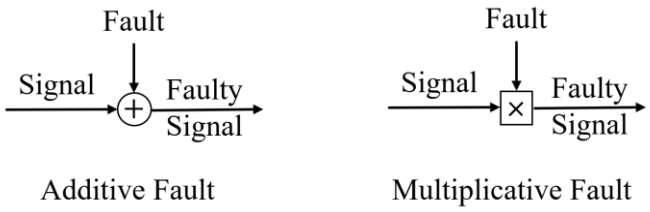

Figure 2.10. Basic fault models (Source: Verhaegen et al, 2010)

Faults in the system can be modelled in two ways as additive and multiplicative faults Figure 2.10. Although additive faults affect the stability of the system,

multiplicative faults do not affect stability. Offset in the actuator and sensor outputs or drift in the sensor outputs can be given as an example of the additive faults. Parameter changes in process, sensor or motor can be modelled as multiplicative fault (Ding, 2008).

Fault types can be divided into three categories as abrupt, incipient, and intermittent, according to their change over time (Figure 2.11). Abrupt faults can be defined as faults that occur suddenly without any symptoms. Incipient faults increase in severity over time and their effects on the system become evident over time. Intermittent faults can be defined as occasional faults that do not always reveal themselves. Since abrupt faults occur suddenly with no symptoms, they have a rapid impact on the performance and stability of the system. Therefore, a fast compensation strategy is needed for an abrupt fault. It can be said that incipient and intermittent faults are less critical than abrupt faults. In incipient fault, it is possible to diagnose the fault before the severity of the fault reaches a level that seriously affects the system performance and stability. On the other hand, intermittent faults caused by damage to the connection elements of system components such as wires which transmit data measured with a sensor, cause interruptions in system properties. Although interruptions may adversely affect system performance, they may not always cause a critical decrease in system performance.

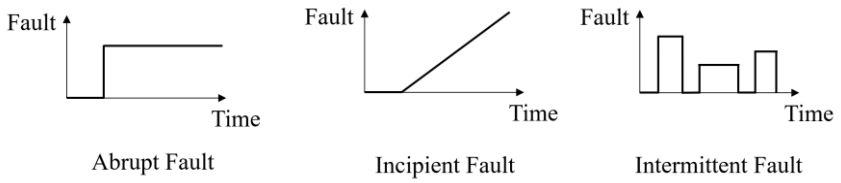

Figure 2.11. Fault types with respect to time characteristic (Source: Isermann, 2005)

2.2.1. Mobile Robot Faults

The subject of FTC has a wide range of applications and the faults that occur in these areas have some unique features, unlike the ones that occur in other areas. Nowadays, researchers are putting forward a lot of work on FTC in the robotic field. Especially in mobile robotics, the FTC issue is of great importance in robots that perform critical tasks, so that the faults that occur during the mission do not interfere with the task. Increasing the risk of fault reduces the reliability of the robot in the task. Reliability analysis of mobile robots is executed in a study by Carlson et al. (2003) in which failures occurred in different types of ground robots are considered over 2 years, in various types

of environments. According to the study, mobile robot reliability is considerably low and the average time between failures is about 8 hours. The study shows that while failures caused by the control system are 29%, hardware failures are 42%.

Before addressing the issue of tolerating faults in mobile robots, it is necessary to know the possible faults that may occur in mobile robots. Therefore, in another work by Carlson et al. (2005) which describes a classification for mobile robot failures caused by component faults, a taxonomy (Figure 2.12) is formed via collecting failure type and failure rate data from seven different mobile robot models (a total of thirteen mobile robots) produced by three manufacturers. According to this study, failures are classified into two main categories, physical and human failures. This classification is first introduced by Luprie (1985), then the sub-categorization of mobile robot failures is introduced by Carlson et al. (2005). In the work by Laprie (1985), only unmanned ground vehicle failures are considered and therefore, physical failures can be different for other types of mobile robots like the physical failures in flying and underwater locomotion systems. Physical failures are investigated under five categories: effector, sensor, control system, power, and communication system. The locomotion system, which is an important subsystem unique to mobile robots, is included in the effector category. The host side computer of the teleoperated mobile robot, the data acquisition devices, and the computer on the mobile robot are also categorized under control system failures.

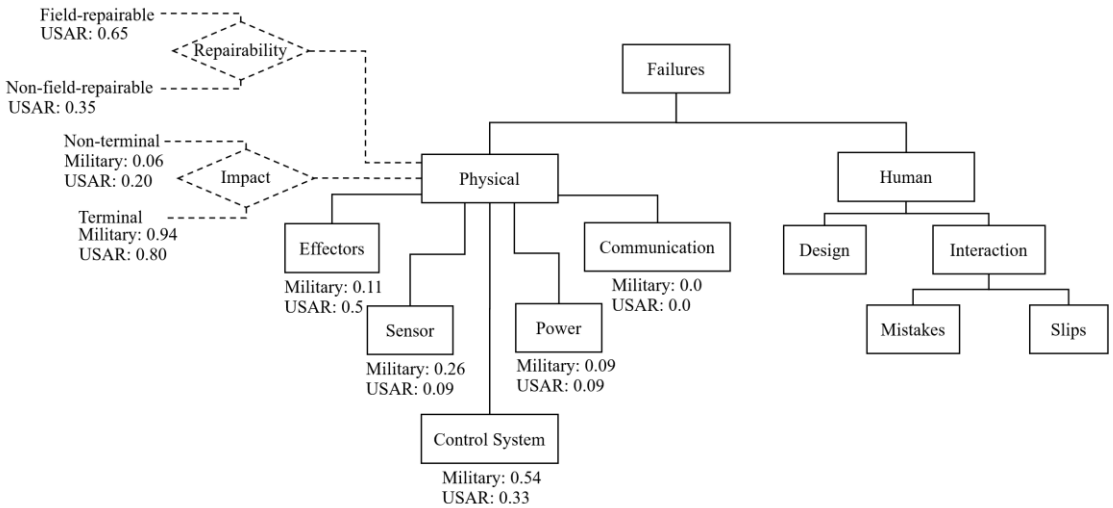

Figure 2.12. Failure taxonomy of unmanned ground vehicles (Source: Carlson et al., 2005)

According to the work by Carlson et al. (2005), physical failures can also be evaluated under two attributes: repairability and impact. Reparability is divided into two categories: field-repairable and non-field-repairable. Field-repairable can be confused with the recovery/reconfiguration part of FTC. However, field repairable is repairing the mobile robot by a trained operator with some required tools in the field. Some physical failures that occurred in a subsystem of the mobile robot can be more important in completing the task. These physical failures are categorized by their impact on the task. While terminal failures in the components of the system terminate the task, non-terminal failures do not stop the mission, but they degrade some capabilities of the robot. The human-made faults can be classified as design faults which are made in the design phase or production of the robot, and as interaction faults which are caused by not complying with the robot's usage conditions during the operation of the robot.

The failures that arise in the mobile robots often cause the robot to become out of order (Carlson et al., 2005). Faults that cause loss of performance in mobile robots or decrease some of the abilities will not prevent the completion of tasks if they are tolerated during the task. Considering the above-mentioned definitions of fault and failure, a failure that permanently disables the subsystem of a mobile robot can be considered as a fault for the mobile robot if such a failure does not completely interrupt the mobile robot work. A mobile robot consists of various subsystems, and any fault in these subsystems may cause the robot to lose the features it has obtained from this subsystem.

Actuators used in mobile robots are often used in the form of actuator-reducer combination. Reduction systems such as gearboxes and belt and pulley systems are used for reducing the speeds of the actuator also increasing the torque of the actuators. In actuation systems, faults can be caused by actuators, as well as due to reasons such as sticking or friction problems that may occur due to wear and lack of lubricant in the reduction system. Therefore, while handling the faults that occur in actuation systems, it is necessary to consider the faults in the reducers as well. Boskovic et. al., (2003) listed faults and failures of control effectors in aircraft as Lock-In-Place, Hard-Over, Float, and Loss of Effectiveness. Actuator faults encountered in mobile robots are similar to aircraft effector faults explained in Boskovic's study. Lock-In-Place fault occurs when the actuator does not give any response for any commands, so the actuator freezes at its last position. The Hard-Over fault is a fault that can be defined as the position of the actuator reaches at its maximum or minimum position limits independent of any commands. When this failure occurs, the actuator reaches the maximum or minimum position with the

maximum speed limit of the actuator. When Float fault occurs in the actuator, the actuator loses its power, so no torque or force can be transmitted by the actuator. In the case of Loss of Effectiveness fault, the actual output of the actuator is less than the nominal value. Actuator faults and failures are represented in Figure 2.13.

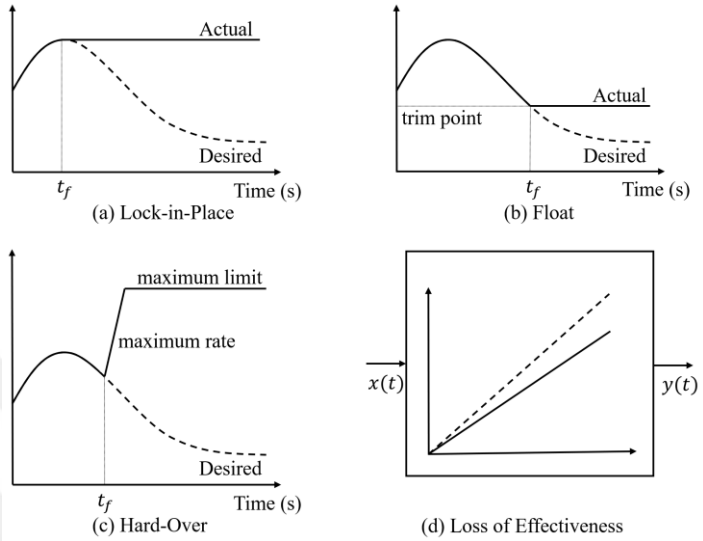

Figure 2.13. Actuator fault and failure types (Source: Alwi et al., 2011)

The Lock-In-Place fault encountered in the actuators of mobile robots can arise due to various reasons. The source of this fault can be abrasion on gears, lack of lubrication, the abrasion on brushes, etc. and because of these kinds of faults, the actuator can become stuck and immovable. Brandstötter et al. (2007) developed an AFTC strategy for Lock-In-Place fault that occurred in one of the wheel actuators on a holonomic mobile robot which uses three omnidirectional wheels. Working on the Lock-In-Place fault is very popular among researchers who work with legged mobile robots (Sarkara et al., 2014; Resceanu, 2011). Because of the locking that occurs in the connecting elements of the actuators in the joints of the leg, the leg with the faulty actuator can be completely out of use. Since most of the legged mobile robots are redundant, faults can be tolerated by applying different gait strategies with the other non-faulty legs. When this type of a fault occurs in the wheel actuator of any wheeled mobile robot, it can make the robot completely inoperative or the robot needs to change its motion strategy. When Lock-In-Place fault occurs in any wheel of a two-wheel differential drive robot, the robot becomes unusable, but the same fault occurred in three omnidirectional wheeled holonomic mobile robots like the robot in Brandstötter's work, the robot can continue the motion with the remaining two wheels.

Float faults that cause actuators to move freely without producing any torque can be caused by various reasons such as disconnection of connection elements between the actuator and link or the disconnection between the power source and the actuator as discussed by Wang (2009). Determination of the type of fault in the case when the actuator becomes completely inoperable is very important in terms of fault recovery. For example, when the Float fault occurs in wheeled robots, it is easier for the robot to tolerate this fault because there is less resistance between the wheel and the ground since the faulty wheel can rotate freely. On the other hand, because of the Lock-In-Place fault occurring in the actuator, the faulty wheel is stuck, and the robot encounters a greater resistance due to the friction between the faulty wheel and the ground during the toleration event. The important factor which affects fault type is whether the reduction mechanism on the actuator is back drivable or not. In the case of a fault occurred in the actuator with a back drivable reducer, the output shaft of the reducer can move freely with some minimal resistance, so the fault can be defined as a Float fault. In non-back-drivable reducers, an actuator fault can cause a Lock-In-Place type of fault.

Loss of Effectiveness is the common fault in studies on faults occurring in mobile robot actuators (Baghernezhad et al., 2016; Li, 2009; Aghili, 2011; Hrizi et al., 2013; Rotonto et al., 2014). This fault is a relatively easy fault to be tolerated compared to the other faults. Performance degradation due to wear and tear can occur in actuators over time. In cases where this fault has occurred, problems such as involuntary orientation and position changes can occur in robots (Li, 2009). While in case of Hard-over fault, the actuator is out of control and moves to maximum or minimum position limits. This fault can be seen in actuators which have a position control such as legs, robot arms placed on mobile robots and guiding wings used in underwater and air vehicles.

In mobile robots working on the land, the basic elements of the locomotion system are wheels, pallets, legs, and various movement organs. These elements, which come into direct contact with the environment where the robot is working, can easily be affected by environmental conditions and cause various faults. These faults in the locomotion systems of mobile robots may be caused by the problems that occur over time in these organs, or they may be caused by selecting inappropriate elements for the working environment during the design process. Stiction is the most common fault that occurs over time in these elements. (Baghernezhad et al., 2016, Fourlas, 2013). Stiction, that may occur in elements such as wheels and pallets, can make it difficult to hold on to the floor over time and may cause slippage. This can lead to involuntary orientation changes or restriction of the

motion of the robot. If an inflatable wheel is used in wheeled mobile robots, the air pressure in the wheel may change over time (Roumeliotis et al.,1998a; Fourlas, 2013; Fourlas, 2014). The difference in wheel diameters that will arise as a result of this fault can lead to various control difficulties. When the operating conditions of mobile robots are considered, objects such as dust, rocks, or branches squeezed into the locomotion system components may cause periodic inconsistencies, immovability, or slippage on parts of the locomotion system (Carlson et al., 2005; Roumeliotis et al.,1998a; Baghernezhad et al., 2016).

Unlike locomotion systems on terrestrial vehicles, various underwater robots (Remotely Operated Vehicles (ROVs) and Autonomous Underwater Vehicles (AUVs)) use a variety of thrusters which contain fins and motor to enable the robot to navigate underwater. Antonelli' (2003) listed the faults and failures that occurred in the locomotion systems of the robots working underwater (Table 2.3).

Table 2.3. Possible faults and failures in underwater robots (Source: Antonelli, 2003)

Thruster Blocking	This fault can be the result of trapping various particles such as ice and algae in the water between the thruster parts. This fault, which may result like a Lock-In-Place fault in the actors, can cause the robot to become completely out of order if there is no redundancy
Flooded Thruster	Insulation is one of the challenges that have to overcome the difficulty in underwater robots. Problems that arise in insulation can cause thruster to get water, so thruster can become unusable
Fin Stuck or Lost	The object in the sea which trapped between the fins that allow the robot to navigate in the sea or the loss of these fins for various reasons can also have an effect that will make it difficult for the robot to be guided
Rotor Failure	Thrusters in underwater robots usually use DC motors, and all the actuator faults mentioned above can also be found in these thrusters. Because of these faults, thruster may be completely out of order and there may be performance losses.
Hardware-software Failure	Underwater robots are working in difficult to reach environments, so failures in critical hardware parts and the software can stop the mission. Therefore, failures in these components can be tolerated with redundancy techniques

Mobile robots are generally designed to operate in unknown environments. For this reason, mobile robots that interact with their environment contain many sensors to

measure environmental effects such as temperature and pressure. Also, considering that the mobile robot can move freely in the environment, it is important to know the localization of the robot. Therefore, mobile robots should have sensors for localization such as encoders, inertial measurement units, and GPS. In a book by Siegward et al. (2004), the sensors used in mobile robots are classified as shown in Table 2.4.

Table 2.4. Sensor types used in mobile robotics (Source: Siegward, 2004)

General classification (typical use)	Sensor Sensor System
Tactile sensors (detection of physical contact or closeness; security switches)	Contact switches, bumpers Optical barriers Noncontact proximity sensors
Wheel/motor sensors (wheel/motor speed and position)	Brush encoders Potentiometers Synchros, resolvers Optical encoders Magnetic encoders Inductive encoders Capacitive encoders
Heading sensors (orientation of the robot in relation to a fixed reference frame)	Compass Gyroscopes Inclinometers
Ground-based beacons (localization in a fixed reference frame)	GPS Active optical or RF beacons Active ultrasonic beacons Reflective beacons
Active ranging (reflectivity, time-of-flight, and geometric triangulation)	Reflectivity sensors Ultrasonic sensor Laser rangefinder Optical triangulation (1D) Structured light (2D)
Motion/speed sensors (speed relative to fixed or moving objects)	Doppler radar Doppler sound
Vision-based sensors (visual ranging, whole-image analysis, segmentation, object recognition)	CCD/CMOS camera(s) Visual ranging packages Object tracking packages

Faults in the sensors of mobile robots can cause losing or reducing some of the properties of the robot and eventually, may prevent the robot from completing the task. Some sensors used in mobile robots are critical to the operation of the robot. An example of this is camera systems used in mobile robots controlled by the operator from a long distance. Since faults that may arise in these camera systems may cause the operator to lose sight, even though the robot's motion functions can work, it causes the robot to fail. In a study by Boskovic (2003), faults in sensors are classified as Bias, Freezing, Drift, Loss of Accuracy, and Calibration Fault (Figure 2.14). Sensor faults classified by

Burkovic's study can be encountered in some of the sensors used in mobile robots which are also listed in Table 2.4. In the case of Bias fault, there is a constant value difference between the actual value and measured value by the sensor. In the Freezing fault, while the actual value of the physical quantity is changed in time, the measured value freezes at a constant value. The Freezing fault is one of the most common faults in mobile robots (Roumeliotis et al.,1998b; Valdivieso et al., 2006; Filaretov et al., 2015). Considering the operating conditions of mobile robots, vibrations that occur in motion can cause various disconnections of the sensors. Both mechanical mounting problems and cable disconnections due to vibration can cause the Freezing fault in the sensors. The Drift fault is the difference developed between measured and the actual value which increases in time. The localization of mobile robots is provided by various sensors. These sensors may be encoders that receive the position information of the actuators, as well as accelerometers and gyroscopes. The difficulty when localizing the robot with an accelerometer and gyroscope is the Drift fault that occurs in the position information due to the noise in the sensor data since the position is obtained from the measured acceleration and speed with the sensors via integration. Other faults encountered in sensors are Loss of Accuracy caused by noise, and measurement fault caused by incorrect calibration of the sensor (Daigle et al., 2007; L´opez-Estrada et al., 2014). The loss of accuracy is a condition when the measured value of the quantity does not reflect accurately the actual value.

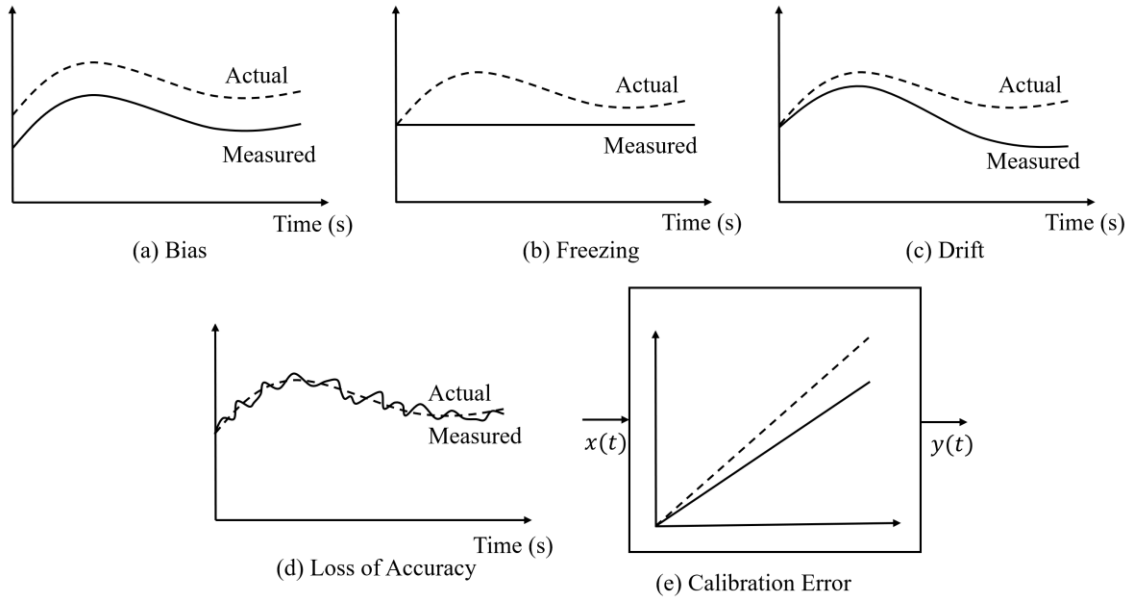

Figure 2.14. Sensor fault and failure types (Source: Alwi et al., 2011)

2.3. Fault Tolerant Control Studies in Mobile Robot Applications

As mentioned in the previous sub-section, fault-tolerant control is divided into two categories as active and passive FTC. It can be said that PFTC is a less preferred method in mobile robots because of the low capacity to tolerate the faults and the variety of faults types in mobile robots. On the other hand, there are studies in which PFTC methods are used to tolerate faults that occur in mobile robots. As an example, Yang et al. (2007) developed a fault tolerant controller based on an artificial immune principle to tolerate loss of effectiveness in one of the actuators on the wheels of a two wheeled mobile robot. Thanks to the method used in this study achieved in simulation, the robot can adapt to the faulty situation and perform the desired motion despite the fault. In another study that applies PFTC principles by Lin et al. (2007), a method which includes computed torque controller and robust FTC to tolerate nonlinear faults and system uncertainties in nine-link biped robot is proposed. While the biped robot is controlled with the computed torque method, the robust FTC used also ensures that the faults which occur in the joints of the robot are tolerated. As mentioned before, the most common diagnosis methods in AFTC systems are model-based and data-based methods. Roumeliotis et al. (1998a), introduced a model-based fault detection and identification method which uses a Kalman filter as the state estimator for a wheeled mobile robot (Pioneer 1). Song et al. (2006) proposed an active model-based fault-tolerant control method for autonomous mobile robots, in which unscented Kalman filter is used for real-time estimation of motion states and actuator effectiveness factor. Duan et al. (2006) used an adaptive particle filter to diagnose faults of a wheeled mobile robot. Although model-based fault diagnosis methods are more widely used for mobile robots, data-based fault-tolerance studies are also being carried out. The neural network is one of the most common methods for data-based fault diagnosis and recovery studies (Li, 2009; Makino et al., 2013; Lin et al., 2015). Liu et al. (2007) proposed a fault diagnosis method for both system and sensor faults of a wheeled mobile robot method based on a multi cerebellar model articulation controller (Multi-CMAC) neural network. Also, in the literature, there are studies that use different models and data-based methods together to improve the reliability of fault diagnosis (Yong et al, 2006). In a study in which the same mobile robot is used with Roumeliotis's work, multiple model estimation method (Kalman filter) and neural network is used together in the fault diagnosis algorithm (Goel et al., 2000). Yong et al. (2006) proposed

a combined Boolean logic reasoning and model-based fault diagnosis in suction foot control of a climbing robot.

One of the major hardware components of mobile robots is sensors. Sensors, used to measure the interactions with the environments and internal states of the robots, can sometimes give faulty outputs. For example, although there is no problem in the locomotion system of the robot, the robot may follow a wrong path due to faulty measurement. In a study by Roumeliotis et al. (1998b), the diagnosis of a fault that may occur in the gyroscope is carried out by a model-based method in which a Kalman filter is used. Duan et al. (2009) used particle filter to diagnose faults that occurred in internal sensors (motor encodes and gyroscope) of a mobile robot.

Many robots are moving on unknown environments, so a reliable navigation system (consists of various sensors) is an important part of mobile robots. Navigation reliability can be explained as; when a robot moves from one place to another, it does not lose or miscalculate its actual position. If the actual position of the robot is different from the measured position given by the navigation system, operation success will be decreased. Also, it can cause a collision with obstacles. For reliable navigation, many researchers are focused on dealing with faults that occur in parts and sensors of the navigation system (Dharmaweera et al., 2010; Forlas, 2013; Filaretov et al., 2015). Sundvall et al. (2006) proposed a fault detection algorithm that detects faults on odometry data. One of the problems in the position estimation with odometry is wheel slippage. In this study, they proposed and algorithm to find out whether there is a fault in odometry data due to wheel slippage by comparing this data with the position information received from a different source (laser scanner). Mobile robots may work in a crowded environment like factory floors and hospitals and thus, these robots can face the risk of collision at any moment. Therefore, a reliable path planning algorithm is essential for these robots. For this purpose, Mass et al. (2012) proposed an adaptive path planning algorithm that can avoid crashes with obstacles.

Mobile robots need a processor in which various calculations are made. A fault toleration mechanism that can tolerate faults or failures should be developed in these processors for the success of the task. Redundancy based fault toleration approach is generally used to compensate for faults that occur in robots' processors. In literature there are works focused on the CPU faults of mobile robots. One of them is Murakami’s study (2006) that proposes a dynamic fault tolerance algorithm for a humanoid robot engine based on hardware redundancy. In another work by Wang et al. (2008), a redundancy-

based fault-tolerant central controller is developed for space robot systems and it has two processing modules: a 32bit ARM RISC processor and Commercial-Off-The-Shelf (COTS) devices.

The locomotion systems are one of the most important systems of mobile robots so there are many studies in the literature on tolerating the faults that occur in these systems. Many terrestrial mobil robots are operating in tough environmental conditions, so they can influence by external factors and easily failed. Therefore, FTC is an important topic for these robots. In a study of Washington et al. (2000), a Markov and Kalman State Identification technic (MaKSI) is applied to fault identification of a rover. For mobile robots that use conventional wheels, there are many fault-tolerant control studies in addition to the studies mentioned before (Axenie et al., 2010; Li et al., 2013). Other than standard wheels, another preferred type of wheel is the omnidirectional wheels, which give the robot to holonomic movement ability. In the literature, there are some studied that propose fault diagnosis and reconfiguration algorithm for actuator faults of holonomic mobile robots instead of structural faults of omnidirectional wheels (Valdivieso et al., 2006; Song et al., 2006; Rotondo et al., 2014). Legged mobile robots are preferable when operational space is terrain or difficult to walk for wheeled mobile robots. Many researchers are interested in developing fault-tolerant locomotion strategies to increase terrain adaptability and efficiency of legged mobile robots. In the literature, some studies focused on the fault-tolerant control strategy for legged mobile robots (Wang et al., 2010; Mösch et al., 2007; Agarwal et al.,2007; Hoshino et al., 2011). For instance, in a work by Yang et al. (2000), a fault-tolerant gait for fault-tolerant locomotion of a hexapod on uneven terrain is proposed. In their scenario, a legged mobile robot (hexapod) is lost one leg during operation but according to the proposed gait strategy it can move without losing locomotion ability.

Underwater applications are very crucial like search and rescue missions so mobile robots operating in underwater must have reliable locomotion and control systems. These robots should have a fault-tolerant control strategy for unexpected situations to increase the reliability of the robot. Filaretov et al. (2015) applied an active FTC method that uses a model-based diagnosis to tolerate sensor faults in the navigation system of an autonomous underwater robot. In another study by Wang et al. (2009) a data-based fault diagnosis algorithm that uses a recurrent neural network is utilized to tolerate thruster fault of glider type underwater robot.

In the last two decades, the usage of drones and unmanned aerial vehicles (UAV) have been increased day by day in both military and civil applications such as rescue, surveillance, geographic studies, search, remote sensing, recognition, aerial transportation, inspection, and maintenance, etc. L´opez-Estrada et al. (2014) used a model-based fault diagnosis method that uses a linear parameter varying method for sensory faults of quadrotor type UAV.

In mobile robotic, fault-tolerant control strategies are not only focused on tolerating faults occurred in hardware and software systems but also developing fault-tolerant multi-robot applications (Khan et al., 2009; Marino et al., 2009; Hoshino et al., 2011; Amory et al., 2013; Portugal et al., 2013; Carrasco et al., 2007). In 2014, Arrichiello et al. proposed a distributed fault-tolerant strategy for a networked team of the autonomous robot. According to their recovery strategy, if any robot of the team is faulty due to any reason, this robot is taken out by the recovery algorithm then reorganize remaining team members to accomplish the mission.

2.4. Wheeled Mobile Robots

Although there are various locomotion systems, such as legs and pallets, for the motion of terrestrial mobile robots, wheels are the commonly employed and efficient locomotion system. Wheels used in wheeled mobile robots (WMRs) vary in terms of their design and material types. The wheel types used in mobile robotics are represented in Figure 2.15.

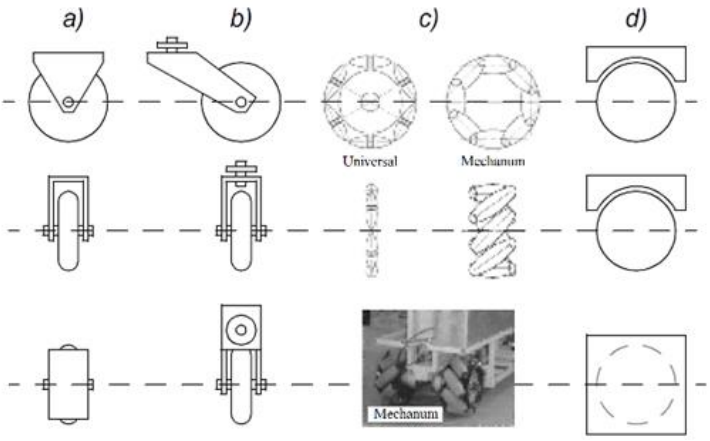

Figure 2.15. The four basic wheel types used in mobile robotics. (a) Standard Wheel (b) Castor Wheel (c) Omnidirectional Wheels (Universal and Mecanum wheels) (d) Spherical Wheel (Source: Siegwart et al., 2004)

Although, there are wheels specially designed for the purpose of increasing the mobility of the mobile robot or to enable more convenient motion in the working area (Tadakuma et al., 2007, Han et al., 2009, Ishida et al., 2010, Al Mamun et al., 2018), many wheels used in mobile robots are actually designed for different purposes (Oftadeh et al., 2013, Li et al., 2016, Yi et al., 2009). Nevertheless, there is no standard friction model that is applied to these different types of wheels.

The friction characteristic of the wheel is an important factor affecting the motion ability of WMRs. Having knowledge about this characteristic is helpful for improving the control of mobile robots (Tian et al., 2014) when absolute position measurements for localization are not available. In fact, for the localization of mobile robots working in indoor applications, such as automated guided vehicles (AGVs) and household robots, global positioning systems (GPS) are not available. Instead, sensor fusion which combines odometry data taken from the wheel's angular speed sensor (commonly an encoder or a tachometer) and other sensors like inertial measurement units (IMU) or laser sensors are more suitable for indoor robot positioning tasks (Jetto et al., 1998, Ganganath et al., 2012, Marin et al., 2014, Peela et al., 2018). The difficulty of the positioning with odometry data is that because of the wheel slippage, the actual position of the robot cannot be calculated precisely. Therefore, the estimation of the wheel slippage with the help of friction force models becomes an important topic in improving robot positioning with odometry data (Iagnemma et al., 2009).

Wheels used in mobile robot applications are quite different than the tires used in automobiles. Although in the literature there are various studies that describe friction characteristics of automobile tires (Erdogan et al., 2011, Rath et al., 2015, Madhusudhanan et al., 2016, Liu et al., 2017, Li et al., 2006), there are few studies which deal with modeling mobile robot wheel friction with static and kinetic friction coefficients (Balakrishna et al., 1995, Williams et al., 2002) or steady-state friction model (Tian et al., 2014). Achieving traction control of the mobile robot and improving localization with odometry data requires information on the wheel's friction characteristics. Therefore, these characteristics must be revealed before these kinds of studies can be carried out with an actual mobile robot.

WMRs need motion ability which allows them to move over rocks or holes and avoid obstacles in outdoor operations. In contrast to outdoor environments, indoor environments have relatively smooth and clean surfaces. However, there are many obstacles and narrow passages in indoor tasks that require increased mobility capabilities.

Among the tasks that require maneuvering in tight spaces and avoiding obstacles, the following can be named as examples: transporting of goods in hospitals or factories, public area cleaning, and sheltered workshops for disabled people. Consequently, special omnidirectional wheels have been developed in the past years to increase the mobility capabilities of WMRs. Using these types of wheels, WMRs can be developed with holonomic motion ability. Holonomic mobile robots (HMR) are capable of translating in two orthogonal directions and rotating about the normal of the surface independently and simultaneously.

Holonomic motion of ground vehicles can be constructed with ordinary castor wheels or special omnidirectional wheels (mecanum and universal). HMR, which have caster wheels, firstly changes wheel orientation according to motion direction and then robot moves. This procedure brings delay in operation and robot cannot perform a smooth continuous motion. Omnidirectional wheels allow motion that is perpendicular to the rotating direction of the wheel through smaller free rollers which are placed on the outer circle of the wheel. In holonomic mobile robots that use caster type of wheels, at least three caster wheels and six actuators among which three actuators are required for rotation of wheels and three actuators are required for changing the wheels' orientation. In holonomic mobile robots that use omnidirectional wheels, only three universal or four mecanum wheels and an actuator for every wheel are enough. Therefore, omnidirectional wheels are more efficient for holonomic ground robots in terms of minimized use of the actuators.

2.5. Conclusions

According to some study results discussed in this chapter (Carlson et al., 2003; Carlson et al., 2005) mobile robots frequently experience failure due to difficulties in working conditions and these failures cause disruptions in the task performed by the robot. The tolerance of the faults that occur in mobile robots is a very important issue considering the tasks these robots perform. In this chapter, faults that occur during the tasks of mobile robots and the methods for tolerating these faults are discussed. First, fault recovery methods are classified and application methods of these are explained. There are some features that distinguish mobile robots structurally from other robots, such as their hardware features and locomotion systems. In this chapter, the second topic

discussed is the types of faults that occur in the hardware parts of mobile robots and the methods applied in the literature to tolerate these fault types.

CHAPTER 3

AN INDOOR FOUR-WHEELED HOLONOMIC MOBILE ROBOT

In this chapter, the design of a HMR with four omnidirectional wheels is introduced. Firstly, the hardware features of the robot are presented. Then, kinematic equations and applied control algorithm are described. The dynamic model of the robot is needed for model-based fault diagnosis studies performed with this mobile robot. The friction model between the wheel and the ground is an essential part of the robot's dynamic model. The methods in the literature used to model this friction are firstly described, and then the entire dynamic model of the robot which uses the selected model is given.

3.1. Four-Wheeled Holonomic Mobile Robot

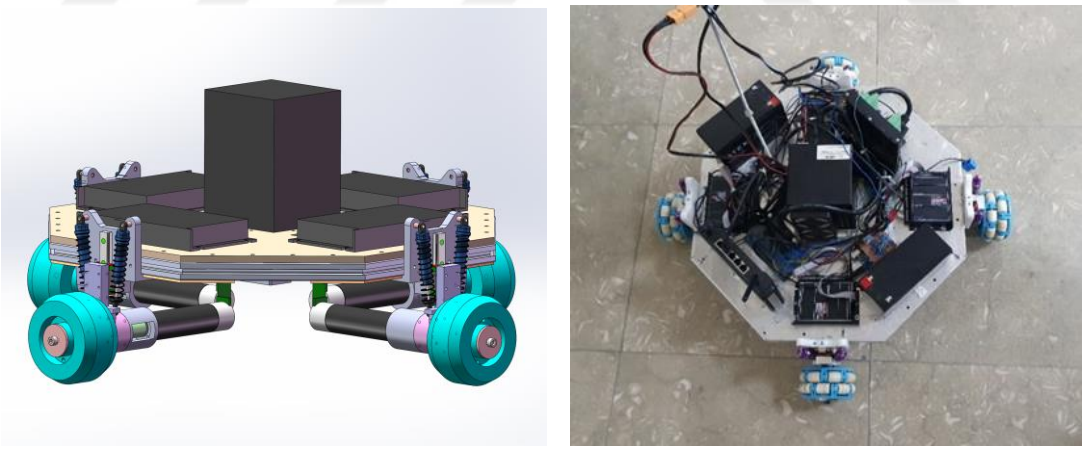

Figure 3.1. Four-wheeled holonomic mobile robot

A HMR (Figure 3.1) is designed and manufactured in IzTech Robotics Laboratory. This mobile robot has four universal-type omnidirectional (UTO) wheels for locomotion. Although holonomic motion in a plane can be achieved with the use of only three UTO wheels, this HMR design aimed at increasing the fault-tolerance capacity of the system. In the worst-case scenario, if any wheel stops working during operation, HMR can tolerate this fault and continue operation with the remaining three UTO wheels

without losing its holonomic property. Additionally, there are relatively less severe cases of faults for this system. Some external factors, such as oil on the surface, can cause nonpermanent deviation on the friction characteristic of the wheel. If this deviation is detected through comparison with a reference friction model (model-based fault detection), HMR can continue to perform the task with a fault recovery strategy.

3.1.1. Kinematics of the Mobile Robot

Figure 3.2 represents the location of the mobile robot according to the global coordinate frame (X_w, Y_w, Z_w) and wheel velocities of the robot, where, V_i is the linear speed of the center of the wheels and $\dot{\varphi}_i$ is the angular speed of wheels for $i = 1,2,3,4$. θ_v is the orientation of the mobile robot, m_v is mass of the robot, I_v is the moment of inertia of the robot with respect to the mass center, $\dot{x}_w$ and $\dot{y}_w$ are linear speed components of the robot with respect to global coordinate frame, $\dot{\theta}_v$ is the angular speed of the robot defined about the normal of the ground, and r is the wheel radius. All four wheels are placed such that the angles between the neighboring wheel axes are 90°. Distances between wheels and center of mass are the same (250 mm) and shown with the parameter l in Figure 3.2.

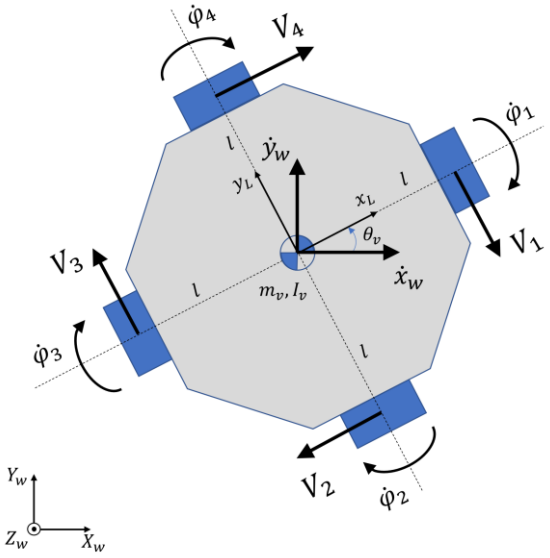

Figure 3.2. Top view of four wheeled mobile robot

Kinematic equations of mobile robot are given below,

$$\dot{x}_w = V_1 sin\theta_v - V_3 sin\theta_v - V_2 cos\theta_v + V_4 cos\theta_v \quad (3.1)$$

$$\dot{y}_w = -V_1 cos\theta_v + V_3 cos\theta_v - V_2 sin\theta_v + V_4 sin\theta_v \tag{3.2}$$

$$\dot{\theta}_v = -(V_1 + V_2 + V_3 + V_4)/l \tag{3.3}$$

$$\begin{bmatrix} \dot{x}_w \\ \dot{y}_w \\ \dot{\theta}_v \end{bmatrix} = J \begin{bmatrix} V_1 \\ V_2 \\ V_3 \\ V_4 \end{bmatrix} \tag{3.4}$$

$$J = \begin{bmatrix} sin\theta_v & -cos\theta_v & -sin\theta_v & cos\theta_v \\ -cos\theta_v & -sin\theta_v & cos\theta_v & sin\theta_v \\ -1/l & -1/l & -1/l & -1/l \end{bmatrix} \tag{3.5}$$

$$V_i = \dot{\varphi}_i r \qquad i = 1,2,3,4 \tag{3.6}$$

Because of the kinematic redundancy, the Jacobian matrix given in Equation 3.5 is not a square matrix. Hence, the pseudo-inverse method can be used to find the minimum norm of wheel speeds. The pseudo-inverse of the Jacobian matrix ,J^+, for the robot is derived as:

$$\begin{bmatrix} V_1 \\ V_2 \\ V_3 \\ V_4 \end{bmatrix} = J^+ \begin{bmatrix} \dot{x}_w \\ \dot{y}_w \\ \dot{\theta}_v \end{bmatrix} \tag{3.7}$$

$$J^+ = J^T (JJ^T)^{-1} \tag{3.8}$$

With the above equations, the wheel speeds can be found according to the speed requests of the robot according to the world coordinate frame. However, there is a need for a method that allows the system to be reconfigured and tolerated if there is a fault in one of the wheels. Therefore, the method of the weighted pseudo-inverse of the Jacobian matrix ($\hat{J}_w^+$) is applied to deal with the hardware faults of the mobile robot. Then Equations 3.7 and 3.8 are modified as

$$\begin{bmatrix} V_1 \\ V_2 \\ V_3 \\ V_4 \end{bmatrix} = \hat{J}_w^+ \begin{bmatrix} \dot{x}_w \\ \dot{y}_w \\ \dot{\theta}_v \end{bmatrix} \tag{3.9}$$

$$\hat{J}_w^+ = \widehat{W}^{-1}\hat{J}^T\left(\hat{J}\widehat{W}^{-1}\hat{J}^T\right)^{-1} \tag{3.10}$$

where, $\widehat{W}$ is a diagonal weight matrix.

$$\widehat{W} = \begin{bmatrix} W_1 & 0 & 0 & 0 \\ 0 & W_2 & 0 & 0 \\ 0 & 0 & W_3 & 0 \\ 0 & 0 & 0 & W_4 \end{bmatrix} \tag{3.11}$$

W_1, W_2, W_3, W_4 each represents the chosen weight constant for the designated wheels. Increasing any W_i $(i = 1,2,3,4)$ parameter with respect to the other three decreases the corresponding wheel's contribution in operation. If any weight is to be chosen infinite, the desired motion is carried out with the other three since the system is already redundant. The calculation of the linear speed requirement of one of the wheels for a desired task space speed profile are given in Equations 3.12, 3.13, 3.14 and 3.15.

$$\begin{aligned} V_1 = -[0{,}5/(W_1 + W_2 + W_3 + W_4)][&\dot{\theta}_v l(W_2 + W_4) + \dot{y}_w(sin\theta_v\,(W_2 - W_4) \\ &+ cos\theta_v(W_2 + 2W_3 + W_4)) + \dot{x}_w(cos\theta_v(W_2 - W_4) \\ &- sin\theta_v(W_2 + 2W_3 + W_4))] \end{aligned} \tag{3.12}$$

$$\begin{aligned} V_2 = -[0{,}5/(W_1 + W_2 + W_3 + W_4)][&\dot{\theta}_v l(W_1 + W_3) + \dot{x}_w(sin\theta_v(W_3 - W_1) \\ &+ cos\theta_v(W_1 + W_3 + 2W_4)) + \dot{y}_w(cos\theta_v(W_1 - W_3) \\ &+ sin\theta_v(W_1 + W_3 + 2W_4))] \end{aligned} \tag{3.13}$$

$$\begin{aligned} V_3 = -[0{,}5/(W_1 + W_2 + W_3 + W_4)][&\dot{\theta}_v l(W_2 + W_4) + \dot{x}_w(cos\theta_v\,(W_2 - W_4) \\ &+ sin\theta_v(W_2 + 2W_1 + W_4)) + \dot{y}_w(sin\theta_v(W_2 - W_4) \\ &- cos\theta_v(2W_1 + W_2 + W_4))] \end{aligned} \tag{3.14}$$

$$\begin{aligned} V_4 = [0{,}5/(W_1 + W_2 + W_3 + W_4))(&-\dot{\theta}_v l(W_1 + W_3) + \dot{x}_w(sin\theta_v(W_1 - W_3) \\ &+ cos\theta_v(W_1 + 2W_2 + W_3)) + \dot{y}_w(cos\theta_v(W_3 - W_1) \\ &+ sin\theta_v(W_1 + 2W_2 + W_3))] \end{aligned} \tag{3.15}$$

3.1.2. The Mobile Robot's Control Algorithm

A cascade control algorithm is designed for the speed demands given according to the world coordinate frame (Figure 3.3). In top-level control which is indicated with blue dashed line in Figure 3.3, the linear speeds of the robot at X_w and Y_w directions are controlled with an open-loop controller due to there is no chance to measure the actual speed of the mobile robot (getting this information by taking integral of the acceleration of the robot is not reliable due to measurement noise) to make the close-loop controller. Also, at this level, the angular speed at Z_w direction is controlled by a close-loop proportional controller (P-controller) by using angular speed information measured by an analog gyroscope placed on the robot. Although fault-tolerant capability is limited, this controller also makes passive fault toleration for orientation changes due to manufacturing faults at the wheel arrangements and wheel slippage.

Due to the special structure of the mobile robot, each wheel should be driven independently from the others (there is no differential system). Therefore, each omnidirectional wheel is driven by a DC motor connected to the wheel. The joint space control algorithm includes a current control loop in the motor driver and a speed control loop for each motor. Because the motor drivers on the robot enable the control of the motors in the current mode, in joint space, current control (indicated with green dashed line in Figure 3.3) of the motors that actuate the omnidirectional wheels is employed. In the top-level, speed demands for each wheel are obtained from inverse kinematic. To control wheel speeds, in the upper-level speed controller at the joint space, a PI type controller is used. Here, the reference current values (i_{ref}) generated by the upper-level speed control loop (indicated with red dashed line in Figure 3.3) for the wheel speed requirements are given to the motor driver, and current control is applied inside the motor drivers.

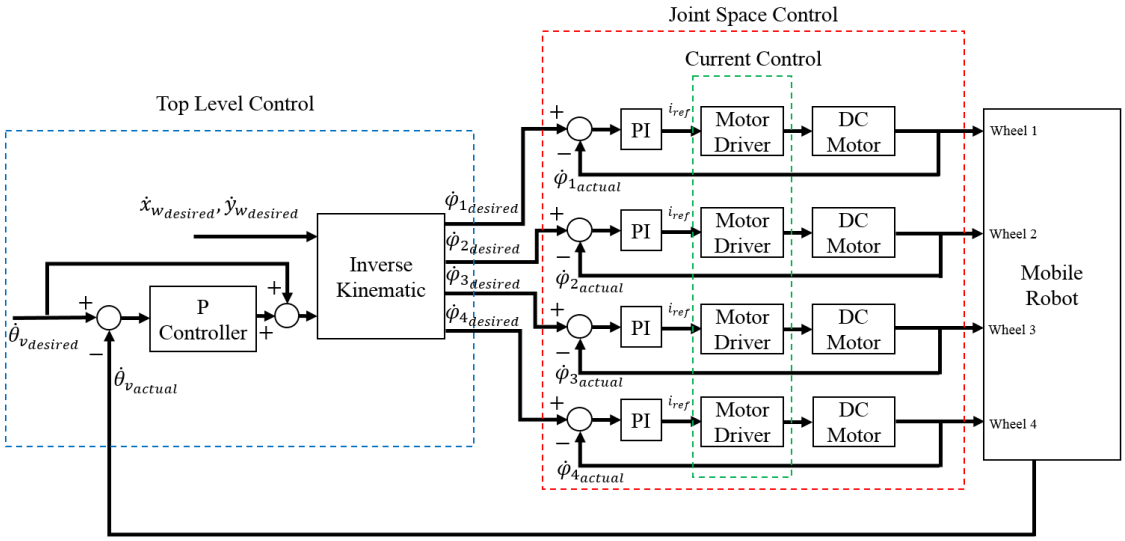

Figure 3.3. Control algorithm of the robot

3.1.3. Dynamics of the Mobile Robot

Wheeled mobile robots have a very similar structure to land vehicles such as automobiles due to their mechanical structure and the systems they include. Wheeled mobile robots also have sub-systems such as chassis, suspension system, and braking system as in automobiles. Considering the overall dynamics of wheeled land vehicles, the dynamics of these sub-systems should be examined separately. Apart from these, the structures of the wheels, wheel-ground friction characteristics and wheel friction models have a significant place in vehicle dynamics.

In order to diagnose wheel slippage and motor fault, firstly, the model of the robot is needed. Therefore, the friction characteristic of the robot between the wheel and the ground should be known. There are various methods in the literature to model the friction characteristic in wheeled land vehicles. The wheel friction models in the literature are explained in the next sub-section.

3.1.3.1. Survey on Wheel Friction Models

Motion of the wheeled vehicles is accomplished by forces which are transmitted to the ground via wheels. Commonly in conventional car-like vehicle models, three forces are used: lateral force (F_{Lat}) which is parallel to the rotation axis of the wheel, longitudinal force (F_{Long}) which is perpendicular to the rotation axis and normal force (F_N) which is

perpendicular to the surface. Also, three moments acting at the contact area between the tire and ground are used, as depicted in Figure 3.4. Unlike the tires of car-like vehicles, the contact between the UTO wheel and the ground can be modelled as a point-type of contact. Therefore, the aligning torque is in negligible range. Also rolling resistance can be neglected for stone like hard materials but if floor material is soft and deformable by UTO wheels, rolling resistance should be considered. On the other hand, while the UTO wheel rolls, at some instances, there are two contact points since a UTO wheel has two rows of rollers. Consequently, the overturning moment cannot be neglected. Although, the lateral force acting on the wheel is considerably small since there are passive rollers that allow lateral motion of the UTO wheel, this force might change longitudinal friction force effects on the wheel. Therefore, longitudinal wheel friction models and effect of the lateral friction force of the omnidirectional wheel on longitudinal motion are considered in this dissertation.

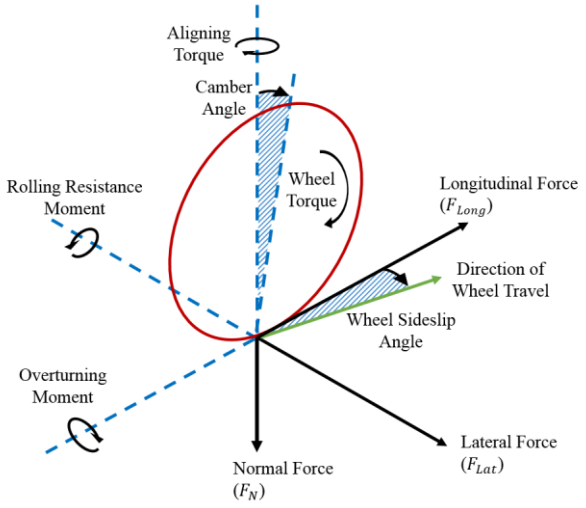

Figure 3.4. Forces and moments acting on the wheels (Source: Wong, 2001)

Longitudinal force is a function of normal force and normalized friction coefficient of the wheel as presented in Equation 1.

$$F_{Long} = \mu F_N \tag{3.16}$$

Longitudinal slip ratio (s) is a ratio between the absolute speed of the vehicle (V) and the speed of the vehicle calculated by using the wheel's angular speed ($r\omega$). Here, ω is the angular speed and r is the radius of the wheel. In the steady-state case, there is a

nonlinear relation between the normalized friction coefficient (μ) and longitudinal slip ratio as represented in Figure 3.5. Longitudinal slip ratio which varies depending on the brake and driving situation as presented in the equation below.

$$s = \begin{cases} s_b = \dfrac{r\omega}{V} - 1 \quad if \quad V > r\omega, \quad V \neq 0 \quad for\ braking \\ s_d = 1 - \dfrac{V}{r\omega} \quad if \quad V < r\omega, \quad \omega \neq 0 \quad for\ driving \end{cases} \tag{3.17}$$

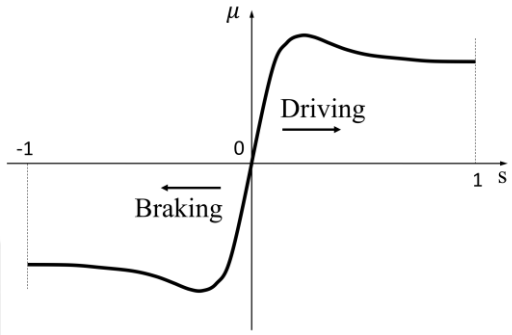

Figure 3.5. Tire friction coefficient characteristic curve (Source: Rajamani, 2006)

Additionally, the friction coefficient depends on some other factors like surface construction and contaminants, wheel parameters and tread wear, and vehicle speed. Harned et al. (1969) present effects of these factors on wheel brake force.

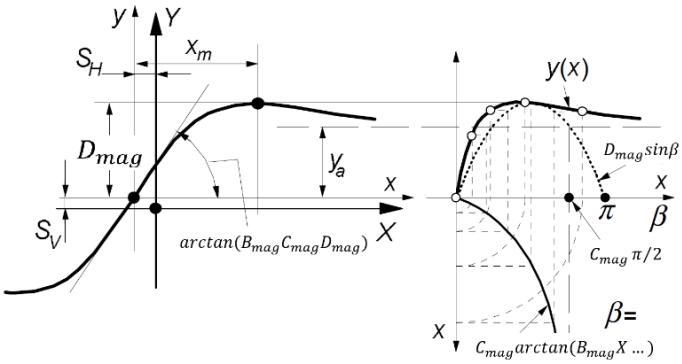

Figure 3.6. Magic formula parameters to produce steady-state wheel friction curve (Source: Pacejka, 2012)

In the literature, there are some semi-empirical models which represent steady-state behavior of the wheel friction. These models fit the friction coefficient characteristic curve to obtained empirical data. The most commonly used semi-empirical wheel friction

model is Pacejka's model which is called "Magic Formula" (Pacejka, 2012). Steady-state force and moment characteristics of the wheel is described by a number of parameters in this "Magic Formula" (Equation 3.18). The meaning of the parameters that appear in the "Magic Formula" are represented in Figure 3.6. This formula is the equation of a curve designed to fit the experimental data.

$$Y = D_{mag} sin\left[C_{mag} \arctan\left\{B_{mag}X - E_{mag}\left(B_{mag}X - \arctan B_{mag}X\right)\right\}\right] \quad (3.18)$$

In the magic formula, which is given in Equation 3.18, B_{mag} is the stiffness factor, C_{mag} is the shape factor, D_{mag} is peak value and E_{mag} is curvature factor. Steady-state behavior of the wheel according to different road conditions can be modeled by adjusting these parameters. Parameters of magic formula for some road conditions are listed in Table 3.1.

Table 3.1. Magic formula parameters for common road conditions

Road Condition	B_{mag}	C_{mag}	D_{mag}	E_{mag}
Dry Asphalt	10	1.9	1	0.97
Wet Asphalt	12	2.3	0.82	1
Snow	5	2	0.3	1
Ice	4	2	0.1	1

These kinds of models do not represent the transient behavior of the wheel. In fact, friction characteristic models are investigated based on two types of models, static friction models and dynamic friction models. Static friction models are used for studying steady-state behavior of the wheel friction. These models define the wheel friction characteristics when the linear speed of the vehicle and angular speed of the wheel are constant. Dynamic wheel friction models are used to model both transient and steady-state behavior of the wheel friction. The major difference of the dynamic models with respect to static friction models is that dynamic models are useful for modeling behavior of the wheel when the vehicle accelerates or decelerates. Hence, dynamic wheel friction models should be able to represent both steady-state and transient behavior of the wheel

(Canudas-de-Wit et al., 2003). Dynamic models for longitudinal wheel friction are separated from each other according to contact definition between wheel and ground:

(1) Lumped models assume the point-type of contact with the ground and

(2) Distributed models assume the contact patch is an area (Figure 3.7).

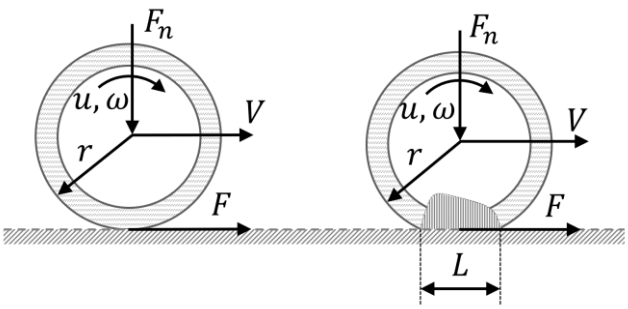

Figure 3.7. Wheel contact patch types: Left: Lumped, Right: Distributed (Source: Canudas-de-Wit et al., 2003)

Distributed wheel friction models are more realistic but relatively more complex models compared to the lumped models. In reality, all wheels have a force distribution area. Nevertheless, since this area is relatively smaller for solid wheels which are made by rubber-like materials, the point-type of contact is used in the model for these kinds of wheels. Distributed models are more suitable in modelling the friction of the tires of conventional car-like vehicles which have pressurized air inside. In UTO wheels, located at the outer circle of the wheel, there are passive rollers which are produced by a solid material. Consequently, the contact area of a UTO wheel is very small. Therefore, lumped friction models are more appropriate for modelling these wheels.

In the literature, there are various lumped friction models for representing longitudinal wheel friction. One of them is Clover's longitudinal wheel friction model (Clover et al., 1998). This model is based on the relation between the speed of the wheel and deformation of a virtual brush which is deformed by longitudinal force at a hypothetical point at the contact patch of the wheel. Another model is the Dahl model (otherwise known as solid friction model), which is designed for modelling friction in simulations of dynamic systems (Dahl, 1968). This model represents friction characteristics in terms of the strength properties of solid materials. According to the Dahl model, static friction and Coulomb friction characteristics resemble ultimate and rupture stresses which are defined in stress-strain diagrams. Canudas-de-Wit et al. (1999) proposed the LuGre model which is an extension of the Dahl model by including the

Stribeck friction effect. In order to receive similar results for both actual steady-state and transient friction characteristic of a wheel, the LuGre model used to model the longitudinal friction characteristics of the UTO wheel in this dissertation is represented as follows:

$$\dot{p} = V_r - \frac{\sigma_0 |V_r|}{g(V_r)} p \tag{3.19}$$

$$F = (\sigma_0 p + \sigma_1 \dot{p} + \sigma_2 V_r) F_N \tag{3.20}$$

$$g(V_r) = \mu_c + (\mu_s - \mu_c) e^{-|V_r/V_s|^{1/2}} \tag{3.21}$$

where, V_r is the relative speed, σ_0 and σ_1 are longitudinal lumped stiffness and damping of the wheel respectively, σ_2 is viscous relative damping, μ_c and μ_s are normalized coulomb and viscous friction coefficients respectively, p is internal relative state, V_s is stribeck relative speed, and F_N is normal force acting on the wheel.

3.1.3.2. Dynamic Equations of the Four-Wheeled Holonomic Mobile Robot

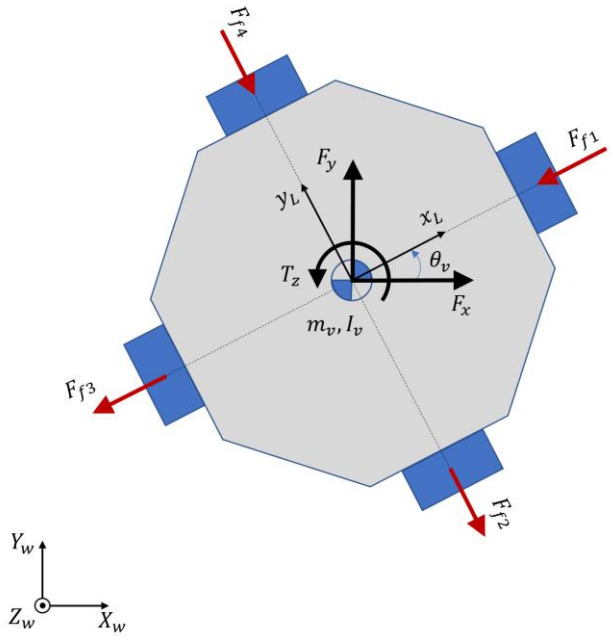

Figure 3.8. Generalized forces and torque of the mobile robot

In order to derive dynamic equations of the holonomic mobile robot Lagrange's method is implemented. The Lagrange equation and generalized coordinates are

$$\frac{\partial}{\partial t}\left(\frac{\partial L}{\partial \dot{q}}\right) - \frac{\partial L}{\partial q} + \frac{\partial D_{dis}}{\partial \dot{q}} = \boldsymbol{Q_K} \tag{3.22}$$

$$\boldsymbol{q} = \begin{bmatrix} x_w \\ y_w \\ \theta_v \end{bmatrix} \tag{3.23}$$

where, L is the Lagrange function, $\boldsymbol{q}$ is the column vector of generalized coordinates, D_{dis} is dissipation function and $\boldsymbol{Q_K}$ is k^{th} generalized force. The mobile robot assumed to be one rigid body which is moving on the plane (Figure 3.8), potential energy change can be assumed to be zero so the Lagrange function of the system is composed by the kinetic energy functions as follows:

$$L = \frac{1}{2} m_v V_v^2 + \frac{1}{2} I_v \dot{\theta}_v^2 \tag{3.24}$$

$$V_v^2 = \dot{x}_w^2 + \dot{y}_w^2 \tag{3.25}$$

$$L = \frac{1}{2} m_v \dot{x}_w^2 + \frac{1}{2} m_v \dot{y}_w^2 + \frac{1}{2} I_v \dot{\theta}_v^2 \tag{3.26}$$

where, V_v is speed of the mobile robot at X_w-Y_w plane. Here, the mass center of the mobile robot is assumed to be at the geometric center of the mobile robot. The virtual work of the system is

$$\delta \widetilde{W} = \tilde{Q}_{x_w} \delta_{x_w} + \tilde{Q}_{y_w} \delta_{y_w} + \tilde{Q}_{\theta_v} \delta_{\theta_v} = F_x \delta_x + F_y \delta_y + T_z \delta_{\theta_v} \tag{3.27}$$

Therefore, the column vector of generalized forces of the system is

$$\boldsymbol{Q_K} = \begin{bmatrix} \tilde{Q}_{x_W} \\ \tilde{Q}_{y_W} \\ \tilde{Q}_{\theta_v} \end{bmatrix} = \begin{bmatrix} F_x \\ F_y \\ T_z \end{bmatrix} \tag{3.28}$$

$$\frac{\partial}{\partial t}\left(\frac{\partial L}{\partial \dot{x}_W}\right) = m_v \ddot{x}_W \tag{3.29}$$

$$\frac{\partial}{\partial t}\left(\frac{\partial L}{\partial \dot{y}_W}\right) = m_v \ddot{y}_W \tag{3.30}$$

$$\frac{\partial}{\partial t}\left(\frac{\partial L}{\partial \dot{\theta}_v}\right) = I_v \ddot{\theta}_v \tag{3.31}$$

Although, lateral force of the omnidirectional wheels is relatively small according to conventional wheels thanks to passive rollers, the friction forces of the passive rollers should be expressed as dissipative forces of the system. These dissipative forces are assumed to be dry and viscous friction as:

$$F_{f1} = \frac{m_v g}{4}\left[\mu_{R\_dry} sign(\dot{x}_W cos\theta + \dot{y}_W sin\theta) + \mu_{R\_vis}(\dot{x}_W cos\theta + \dot{y}_W sin\theta)\right] \tag{3.32}$$

$$F_{f2} = \frac{m_v g}{4}(\mu_{R\_dry} sign(-\dot{x}_W sin\theta + \dot{y}_W cos\theta) + \mu_{R\_vis}(-\dot{x}_W sin\theta + \dot{y}_W cos\theta)] \tag{3.33}$$

$$F_{f3} = \frac{m_v g}{4}(\mu_{R\_dry} sign(\dot{x}_W cos\theta + \dot{y}_W sin\theta) + \mu_{R\_vis}(\dot{x}_W cos\theta + \dot{y}_W sin\theta)] \tag{3.34}$$

$$F_{f4} = \frac{m_v g}{4}(\mu_{R\_dry} sign(-\dot{x}_W sin\theta + \dot{y}_W cos\theta) + \mu_{R\_vis}(-\dot{x}_W sin\theta + \dot{y}_W cos\theta)] \tag{3.35}$$

Then the dynamic equations of the motion of the mobile robot are

$$m_v \ddot{x}_W + (F_{f1} + F_{f3})cos\theta_v - (F_{f2} + F_{f4})sin\theta_v = F_x \tag{3.36}$$

$$m_v \ddot{y}_W + (F_{f1} + F_{f3})sin\theta_v + (F_{f2} + F_{f4})cos\theta_v = F_y \tag{3.37}$$

$$I_v \ddot{\theta}_v = T_z \tag{3.38}$$

Also, these equations can be written in matrix form as follows:

$$\begin{bmatrix} m_v & 0 & 0 \\ 0 & m_v & 0 \\ 0 & 0 & I_v \end{bmatrix} \begin{bmatrix} \ddot{x}_W \\ \ddot{y}_W \\ \ddot{\theta}_v \end{bmatrix} + \begin{bmatrix} cos\theta_v & -sin\theta_v & 0 \\ sin\theta_v & cos\theta_v & 0 \\ 0 & 0 & 0 \end{bmatrix} \begin{bmatrix} F_{f1} + F_{f3} \\ F_{f2} + F_{f4} \\ 0 \end{bmatrix} = \begin{bmatrix} F_x \\ F_y \\ T_z \end{bmatrix} \quad (3.39)$$

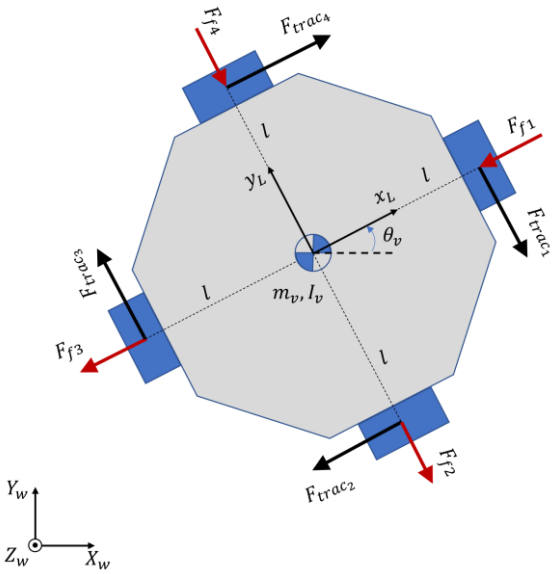

Figure 3.9. Applied traction forces by omnidirectional wheels

The motion of the mobile robot is provided with traction forces $\left(F_{trac_i}, i = 1,2,3,4\right)$ which are generated by the interaction between omnidirectional wheel and the ground (Figure 3.9). The traction forces can be found from this equation:

$$\begin{bmatrix} F_{trac_1} \\ F_{trac_2} \\ F_{trac_3} \\ F_{trac_4} \end{bmatrix} = J^T \begin{bmatrix} F_x \\ F_y \\ T_z \end{bmatrix} \quad (3.40)$$

This traction forces also can be written as LuGre friction model form as follows:

$$\dot{p}_i = V_{r_i} - \frac{\sigma_0 |V_{r_i}|}{g(V_{r_i})} p_i \quad (3.41)$$

$$F_{trac_i} = (\sigma_0 p_i + \sigma_1 \dot{p}_i + \sigma_2 V_{r_i}) F_N \quad (3.42)$$

$$g(V_{r_i}) = \mu_c + (\mu_s - \mu_c) e^{-|V_{r_i}/V_s|^{1/2}} \quad (3.43)$$

$$V_{r_i} = \dot{\varphi}_i r - V_i \qquad i = 1,2,3,4 \tag{3.44}$$

Up to here, dynamic equations of the mobile robot are derived according to world coordinate frame. Since the acceleration and speed measurements, which are necessary for implementing fault diagnosis, are acquired with respect to local coordinate frame, in the model-based fault diagnosis algorithm, dynamic equation of the mobile robot with respect to this frame is used. In local coordinates, dynamic equations of the mobile robot are

$$F_{trac_4} - F_{trac_2} - \left(F_{f1} + F_{f3}\right) = m_v \ddot{x}_L \tag{3.45}$$

$$F_{trac_3} - F_{trac_1} - \left(F_{f2} + F_{f4}\right) = m_v \ddot{y}_L \tag{3.46}$$

$$(-F_{trac_1} - F_{trac_2} - F_{trac_3} - F_{trac_4})l = I_v \ddot{\theta}_v \tag{3.47}$$

Linear velocities of the wheels on the corresponding the longitudinal axis can be calculated with these equations:

$$\vec{V}_i = \vec{V}_L + \vec{V}_{i/l} \tag{3.48}$$

$$\vec{V}_{i/L} = \vec{\omega} \times \vec{r}_{i/l} \tag{3.49}$$

From Equations 3.48 and 3.49 longitudinal speeds can be calculated as follows:

$$V_1 = -\dot{y}_L - \dot{\theta}_v l \tag{3.50}$$

$$V_2 = -\dot{x}_L - \dot{\theta}_v l \tag{3.51}$$

$$V_3 = \dot{y}_L - \dot{\theta}_v l \tag{3.52}$$

$$V_4 = \dot{x}_L - \dot{\theta}_v l \tag{3.53}$$

Then the dynamic equations of the mobile robot can be presented with eleven state variables. These state variables are

$$\{p_1, p_2, p_3, p_4, \dot{\varphi}_1, \dot{\varphi}_2, \dot{\varphi}_3, \dot{\varphi}_4, \dot{x}_L, \dot{y}_L, \dot{\theta}_v\} = \{x_1, x_2, x_3, x_4, x_5, x_6, x_7, x_8, x_9, x_{10}, x_{11}\} \quad (3.54)$$

The linear speed of the wheels can be re-written with these state variables as:

$$V_1 = -x_{10} - x_{11}l \quad (3.55)$$

$$V_2 = -x_9 - x_{11}l \quad (3.56)$$

$$V_3 = x_{10} - x_{11}l \quad (3.57)$$

$$V_4 = x_9 - x_{11}l \quad (3.58)$$

The relative speeds for each wheel are

$$V_{r_1} = x_5 r + x_{10} + x_{11}l \quad (3.59)$$

$$V_{r_2} = x_6 r + x_9 + x_{11}l \quad (3.60)$$

$$V_{r_3} = x_7 r - x_{10} + x_{11}l \quad (3.61)$$

$$V_{r_4} = x_8 r - x_9 + x_{11}l \quad (3.62)$$

Then the Equations 3.41 and 3.42 for each wheel becomes

$$\dot{x}_1 = x_5 r + x_{10} + x_{11}l - \frac{\sigma_0 |x_5 r + x_{10} + x_{11}l|}{g(x_5 r + x_{10} + x_{11}l)} x_1 \quad (3.63)$$

$$\dot{x}_2 = x_6 r + x_9 + x_{11}l - \frac{\sigma_0 |x_6 r + x_9 + x_{11}l|}{g(x_6 r + x_9 + x_{11}l)} x_2 \quad (3.64)$$

$$\dot{x}_3 = x_7 r - x_{10} + x_{11}l - \frac{\sigma_0 |x_7 r - x_{10} + x_{11}l|}{g(x_7 r - x_{10} + x_{11}l)} x_3 \quad (3.65)$$

$$\dot{x}_4 = x_8 r - x_9 + x_{11} l - \frac{\sigma_0 |x_8 r - x_9 + x_{11} l|}{g(x_8 r - x_9 + x_{11} l)} x_4 \tag{3.66}$$

$$F_{trac_1} = F_N \left(\sigma_0 x_1 \left(1 - \frac{\sigma_1 |x_5 r + x_{10} + x_{11} l|}{g(x_5 r + x_{10} + x_{11} l)} \right) + (x_5 r + x_{10} + x_{11} l)(\sigma_1 + \sigma_2) \right) \tag{3.67}$$

$$F_{trac_2} = F_N \left(\sigma_0 x_2 \left(1 - \frac{\sigma_1 |x_6 r + x_9 + x_{11} l|}{g(x_6 r + x_9 + x_{11} l)} \right) + (x_6 r + x_9 + x_{11} l)(\sigma_1 + \sigma_2) \right) \tag{3.68}$$

$$F_{trac_3} = F_N \left(\sigma_0 x_3 \left(1 - \frac{\sigma_1 |x_7 r - x_{10} + x_{11} l|}{g(x_7 r - x_{10} + x_{11} l)} \right) + (x_7 r - x_{10} + x_{11} l)(\sigma_1 + \sigma_2) \right) \tag{3.69}$$

$$F_{trac_4} = F_N \left(\sigma_0 x_4 \left(1 - \frac{\sigma_1 |x_8 r - x_9 + x_{11} l|}{g(x_8 r - x_9 + x_{11} l)} \right) + (x_8 r - x_9 + x_{11} l)(\sigma_1 + \sigma_2) \right) \tag{3.70}$$

Also, Equations 3.45, 3.46 and 3.47 are re-written as

$$\dot{x}_9 = \left[F_{trac_4} - F_{trac_2} - \left(F_{f1} + F_{f3} \right) \right] / m_v \tag{3.71}$$

$$\dot{x}_{10} = \left[F_{trac_3} - F_{trac_1} - \left(F_{f2} + F_{f4} \right) \right] / m_v \tag{3.72}$$

$$\dot{x}_{11} = \left[-F_{trac_1} - F_{trac_2} - F_{trac_3} - F_{trac_4} \right] l / I_v \tag{3.73}$$

In these Equations the friction forces due to passive rollers can be written as

$$F_{f1} = \frac{m_v g}{4}[\mu_{R\_dry} sign(x_9) + \mu_{R\_vis}(x_9)] \quad (3.74)$$

$$F_{f2} = \frac{m_v g}{4}[\mu_{R\_dry} sign(x_{10}) + \mu_{R\_vis}(x_{10})] \quad (3.75)$$

$$F_{f3} = \frac{m_v g}{4}[\mu_{R\_dry} sign(x_9) + \mu_{R\_vis}(x_9)] \quad (3.76)$$

$$F_{f4} = \frac{m_v g}{4}[\mu_{R\_dry} sign(x_{10}) + \mu_{R\_vis}(x_{10})] \quad (3.77)$$

Also, there is a relation between traction force and the applied torque by DC motor as

$$F_{trac_j} r + I_j \ddot{\varphi}_j = T_j \qquad j = 1,2,3,4 \quad (3.78)$$

where, T_j $(j = 1,2,3,4)$ torques are generated by gearhead DC motors, r is radius of the UTO wheel, I_j is moment of inertia of the UTO wheel calculated about the rotation axis of the corresponding actuator. The torque generated by a DC motor is related to the armature current, i, and motor's torque constant, K_t as

$$T_m = K_t i \quad (3.79)$$

The torque value applied by the output shaft of the motor (T_{m_shaft}) is calculated as

$$T_{m\_shaft} = K_t i - T_{nl} - J_r \frac{d\omega}{dt} \quad (3.80)$$

where T_{nl} is no load friction torque of the motor shaft, J_r is motor's rotor moment of inertia calculated about its rotation axis and $\frac{d\omega}{dt}$ is the angular acceleration of the motor shaft. The output torque of the gearbox (T_{gear_shaft}) is formulated as

$$T_{gear\_shaft} = (T_{m\_shaft} - J_g \frac{d\omega}{dt}) E G_r \quad (3.81)$$

where E is efficiency of the gearbox, G_r is the torque amplification ratio (inverse of the speed reduction ratio) of the gear and J_g is the moment of inertia of the gears lumped to the input shaft of the gear.

By using Equation 3.78 and the motor model, time derivative of the states x_5, x_6, x_7, and x_8 can be written as

$$\dot{x}_5 = \frac{1}{I_1 + (J_r + J_g)EG_r{}^2}\left[(K_t i_1 - T_{nl})EG_r - rF_{trac_1}\right] \tag{3.82}$$

$$\dot{x}_6 = \frac{1}{I_2 + (J_r + J_g)EG_r{}^2}\left[(K_t i_2 - T_{nl})EG_r - rF_{trac_2}\right] \tag{3.83}$$

$$\dot{x}_7 = \frac{1}{I_3 + (J_r + J_g)EG_r{}^2}\left[(K_t i_3 - T_{nl})EG_r - rF_{trac_3}\right] \tag{3.84}$$

$$\dot{x}_8 = \frac{1}{I_4 + (J_r + J_g)EG_r{}^2}\left[(K_t i_4 - T_{nl})EG_r - rF_{trac_4}\right] \tag{3.85}$$

3.1.4. The Mobile Robot's Hardware

In the mobile robot, each wheel is actuated with a 24 V DC motor. All motors used in the robot are Dunkermotoren brand G30.0 model DC motors with gearboxes that have 20.25:1 gear ratio. There is an Escon 50/5 model Maxon servo amplifier for each motor on the mobile robot. Motors are driven in current mode with these servo amplifiers. Since the motors used do not have a built-in encoder to measure angular speed, they are modified by connecting a magnetic encoder (AMS AS5040) to the back of the motors. These encoders can give 1024 pulses per revolution. However, since the data acquisition device used in the robot does not have a hardware to read the encoder information, the encoders are connected to the motor driver in order to get the angular speed information of the motors. The motor driver can calculate the angular speeds of the motors with the information it receives from the encoder and can provide this information as an analog value. In addition, there is an analog output port on the motor drives that allows the information about the amount of current used by the motors to be taken as an analog value. From this port, the current information used by the motors can be obtained in real

time during the robot's movement. The data acquisition system used in the mobile robot is shown in Figure 3.10.

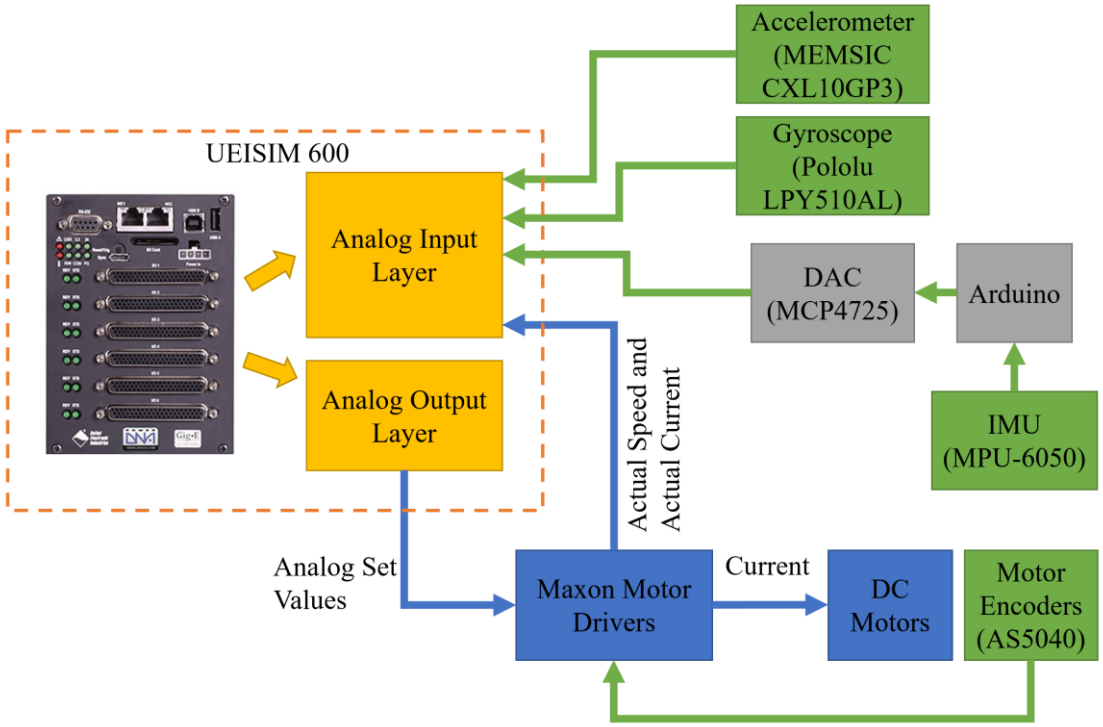

Figure 3.10. Data acquisition scheme of the mobile robot

In the mobile robot, UEISIM 600-1G model control cube is used as the system computer and data acquisition device. This device consists of multiple empty layers and can have different types of signal input and output thanks to the hardware attached to each layer. The device used in the mobile robot has two filled layers with a hardware, analog input layer and analog output layer. Thanks to the analog input layer, the angular speed and acceleration information of the robot taken from various analog sensors on the robot, and the wheel speeds and current information from the motor drivers are read. Thanks to the analog output layer on the device, the desired current information generated by the robot's control algorithm is given to the motor drivers as an analog set value.

The data acquisition device used in the mobile robot allows the models created in Matlab Simulink to be deployed with a Simulink coder. In this way, the control algorithm of the mobile robot fault, also diagnosis and recovery algorithms created in Matlab Simulink are run on the robot. UEISIM 600-1G has one Gigabit Ethernet port. Thanks to the Wi-Fi rooter connected to this port, the wireless communication of the robot with the main computer is provided. In this way, models created on the main computer can be

wirelessly deployed on the mobile robot. This system also allows the robot to be remotely controlled by the human operator with the user interface to be created on the main computer. The communication line between the mobile robot and the host computer is represented in Figure 3.11.

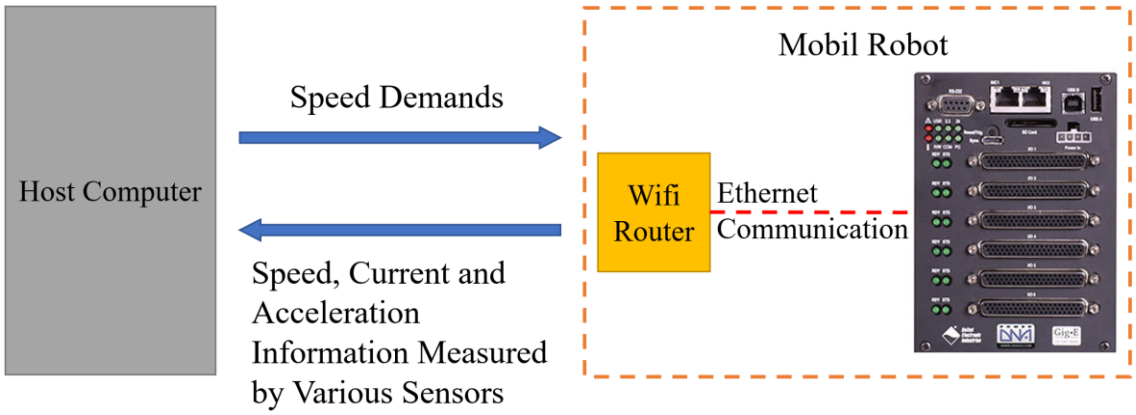

Figure 3.11. Communication line of the mobile robot

There are many sensors on the mobile robot as seen in Figure 3.10. The first of these sensors is the MEMSIC CXL10GP3 model analog accelerometer which has ±10g range. Thanks to this sensor placed under the robot's chassis, the accelerations of the mobile robot in both the x_L and y_L axes are measured. Another sensor used in the robot is the Pololu LPY510AL model gyroscope sensor with ±400°/s range. This sensor is used to measure the angular speed on the Z_w axis. In order to control the mobile robot according to the global coordinate frame, the orientation information (θ_v) of the robot is needed. In order to obtain the orientation information of the robot, an MPU-6050 model IMU, which contains a 3-axis gyroscope and a 3axis accelerometer, is used. The orientation of the robot can be calculated using the acceleration and angular speed information measured with this sensor. However, the sensor transmits this information with the I^2C communication protocol, whereas the data acquisition device used in the mobile robot does not have a hardware that supports this communication protocol. For this reason, the orientation of the robot is calculated in Arduino and this orientation information is transformed into an analog signal with the help of MCP4725 model digital to analog converter. The sensors used in the mobile robot are shown in Figure 3.12.

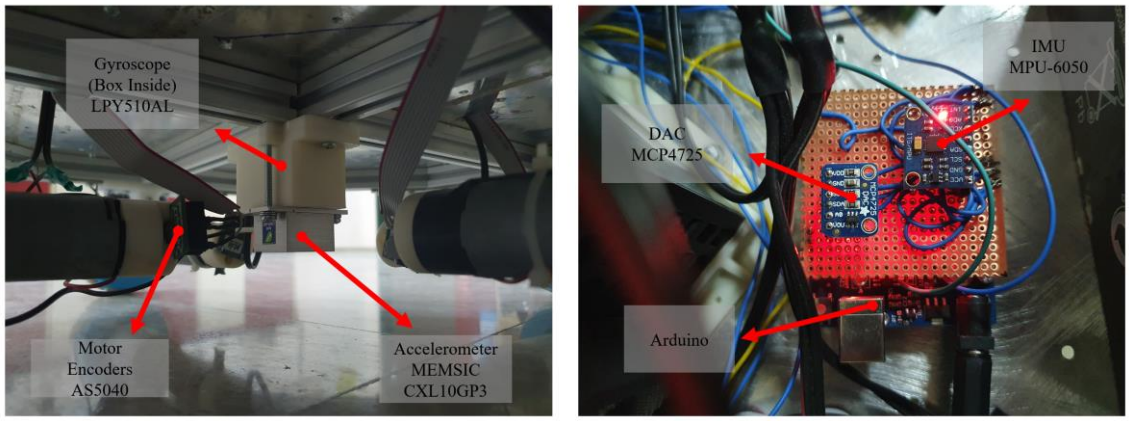

Figure 3.12. Sensors used in the mobile robot

Although the mobile robot is designed as a four-wheeled structure instead of three-wheeled, it provides an advantage in fault toleration, but it also brings along some complications. Although there is no need for a suspension system to ensure the contact of all wheels with the ground in the three-wheeled structure, problems such as loss of contact with the ground may occur in the case of four-wheel structures due to production tolerances. For this reason, the mobile robot needs a suspension system both to ensure the contact of all wheels with the ground and to minimize the impact of minor inconsistencies on the ground, even though the mobile robot is used on flat floors. For this reason, a suspension system is designed for the mobile robot, and the studies performed with the mobile robot are carried out with this system (Çelik, 2016). However, in the suspension system used during these studies, although the contact of each wheel with the ground at the same time is achieved, the parallelism between the wheel and the ground is disrupted because of both the stretching of the 3D printed parts used in this system due to the weight of the robot and the clearance in the joints (Figure 3.13). Since there are double rows of rollers in the omnidirectional wheels used in the mobile robot, if this parallelism is broken, problems such as some of the rollers not contacting the ground may occur. Therefore, the suspension system of the mobile robot is redesigned as a rigid structure to provide this parallelism, and the mobile robot is modified with the new suspension system (Figure 3.14). In the new suspension system, each wheel is mounted to the robot's chassis with a linear guide. On this linear guide, the wheel and motor parts can move up and down, while at the same time maintaining the parallelism of the wheel and the distances of the wheels to each other. In addition, there are two shock absorbers consisting of a spring and a damper in the suspension system.

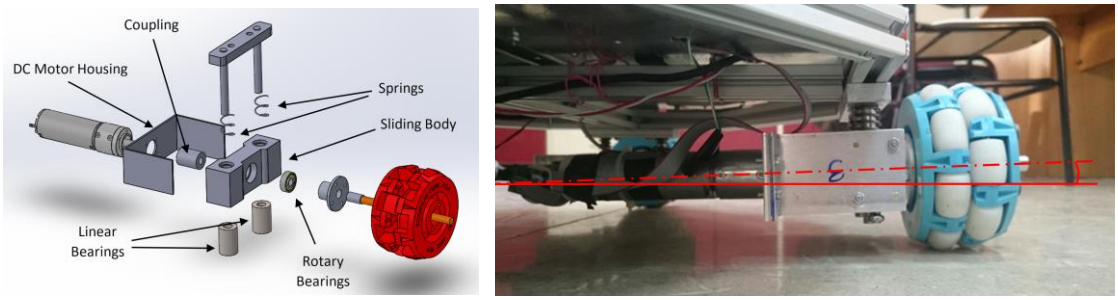

Figure 3.13. Previous version of the suspension system (Source: Çelik, 2016)

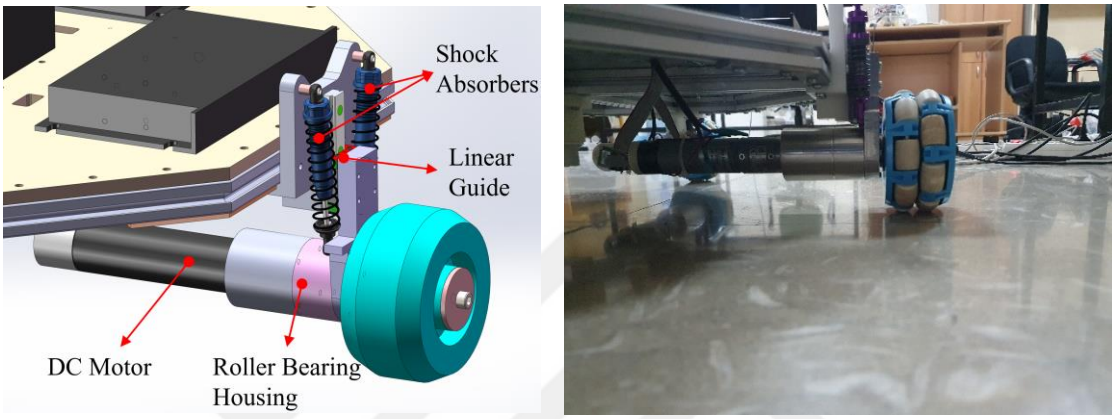

Figure 3.14. Modified version of the suspension system

3.2. Conclusions

In this chapter, firstly, the hardware and structural properties of the mobile robot used in the dissertation are explained and then kinematic equations of the robot are given. Also, the methods applied in the control of the robot are explained. A dynamic model of the robot is needed to be used in studies of diagnosing the faults that occur in the robot. The literature review on the methods used to model the friction between the wheel and the ground is also presented in this chapter. The entire dynamic model of the robot created with the longitudinal friction model chosen for modeling the friction characteristic is given. In the dynamic model of the robot, although the parameters of the DC motor used in the robot are known from the motor manufacturer's catalogue, the parameters of the friction model that characterize the friction between the UTO wheel used in the robot and the ground on which the robot moves are unknown. Studies for identifying these parameters are explained in Chapter 4.

CHAPTER 4

IDENTIFICATION AND VALIDATION OF THE PARAMETERS OF THE FRICTION MODEL FOR THE UTO WHEEL

Although some of the wheels are specially designed for use in WMRs, some wheels used in WMRs are actually designed for different purposes. As a result of this, for each type of wheel used in WMRs, there are different friction characteristics. Also, there are no standards which describe WMR wheel specifications and there are no model parameters which characterize friction of mobile robot wheels in the literature. Therefore, LuGre model parameters which are described in the previous chapter should be estimated to model longitudinal wheel friction between the UTO wheel and floor material of the robot's workspace.

(a) (b)

Figure 4.1. Industrial wheel force/moment measurement equipment; a) Flat belt tire test machine b) Vehicle measurement system (Source: A&D Technology, 2020)

There are industrial test machines to measure steady-state and dynamic force/moment acting on car-like vehicle tires (Figure 4.1a). However, the size and shape of wheels used in mobile robots are quite different, so these commercial test machines are not suitable for testing UTO wheels. There are also specially built sensors that are used in car tire tests to measure forces and moments on wheels of a vehicle (Figure 4.1b). Identification of the model parameters is not possible with experiments on an actual

mobile robot which uses a UTO wheel since it is not easy to find these kinds of special sensors designed for measuring forces on HMR wheels. Therefore, an experimental test setup, which contains one-quarter of an HMR, is designed and built for this purpose.

In the following sections, firstly, the hardware properties and dynamic equations of the test setup are given. Then, studies performed with this test setup for identifying LuGre model parameters for three different floor types are described. Verification of the obtained parameters is carried out by using the dynamic model of the test setup. The obtained results in verification tests are given in section 4.3. UTO wheels have less resistance on the lateral axis than normal wheels due to their special structure. However, this resistance can affect the motion on the longitudinal axis. Studies on the effect of lateral motion on the longitudinal axis are also described and the results of the tests performed to demonstrate this effect are explained in this chapter. Last section of the chapter includes conclusion and discussions about studies explained in this chapter.

4.1. Experimental Test Setup

The experimental test setup shown in Figure 4.2 includes one-quarter of the HMR with a single UTO wheel. This one-quarter part of the mobile robot includes Links 2 to 9 which are represented in schematics of the test setup presented in Figure 4.3. The one-quarter part is mounted on a linear rail on a gantry which is constructed with aluminum sigma profile (Link 11). The linear rail is composed of two small wheels rolling on the aluminum sigma profile; hence, the prismatic joint structure is not form-closed. This makes the tilt of the vehicle free and the effects of the overturning moment are observable in this test setup. The gantry is responsible for both balancing the one-quarter part and guiding the motion of the part along the direction which is perpendicular to the rotation axis of the UTO wheel. The gantry is mounted on two rails, which are located on the ground, at points E and F with two prismatic joints. Motion on these two rails provides translation of the gantry and the one-quarter part along the axis which is parallel to the rotation axis of the wheel. The dimensions of the test setup are $a = 1000$ mm, $b = 2100$ mm and $c = 250$ mm. The workspace of the one-quarter part inside of the test setup is 600 mm by 1700 mm.

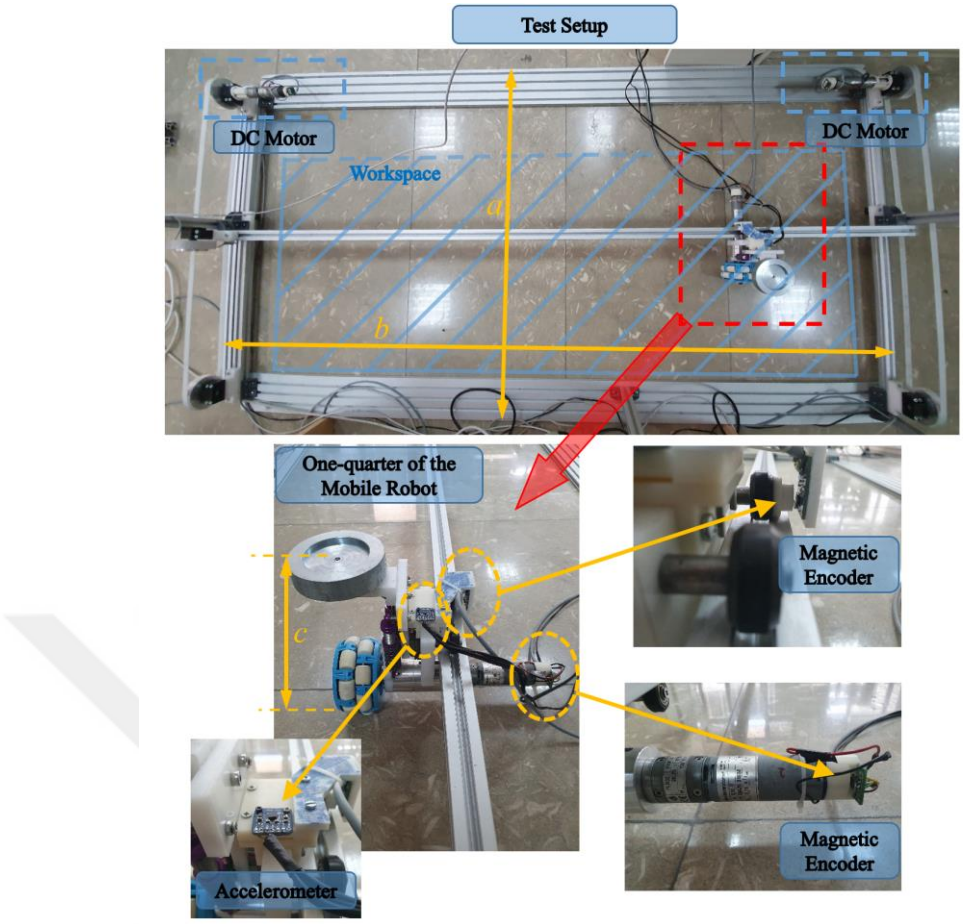

Figure 4.2. Experimental test setup

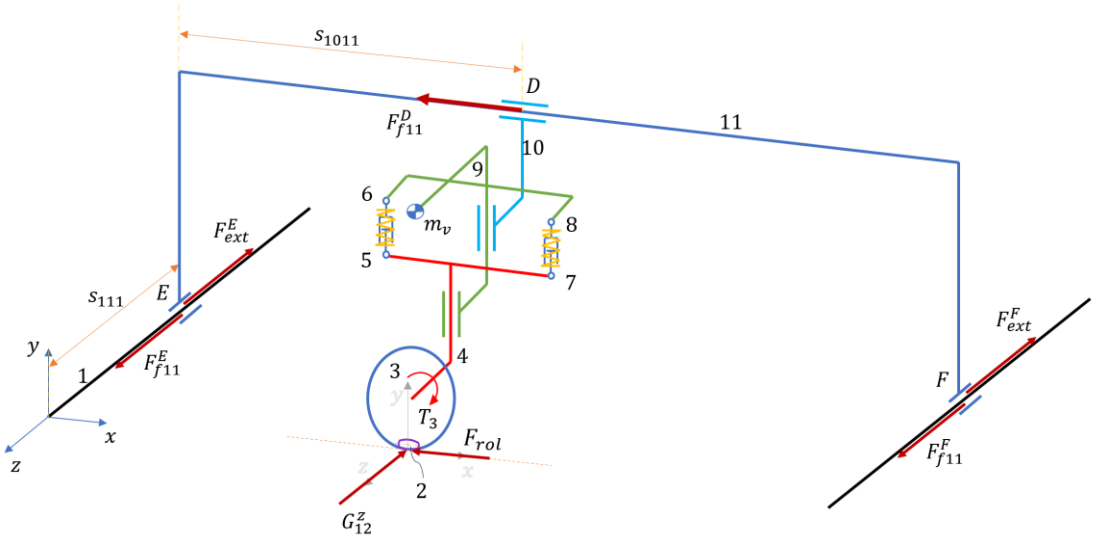

Figure 4.3. Schematic representation of the test setup

One of three DC motors used in this setup is coupled to the shaft of the UTO wheel and the other two are connected to belt-pulley systems that are responsible for

linear motion of the wheel in two translational axes of the surface. All motors used in the test setup are Dunkermotoren brand G30.0 model DC motors with gearboxes which have 20.25:1 gear ratio. These motors are driven with three Maxon ADS 50/10 4-Q-DC Servo amplifiers. The motor mounted on the UTO wheel is driven in current mode in order to obtain the actuation torque and traction force relation. Humusoft MF624 model data acquisition card, which is attached to the PCI port of a desktop PC, is used to collect the information from the various sensors and to provide input to the servo amplifiers.

In order to estimate wheel traction force with the LuGre model, relative speed, which is the difference between the speed of the vehicle calculated by using the wheel speed ($\dot{\theta}_3$) and the absolute speed of the vehicle ($\dot{s}_{1011}$), should be known. The wheel speed is measured by using an AMS AS5045B model magnetic encoder, which is mounted on the rear end of the motor. The same type of magnetic encoder, which is mounted on one of the linear guide wheels, is used for measuring the absolute speed of the vehicle. The acceleration of the vehicle is measured by an analog accelerometer (Adafruit ADXL335). The total mass of the one quarter part is adjusted with additional mass (m_v) to represent a quarter of the HMR's mass. The test-model is created with desktop real-time blocks in Matlab Simulink environment.

4.1.1. The Dynamic Equations of The Test Setup

In order to derive dynamic equations of motion for the test setup, Lagrange's method is implemented (Equation 3.19). The dynamics along the y-axis is neglected as it does not affect the longitudinal dynamics of the wheel on the horizontal plane. For test setup, generalized coordinates are identified as

$$\boldsymbol{q} = \begin{bmatrix} s_{111} \\ \theta_3 \end{bmatrix} \tag{4.1}$$

Since the potential energy change can be assumed to be zero, the Lagrange function of the system is composed by the kinetic energy functions as follows:

$$L = \frac{1}{2} m_T V_T^2 + \frac{1}{2} m_{11} V_{11}^2 + \frac{1}{2} I_3 \dot{\theta}_3^2 \tag{4.2}$$

where V_T is speed of the total mass (m_T) of links 2 to 10 and attached additional mass (m_v) in order to simulate mass of the mobile robot, m_{11} is mass of link 11, V_{11} is speed of link 11, I_3 is moment of inertia of link 3, which is the UTO wheel, calculated about the UTO wheel's rotation axis and ω_3 is angular speed of link 3.

$$m_T = \sum_{i=2}^{10} m_i + m_v \tag{4.3}$$

$$V_T^2 = \dot{s}_{1011}^2 + \dot{s}_{111}^2 \tag{4.4}$$

$$V_{11} = \dot{s}_{111} \tag{4.5}$$

Consequently, the Lagrange function is re-written as follows:

$$L = \frac{1}{2}(m_T + m_{11})\dot{s}_{111}^2 + \frac{1}{2}m_T\dot{s}_{1011}^2 + \frac{1}{2}I_3\dot{\theta}_3^2 \tag{4.6}$$

For no-slip condition, the relation between the angular speed of link 3 and speed of the total mass along the x-direction is determined as

$$\dot{s}_{1011} = r\dot{\theta}_3 \tag{4.7}$$

Total virtual work of the system is formulated in order to find generalized forces in Equation 4.8. Here, F_{ext}^E and F_{ext}^F are the forces acting on the system along the z-direction to move the wheel along the z-direction in order to observe the effects of the side motion enable by the passive rollers.

$$\delta\widetilde{W} = \tilde{Q}_\theta\delta_\theta + \tilde{Q}_z\delta_z = (F_{ext}^E + F_{ext}^F)\delta_z + T_3\delta_\theta \tag{4.8}$$

Therefore, the column vector of generalized forces of the system is

$$\boldsymbol{Q} = \begin{bmatrix} \tilde{Q}_z \\ \tilde{Q}_\theta \end{bmatrix} = \begin{bmatrix} F_{ext}^E + F_{ext}^F \\ T_3 \end{bmatrix} \tag{4.9}$$

There are also five dissipative forces acting on the system due to the friction forces at the prismatic joint at points D, E and F (F_{f11}^{D} , F_{f11}^{E}, F_{f11}^{F}) and friction forces due to the passive rollers (G_{12}^{z}) and rolling resistance force of the wheel (F_{rol}). These friction forces are assumed to be results of dry and viscous friction between the surfaces. The dry and viscous friction coefficients at points E and F are denoted with μ_{E_dry} and μ_{F_dry}, and μ_{E_vis} and μ_{F_vis}, respectively. Accordingly, friction forces at points E and F and rolling resistance force are calculated as follows:

$$F_{f11}^{E} = [\mu_{E\_dry} sgn(\dot{s}_{111}) + \mu_{E\_vis}\, \dot{s}_{111}] G_{111}^{Ey} \tag{4.10}$$

$$F_{f11}^{F} = [\mu_{F\_dry} sgn(\dot{s}_{111}) + \mu_{F\_vis}\, \dot{s}_{111}] G_{111}^{Fy} \tag{4.11}$$

$$F_{rol} = \mu_{rol} m_T g \tag{4.12}$$

where G_{111}^{Ey} and G_{111}^{Fy} are normal forces acting on the point E and F, μ_{rol} is coefficient of the rolling resistance.

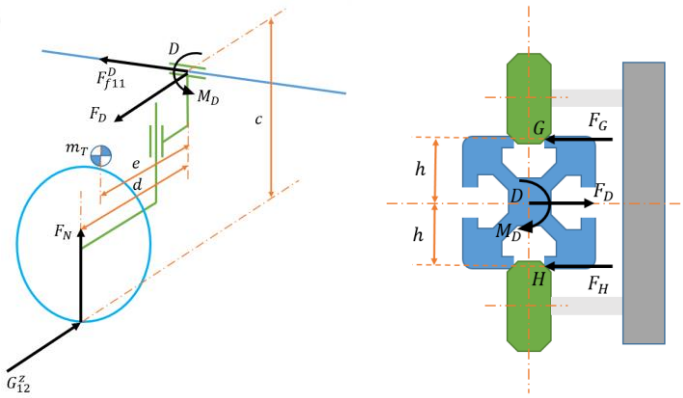

(a) (b)

Figure 4.4. (a) Simplified representation of the one quarter part (b) Forces/moments acting at point D

Friction force at point D is affected by the abovementioned lateral friction force. In Figure 4.4, a specific direction of lateral motion is investigated. Accordingly, if the lateral motion is in the other direction, the forces and moment identified as F_D, F_G, F_H and M_D on Figure 4.4b will be in the opposite directions. Friction force at point D is

calculated by using the dry and viscous friction coefficients denoted by μ_{D_dry} and μ_{D_vis} as

$$M_D = F_N d - m_T g\, e - G_{12}^z c \tag{4.13}$$

$$F_D = -G_{12}^z \tag{4.14}$$

$$F_H = \frac{F_D h - M_D}{2h}, \qquad F_G = \frac{F_D h + M_D}{2h} \tag{4.15}$$

$$F_{f11}^D = [\mu_{D\_dry} sgn(\dot{s}_{1011}) + \mu_{D\_vis}\, \dot{s}_{1011}](|F_H| + |F_G|) \tag{4.16}$$

where F_N is the total normal force acting on the wheel.

On the UTO wheel, there are two rows of passive rollers. During the lateral motion of the UTO wheel, lateral friction force is generated while these rollers roll about their own axes. Due to the lateral friction force, the normal force on the ground applied by the rollers change. This situation is represented in Figure 4.5. Each component of the quarter model is weighed and then this information is used in the assembly of the test setup in computer-aided-design (CAD) software. The mass center location is calculated by using this assembly file in CAD environment.

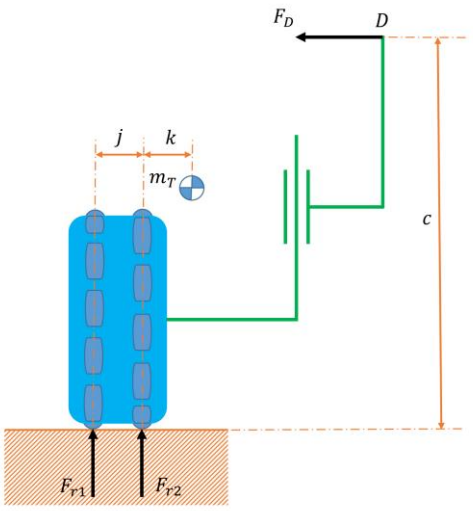

Figure 4.5. Reaction forces acting on passive rollers

The reaction forces from the ground to the rollers are calculated in Equation 4.17. The assumption made here is that both rollers touch the ground at all times.

$$F_{r1} = \frac{-m_T g k + F_D c}{j}\ , \qquad F_{r2} = \frac{m_T g (k+j) - F_D c}{j} \tag{4.17}$$

Accordingly, lateral friction force on the wheel is determined from Equation 4.14. Here, the dry and viscous friction coefficients between the rollers and the surface are denoted by μ_{R_dry} and μ_{D_vis}, respectively.

$$G_{12}^{z} = -F_D = [\mu_{R\_dry} sgn(\dot{s}_{111}) + \mu_{R\_vis}\, \dot{s}_{111}](|F_{r1}| + |F_{r2}|) \tag{4.18}$$

Using Equations 4.13 and 4.15, F_D is calculated and substituted in Equation 4.17 to calculate F_{r1} and F_{r2}. Consequently, the normal force acting on the wheel is determined by $F_N = F_{r1} + F_{r2}$. Based on the abovementioned equations for the Lagrange function and dissipative forces, equations of motion are determined as presented in Equations 4.19 and 4.20.

$$(m_T + m_{11})\ddot{s}_{111} + G_{12}^{z} + F_{f11}^{E} + F_{f11}^{F} = F_{ext}^{E} + F_{ext}^{F} \tag{4.19}$$

$$(m_T r^2 + I_3)\ddot{\theta}_3 + (F_{f11}^{D} + F_{rol})r = T_3 \tag{4.20}$$

Then, the equations of motion of the test setup can be written in the matrix form as follows:

$$\boldsymbol{M(q)}\ddot{\boldsymbol{q}} + \boldsymbol{F}(\dot{\boldsymbol{q}}) = \boldsymbol{B(q)\tau} \tag{4.21}$$

$$\underbrace{\begin{bmatrix}(m_T + m_{11}) & 0\\ 0 & (m_T r^2 + I_3)\end{bmatrix}}_{\boldsymbol{M(q)}} \underbrace{\begin{bmatrix}\ddot{s}_{111}\\ \ddot{\theta}_3\end{bmatrix}}_{\ddot{\boldsymbol{q}}} + \underbrace{\begin{bmatrix}G_{12}^{z} + F_{f11}^{E} + F_{f11}^{F}\\ (F_{f11}^{D} + F_{rol})r\end{bmatrix}}_{\boldsymbol{F}(\dot{\boldsymbol{q}})} = \underbrace{\begin{bmatrix}1 & 0\\ 0 & 1\end{bmatrix}}_{\boldsymbol{B(q)=I}} \underbrace{\begin{bmatrix}F_{ext}^{E} + F_{ext}^{F}\\ T_3\end{bmatrix}}_{\boldsymbol{\tau}} \tag{4.22}$$

Up to now, the equations of motion are found assuming that there is no slip between the wheel and the ground. In fact, the friction force between the wheel and the ground varies according to the amount of wheel slippage as described in the previous sections. The state of slip between the wheel and the ground can be expressed as follows:

$$\dot{s}_{1011} = r\dot{\theta}_3 \rightarrow No\ slip\ case \tag{4.23}$$

$$\dot{s}_{1011} \neq r\dot{\theta}_3 \rightarrow Slip\ case \tag{4.24}$$

For slip case Equation 4.20 becomes

$$m_T\ddot{s}_{1011}r + I_3\ddot{\theta}_3 + (F_{f11}^D + F_{rol})r = T_3 \tag{4.25}$$

Traction force, F_{trac}, applied to the vehicle is calculated as follows:

$$F_{trac} = m_T\ddot{s}_{1011} + (F_{f11}^D + F_{rol}) \tag{4.26}$$

This force is related to the friction force between wheel and ground. Traction force can be also estimated with the LuGre model whose formulation is given in the previous section in Equation 3.17. Then, the longitudinal dynamic model is represented with the following four state variables:

$$x_{12} = \dot{s}_{1011} \tag{4.27}$$

$$x_{13} = \dot{\theta}_3 \tag{4.28}$$

$$x_{14} = p \tag{4.29}$$

$$x_{15} = \dot{s}_{111} \tag{4.30}$$

Equations 3.16 and 3.17 can be rewritten with by using these states that are defined above as follows:

$$V_r = x_{13}r - x_{12} \tag{4.31}$$

$$\dot{x}_{14} = (x_{13}r - x_{12}) - \frac{\sigma_0|x_{13}r - x_{12}|}{g(x_{13}r - x_{12})}x_{14} \tag{4.32}$$

$$F_{trac} = F_N \left[\sigma_0 x_{14} + \sigma_1 \left[(x_{13}r - x_{12}) - \frac{\sigma_0 |x_{13}r - x_{12}|}{g(x_{13}r - x_{12})} x_{14}\right] + \sigma_2 (x_{13}r - x_{12})\right] \tag{4.33}$$

$$F_{trac} = F_N \left[\sigma_0 x_{14} \left[1 - \frac{\sigma_1 |x_{13}r - x_{12}|}{g(x_{13}r - x_{12})}\right] + (x_{13}r - x_{12})[\sigma_1 + \sigma_2]\right] \tag{4.34}$$

Also, the first two state equations based on Equations 4.25 and 4.26 are written as

$$\dot{x}_{12} = \frac{1}{m_T}[F_{trac} - (F_{f11}^D + F_{rol})] \tag{4.35}$$

$$\dot{x}_{13} = \frac{1}{I_3}[T_3 - rF_{trac}] \tag{4.36}$$

The normal forces acting on the bearings change due to lateral motion of the wheel and this is represented in Figure 4.6.

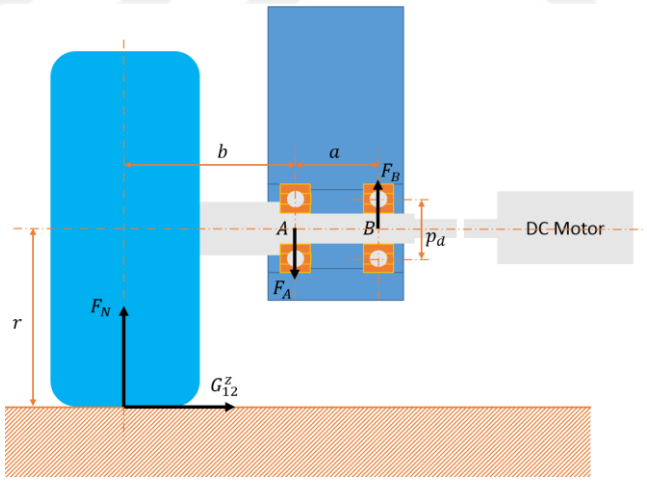

Figure 4.6. Reaction forces acting on the bearings of the wheel shaft

Total friction torque acting the bearings is calculated by determining the normal forces acting on the bearings (F_A and F_B).

$$F_A = \frac{F_N(a+b) - G_{12}^z r}{a} \quad , \qquad F_B = \frac{F_N b - G_{12}^z r}{a} \tag{4.37}$$

$$T_{friction} = [\mu_{bearing\_dry} sign(x_{13}) + \mu_{bearing\_vis}\, x_{13}](|F_A| + |F_B|)(\frac{p_d}{2}) \tag{4.38}$$

where $\mu_{bearing\_dry}$ and $\mu_{bearing\_vis}$ are the dry and viscous friction coefficients of the bearing and p_d is pitch diameter of bearing. The effective applied torque on the wheel is calculated as

$$T_3 = T_{gear\_shaft} - T_{friction} \tag{4.39}$$

Consequently, Equation 4.36 is re-written as

$$\dot{x}_{13} = \frac{1}{I_3 + (J_r + J_g)EG_r{}^2}\left[(K_t i - T_{nl})EG_r - T_{friction} - rF_{trac}\right] \tag{4.40}$$

4.2. Parameter Identification

Parameter identification tests are carried out on three different floor types. The surfaces where the tests are carried out are natural stone (studies explained in following chapters are carried out on this floor type), PVC floor covering, and paperboard surface placed on the floor. In order to identify the LuGre wheel friction model parameters for these floor types, the relation between the relative speed and the traction force must be measured. Tests are carried out by supplying 24 VDC and different levels of constant current to the DC motor that actuates UTO wheel. In the first test, the current value supplied to the motor is set to a constant 0,15 A. A larger constant current value is used for the next tests, and is raised up to the maximum constant current value of 1,5 A. The traction force corresponding to each test is calculated by applying Equation 4.26. The total mass of the one-quarter part of the test setup and the friction force of the linear guide are measured to be $m_T = 3{,}9593$ kg and $0{,}304\ N$, respectively. The identification test procedure is set respectively for each floor types as follows:

1. Supply the selected constant current to the DC motor mounted to the UTO wheel within the predefined working range.

2. Calculate the speed of the one-quarter model by using the measurements from the encoders at the rear side of the DC motor
3. Calculate the speed of the one-quarter model (actual speed) by using the measurements from the encoders located on the measurements wheel moving on the linear guide.
4. Calculate the relative speed by the difference between the two calculations of one-quarter model's speed.
5. Measure acceleration of the one-quarter model with an accelerometer mounted on it.
6. Compute traction force by applying Equation 4.26 and using the measured acceleration at step 5.
7. Move the one-quarter model back to the starting position, set the constant current value to an increased value and repeat the test.
8. After the tests are completed, supply the measured relative speed data for each test to the LuGre model as inputs and calculate the corresponding traction forces.
9. Identify optimal model parameters that satisfy each test traction force result and LuGre model traction force outputs.

The whole test procedure is represented in Figure 4.7.

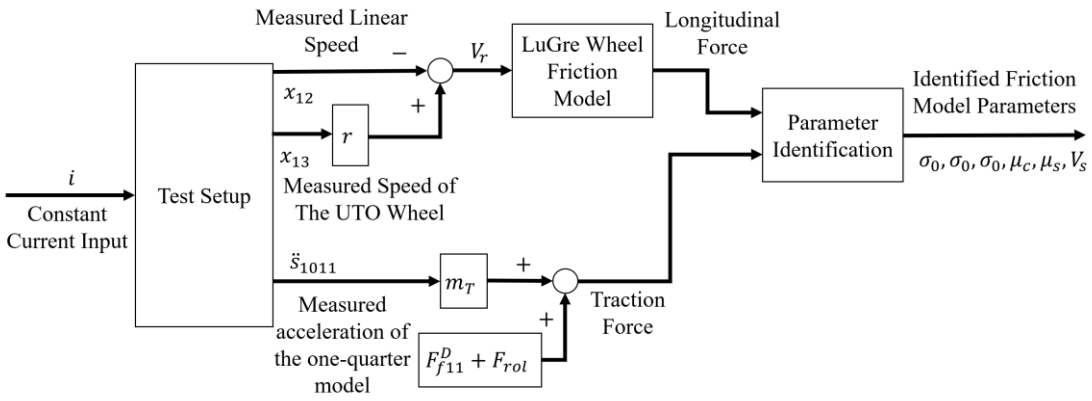

Figure 4.7. Parameter identification test procedure

4.2.1. Parameter Identification Tests

A Humusoft data acquisition card (DAQ) is used for data acquisition with a sampling frequency of 1 kHz during the identification and validation tests. The calculated speeds of the one-quarter model from the encoder data received from the linear guide ($\dot{s}_{1011}$) and from the encoder attached to the rear end of the motor driving the UTO wheel

($r\dot{\theta}_3$) (UTO wheel speed), during one of the tests on natural stone floor carried out with 1,35 A constant current, are represented in Figure 4.8.

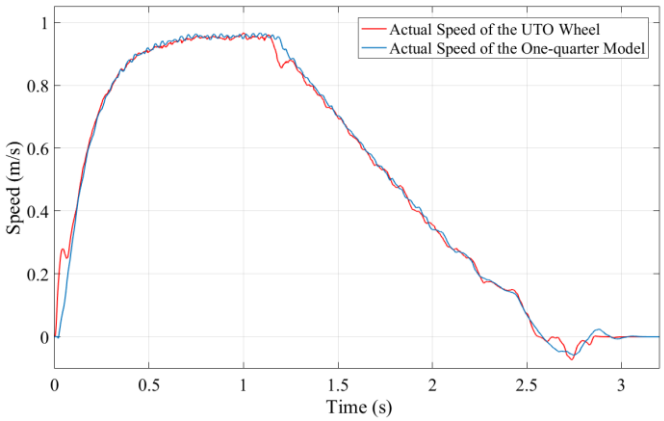

Figure 4.8. Calculated speed of the one-quarter model from UTO wheel and the actual speed during the test on natural stone floor carried out with 1,35 A constant current

As it is observed from Figure 4.8, when constant current is applied to the motor which actuates the UTO wheel, the one-quarter model accelerates until the motor reaches the maximum speed. After the motor reaches the maximum speed at 0,7 s of the test, one-quarter model continues the motion at this constant maximum speed until a safe location after which the one-quarter model can come to a full stop within the test setup's workspace. While the speed calculated from the UTO wheel is larger than the actual speed of the one-quarter model during the acceleration regime of the motion, these values are close to each other during the constant speed portion of the motion. The relative speed which shows the difference between the speed calculated from the UTO wheel and the actual speed of the one-quarter model during experiments on different floor types are presented in Figure 4.9.

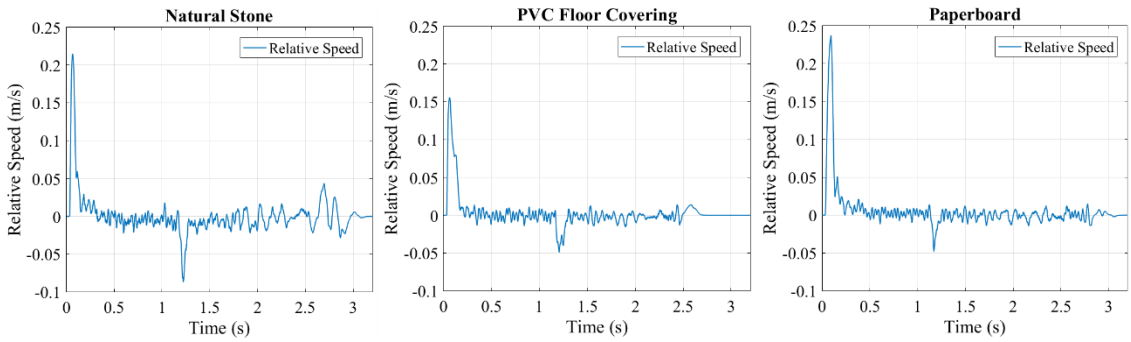

Figure 4.9. The relative speed during the tests on three floor types carried out with 1,35A

After collecting data for each test with different constant current values, the parameters of the LuGre wheel friction model that produce the most similar results for each test's traction forces are identified. In this identification routine, the measured relative speed values are given as the input in the constructed Matlab Simulink model and then, estimated traction forces, which are the output of the LuGre model, are compared with the actual traction forces. The Matlab parameter estimation toolbox is used during this identification of the LuGre model parameters process. The identified LuGre friction model parameters for three floor types are presented in Table 4.1. The measured and the estimated traction force values with the identified parameters for 1,35 A constant current test is shown in Figure 4.10.

Table 4.1. Identified LuGre friction model parameters

Floor Type	Identified Parameters					
	$V_s\ (m/s)$	μ_c	μ_s	$\sigma_0\ (m^{-1})$	$\sigma_1\ (s/m)$	$\sigma_2\ (s/m)$
Natural Stone	1,9643	0,12	0,1205	11,451	0,0809	2,4490
PVC Floor Covering	0,0044	0,12	0,15	49,933	0,3720	2,8084
Paperboard	0,8170	0,04	0,07	54,724	0,6146	2,4028

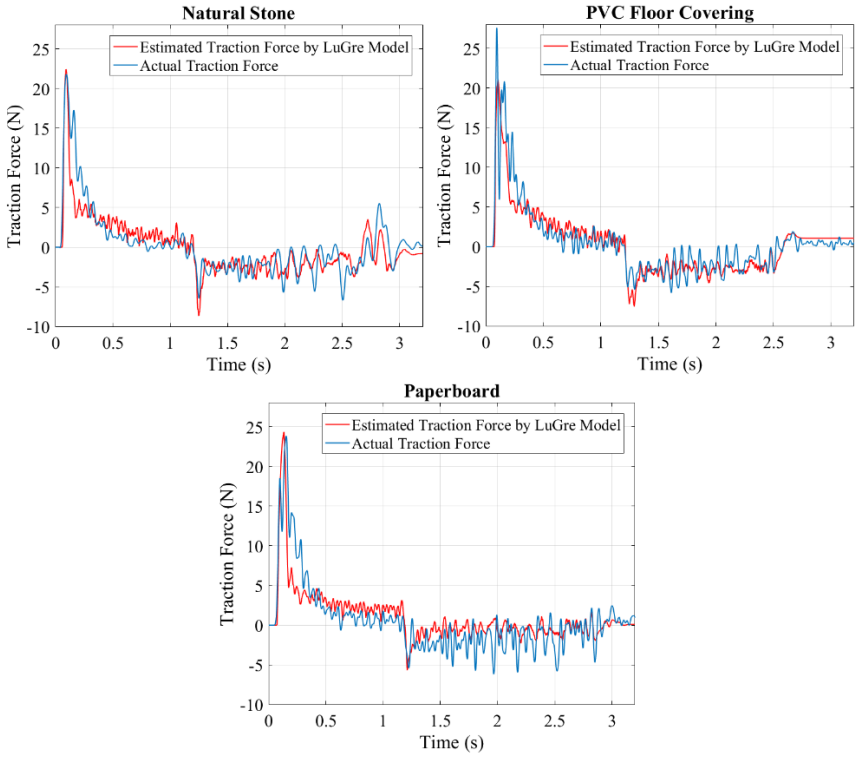

Figure 4.10. Estimated and actual traction forces during the tests with 1,35 A

4.3. Model Validation

After identifying model parameters, validation procedure of the longitudinal system dynamics given in the Section 4.1.1 is carried out. In the validation tests, motor is driven with a constant current value from starting position until the safe position from which the system can come to a full stop within the limits of the workspace. During the total motion, the actual current value is measured via the motor driver's current monitor output port. Throughout the test, the constant current value is set to 1,35 A. As it is depicted in Figure 4.11, the current value is the constant 1,35 A while the one-quarter model is in acceleration regime. After the one-quarter model reaches the maximum speed, the current supplied to the motor slowly decreases until a constant current value. This constant current value produces the necessary amount of torque to compensate for the friction force at the linear guide and no-load torque value of the motor, which is due to motor's internal friction and armature resistance and rolling resistance of the wheel. As it seen in the Figure 4.11, when the measured current value is about 0,2 A at constant speed part of the motion for natural stone and paperboard floor types, this value is higher than the 0,2 A for PVC floor covering for due to higher rolling resistance.

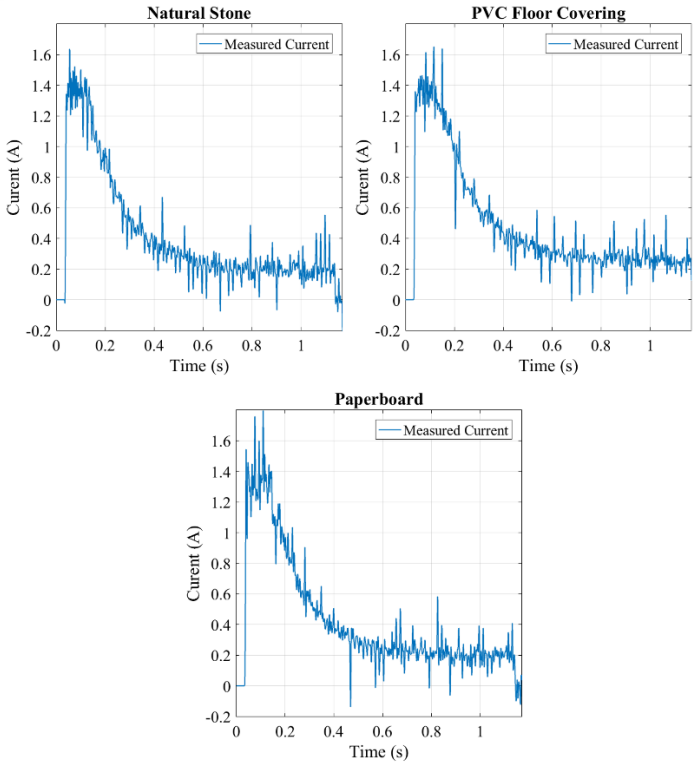

Figure 4.11. Measured current via the current monitor output of the motor driver during the validation tests with a constant set value of 1,35 A

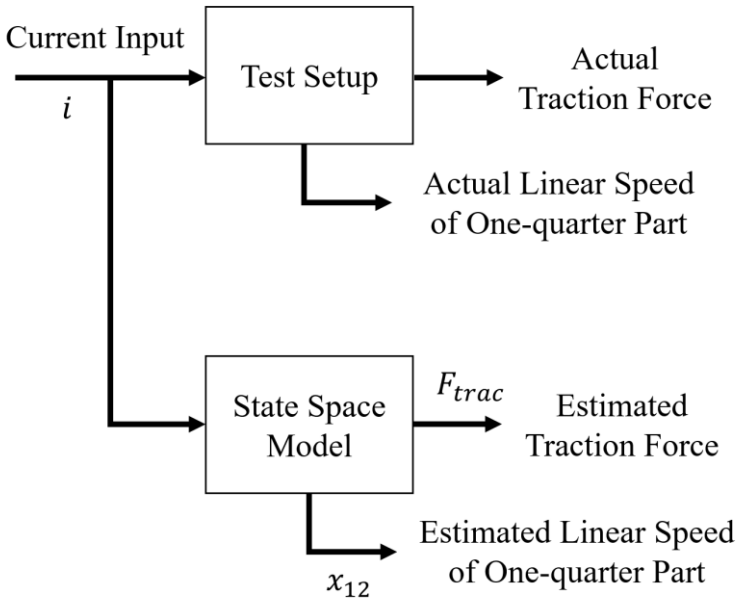

Figure 4.12. Model validation test procedure

These measured current values for each test are supplied as inputs to the model with the identified parameters, whose equations are given in Section 4.1.1, and the estimated traction forces and estimated speed for the one-quarter model for each test data are the outputs of the state space model (Figure 4.12). These estimated traction forces and speed of the one-quarter model are compared with the measured actual values. These comparisons for each test with different constant current values are presented in Figure 4.13a and 4.13b for traction forces and speeds, respectively. In addition, the tests are repeated with changing the weight of the one-quarter model of the mobile robot and the estimated and measured speed values are compared. Root-mean-square (RMS) values of the errors between measured and estimated speeds of the one-quarter model for each test result is presented in Table 4.2.

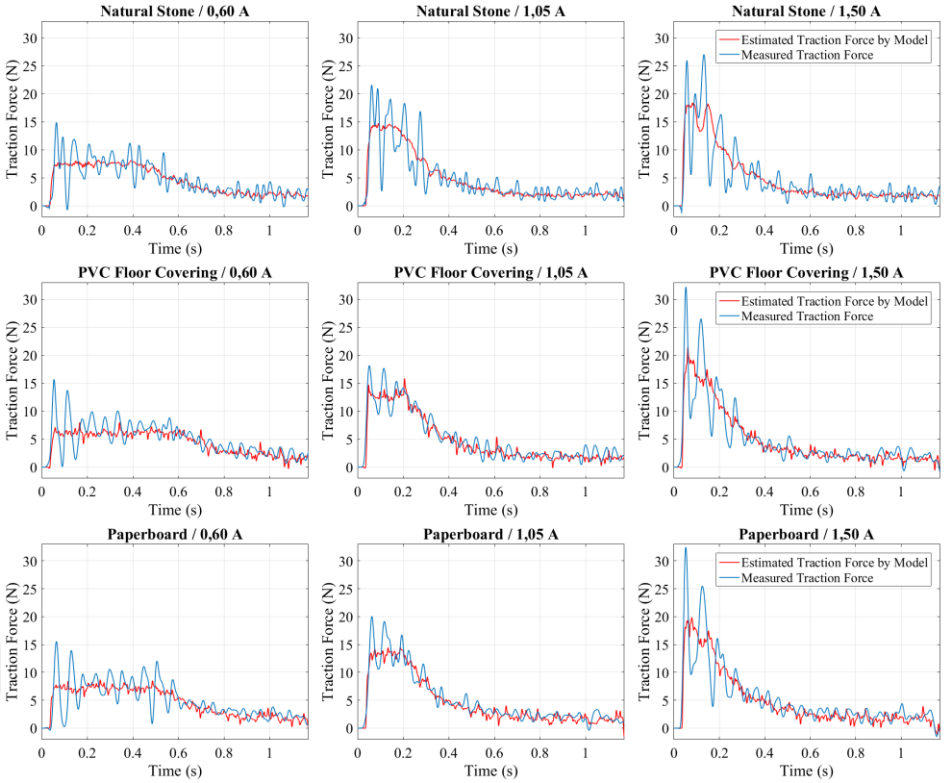

(a)

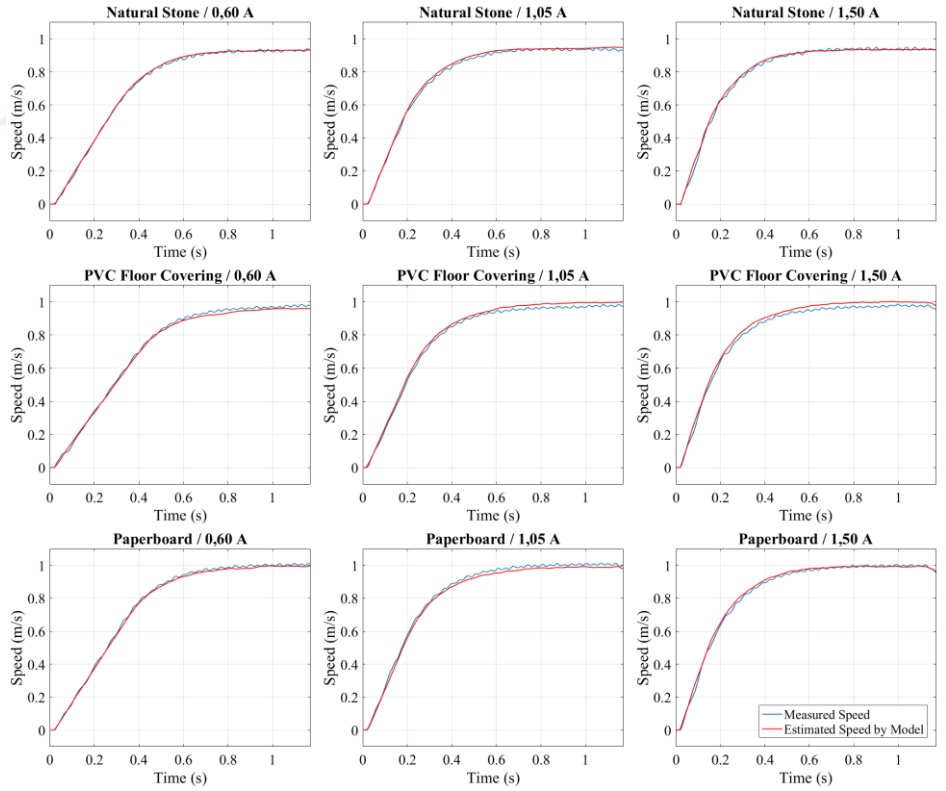

(b)

Figure 4.13. Model validation test results; a) The comparison between measured and estimated traction forces b) The comparison between estimated and actual linear speed of the one-quarter model

Table 4.2. RMS values of the errors between measured and estimated speeds of the one-quarter model for each test

Mass of the One-quarter Model (kg)	Current Input (A)	Floor Types		
		Natural Stone	PVC Floor Covering	Paperboard
		RMS Values of Error (m/s)	RMS Values of Error (m/s)	RMS Values of Error (m/s)
3,9593	0,45	0,024	0,037	0,035
	0,60	0,016	0,035	0,006
	0,75	0,007	0,014	0,010
	0,90	0,010	0,008	0,021
	1,05	0,012	0,019	0,017
	1,20	0,016	0,009	0,011
	1,35	0,020	0,017	0,021
	1,50	0,012	0,024	0,013
2,9593	0,45	0,022	0,036	0,031
	0,60	0,015	0,013	0,012
	0,75	0,013	0,011	0,011
	0,90	0,008	0,010	0,008
	1,05	0,022	0,011	0,015
	1,20	0,016	0,010	0,014
	1,35	0,025	0,014	0,012
	1,50	0,029	0,015	0,025
1,9593	0,45	0,035	0,019	0,022
	0,60	0,015	0,016	0,022
	0,75	0,029	0,016	0,019
	0,90	0,018	0,018	0,022
	1,05	0,028	0,026	0,025
	1,20	0,038	0,033	0,025
	1,35	0,037	0,031	0,032
	1,50	0,025	0,029	0,015

4.4. Effect of the Lateral Friction Force on Longitudinal Motion of the One-quarter of the Mobile Robot

In this part of the dissertation, the effect of lateral friction force of the wheel on longitudinal motion of the one-quarter of the mobile robot is investigated. Longitudinal motion of the one-quarter of the robot in the test setup is influenced by various frictional forces. Although the lateral friction forces of the UTO wheels are very small compared to the conventional wheels, ignoring the friction in lateral direction degrades the accuracy of the longitudinal model. In order to observe this situation, tests are carried out at different lateral speeds with the test setup on natural stone floor. To observe the effect of lateral motion, while the one-quarter model is in the initial position, constant lateral speed demand is given to the linear guide. As soon as the linear guide reaches a constant lateral speed, the one-quarter model is driven with constant current from the initial position to the safe position. The test is repeated with various lateral speed and current values.

Initially, the lateral friction force is assumed to be zero in the model and the actual speed of the one-quarter model is compared with the estimated speed. Test results achieved with different lateral speeds are represented in Figure 4.14. The RMS values of the error between the actual and the estimated longitudinal speed of the one-quarter of the robot for tests achieved with different lateral speeds are given in Table 4.3.

Table 4.3. RMS values of the errors between measured and estimated speeds of the one-quarter model for each test achieved with zero lateral friction force assumption

Lateral motion at positive direction				
	0,6 A	0,9 A	1,2 A	1,5 A
0,2 m/s	0,045	0,029	0,033	0,024
0,35 m/s	0,068	0,054	0,040	0,027
0,5 m/s	0,075	0,038	0,033	0,029
0,65 m/s	0,072	0,040	0,028	0,033
Lateral motion in negative direction				
	0,6 A	0,9 A	1,2 A	1,5 A
-0,2 m/s	0,023	0,055	0,051	0,078
-0,35 m/s	0,047	0,066	0,079	0,102
-0,5 m/s	0,034	0,064	0,067	0,093
-0,65 m/s	0,057	0,082	0,088	0,103

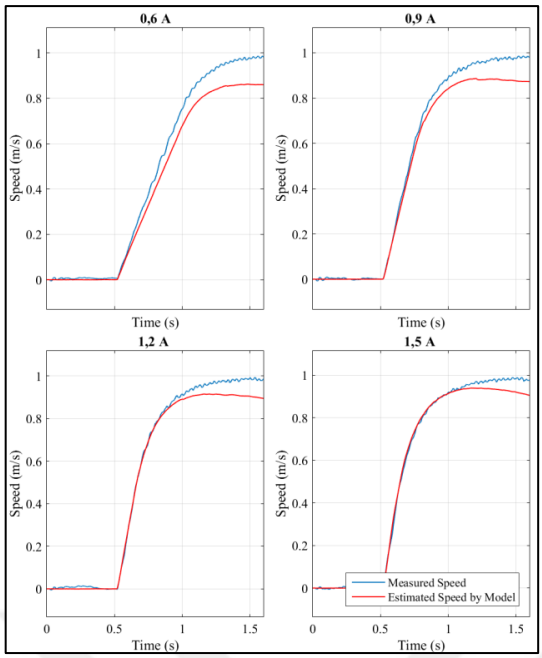

(a)

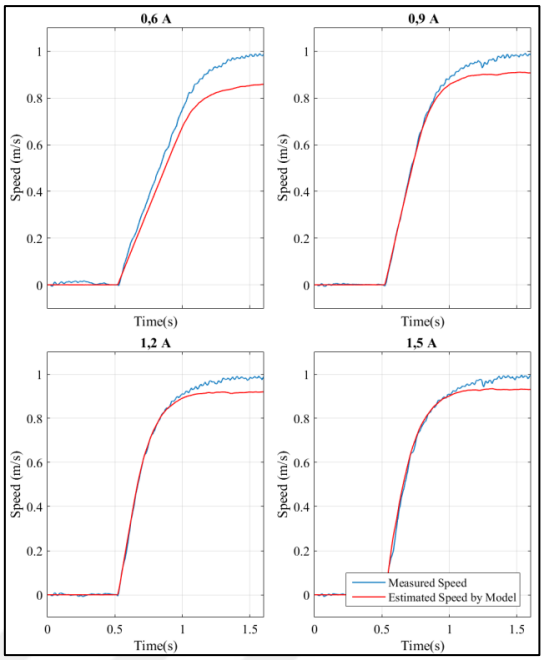

(b)

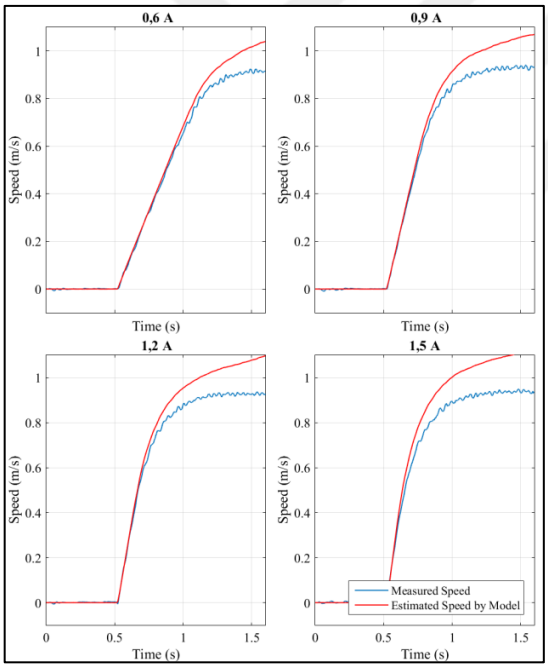

(c)

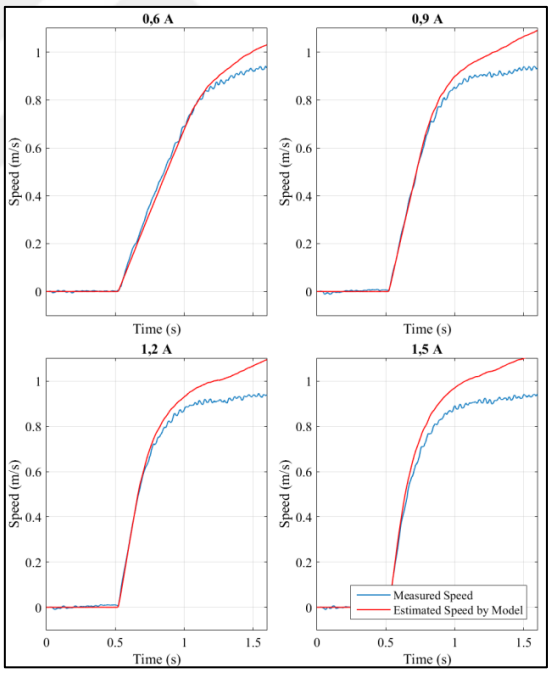

(d)

Figure 4.14. Test results for zero lateral friction force assumption a) 0.35 m/s lateral speed b) 0.50 m/s lateral speed c) -0.35 m/s lateral speed d) -0.50 m/s lateral speed

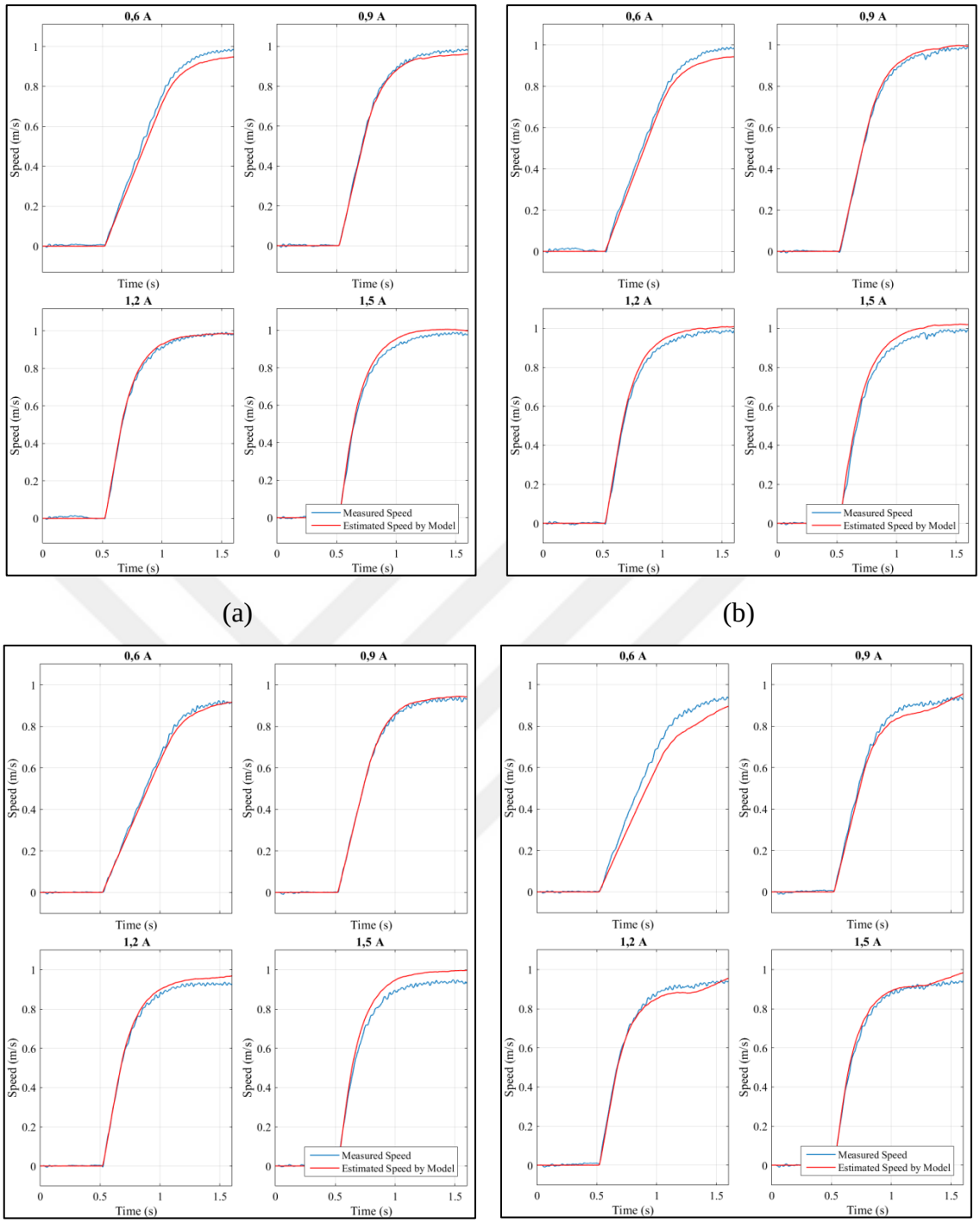

Figure 4.15. Test results for considering lateral friction force in the model a) 0.35 m/s lateral speed b) 0.50 m/s lateral speed c) -0.35 m/s lateral speed d) -0.50 m/s lateral speed

As a next step, the effect of lateral friction force caused by lateral motion is considered in the model. Same test results that are analyzed against the no lateral friction model are used in this analysis. The results with the lateral friction model are represented

in Figure 4.15. The RMS values of the errors between the actual and the estimated speed values obtained as a result of this analysis with lateral friction model are given in Table 4.4.

Table 4.4. RMS values of the errors between measured and estimated speeds of the one-quarter model for each test achieved with considering effect of the lateral friction force in the model

Lateral motion in positive direction				
	0,6 A	0,9 A	1,2 A	1,5 A
0,2 m/s	0,021	0,005	0,008	0,009
0,35 m/s	0,029	0,013	0,011	0,024
0,5 m/s	0,029	0,014	0,022	0,032
0,65 m/s	0,024	0,019	0,029	0,028
Lateral motion in negative direction				
	0,6 A	0,9 A	1,2 A	1,5 A
-0,2 m/s	0,018	0,018	0,015	0,041
-0,35 m/s	0,016	0,008	0,020	0,044
-0,5 m/s	0,059	0,023	0,019	0,018
-0,65 m/s	0,047	0,018	0,014	0,024

4.5. Conclusion

The friction characteristic between the wheel and the ground is an important part of vehicle dynamics studies, which is also important for improving the control of mobile robots. In this chapter, the longitudinal friction characteristic of a UTO wheel is studied via implementing the LuGre friction model. As a result of the tests, LuGre friction model parameters are identified between the omnidirectional wheel and three different floor types. Also, full system model validation tests with the identified wheel friction model parameters are carried out in which the measured traction forces and the actual speeds of the one-quarter model are compared with estimated speeds and traction forces.

During the validation tests, the current inputs to the motor coupled to the UTO are obtained via the driver of the motor. Consequently, the output signals received from the model are noisy due to the use of these measured currents as input signals. Relatively higher magnitude oscillations are observed in the measured results for the traction forces, due to vibrations during the motion of this special structured UTO. The main reason for

this vibration is the transition of contact from one free roller on the UTO wheel to the next free roller. Irrespective of these oscillations, when plots in Figure 4.13a are investigated, it can be concluded that the estimated traction forces closely match the measured ones. Additionally, the measured speed of the one-quarter model is compared with the speed output received from the model. The difference between them is considerably low, which means that a reliable model for the one-quarter model with the UTO wheel is obtained. Therefore, the obtained friction model can be used for traction control and odometry studies.

Omnidirectional wheels have passive rollers that allow motion in the parallel direction to the rotation axis of the wheel which significantly reduce the lateral frictional force. However, this friction force must still be considered in the vehicle model. In the literature, the effect of lateral friction force in the dynamic equations of such robots is considered only in two-dimensional space as the robot moves on the plane. However, when the effect of the lateral friction force is examined from a three-dimensional perspective, this force changes the reaction forces and moments on the various rotating and moving elements. Ignoring the effect of lateral friction force on these elements causes inaccuracies in the friction model of the robot. In the last part of this chapter, the effect of lateral friction force on the motion of the robot is investigated. According to the test results, when the lateral friction force is ignored in the model, it is observed that estimated speed by model does not match with measured speed and the error between the estimated speed and actual speed increased drastically. However, when the lateral friction is considered in the longitudinal model, the error in speed estimation is considerably reduced.

UTO wheels used in mobile robots have single-row or double-row rollers. UTO wheel which has double-row rollers are used in this dissertation. It is not possible to talk about a continuous friction characteristic on the longitudinal axis due to the spaced structure of the rollers in UTO wheels using single-row rollers. Therefore, it is not possible to model longitudinal friction in UTO wheels which has single-row rollers. Urethane material which is the material used in the UTO wheel in the dissertation, or rubber, which has very close friction characteristics, are used in the rollers of UTO wheels suitable for use in mobile robots. These two materials are also used in many robot wheels. Another factor that specifies the friction between the wheel and the ground is the type of the ground. The identified parameters of the LuGre friction model for three different floor types can be used for modelling the friction between a mobile robot wheel using the same

material and ground types which are similar structure with this dissertation. In order to model the friction between mobile robot wheels using different types of materials and ground types which have different structures, the model parameters should be identified with the procedure described in section 4.4.

In traction control systems used in wheeled terrestrial vehicles, it is aimed to estimate the amount of slippage between the wheel and the ground and to reduce the speed of the slipped wheel to ensure the holding onto the ground. Thanks to the model obtained in this dissertation, the wheel slippage can be estimated for usual cases. In the case of an unusual slippage on one of the wheels in the mobile robot, the estimated value differs from the actual value. In this way, a control algorithm similar to the traction control systems used in terrestrial vehicles can be applied in mobile robots, by determining the unusual wheel slippage.

The dynamic model of the mobile robot is completed with the identified model parameters. In Chapter 5, the studies to diagnose the wheel slippage and performance degradation in the motor are presented.

CHAPTER 5

FAULT DIAGNOSIS

As explained in Chapter 2, mobile robots have several system components. Faults that may arise from these components may cause deterioration in the robot's behavior or completely disrupt the operation of the robot. For this reason, tolerating the faults that occur in the robot is important in mobile robots that carry out critical tasks. In this dissertation, tolerating the faults that may occur during the task of the holonomic mobile robot is studied. One of the faults encountered in previous studies with the HMR, which causes control difficulties in the robot, is the slippage on the wheel. Therefore, wheel slippage and performance degradation that may occur in motors, are hardware faults that are issued in this dissertation. As mentioned before, because of the redundant structure of the robot, the robot can tolerate these faults by adjusting a suitable control strategy according to the fault type without interrupting the motion. Therefore, it is important to determine which fault occurrs in the mobile robot to implement the suitable fault recovery strategy. The diagnosis of these faults is aimed to be accomplished with the model-based fault diagnosis algorithm, as described in the previous chapters. Therefore, the dynamic model of the robot needed for model-based fault diagnosis is developed by identifying the parameters of the wheel friction model. Fault diagnosis studies performed using the dynamic model of the HMR are described in this chapter. Initially, fault diagnosis studies are carried out in the test setup consisting of a one-quarter model of the robot. After this process, the diagnosis method applied is implemented in the mobile robot. In the next section, fault diagnosis studies performed with the test setup are explained, and in the following section, the studies carried out with the HMR to diagnose the wheel slippage and the performance degradation in the motors that actuate the wheels are explained.

5.2. Fault Diagnosis Studies with the Test Setup

In the studies of diagnosing the wheel slippage, it is necessary to provide the appropriate condition for the wheel to slip. This may be made possible by the use of an external factor, such as oil-like materials contamination on the wheel or substances

entering between the wheel and the ground, which causes degradation of the friction characteristics between the wheel and the ground. Therefore, in the tests carried out with the test setup, the wheel slippage is generated by placing a nylon material between the wheel and the ground which causes a distorting effect on the friction characteristics of the wheel. Because of the distorted friction characteristics, the resultant wheel slippage appears to be more than the slippage in a normal state and the wheel produces less traction force.

To make a model-based fault diagnosis using the dynamic model of the test setup described in the previous section, firstly, the residual signal should be generated, then, the threshold value should be determined according to variation of the residual signal in the case where there is no fault in the system. The wheel slippage is directly correlated with the wheel speed and wheel speed information is the easiest state to measure on the mobile robot via the encoders attached to the wheel shafts. Therefore, the residual signal can be generated by calculating the difference between the measured wheel speed and the estimated wheel speed, which is found with the help of the dynamic model. Since the friction characteristic model is developed for the friction between the UTO wheel and the ground with natural stone, in the case of wheel slippage due to the nylon sheet inserted between the wheel and the ground, the estimated wheel speed, and the measured wheel speed do not match. Hence, thanks to the generated residual signal to be generated in this way, wheel slippage can be detected. Accordingly, the residual signal is generated by the following equation:

$$r_1 = x_{13} - \hat{x}_{13} \tag{5.1}$$

Although the measured wheel speed and estimated wheel speed values are expected to be equal when there is no fault in the system, in the actual case, there is a difference between these two values due to uncertainty and disturbances in the system. Therefore, the threshold values for the residual signal should be determined in the fault-free condition. In this way, if the residual signal exceeds the specified threshold value, it is possible to detect the presence of a fault in the system. To determine the threshold value in the fault-free case, similar to the tests described in the previous section, constant current values are supplied to the motor connected to the wheel and the estimated and measured wheel speeds are compared. The comparison of these speed values is given in Figure 5.1 for various constant current values.

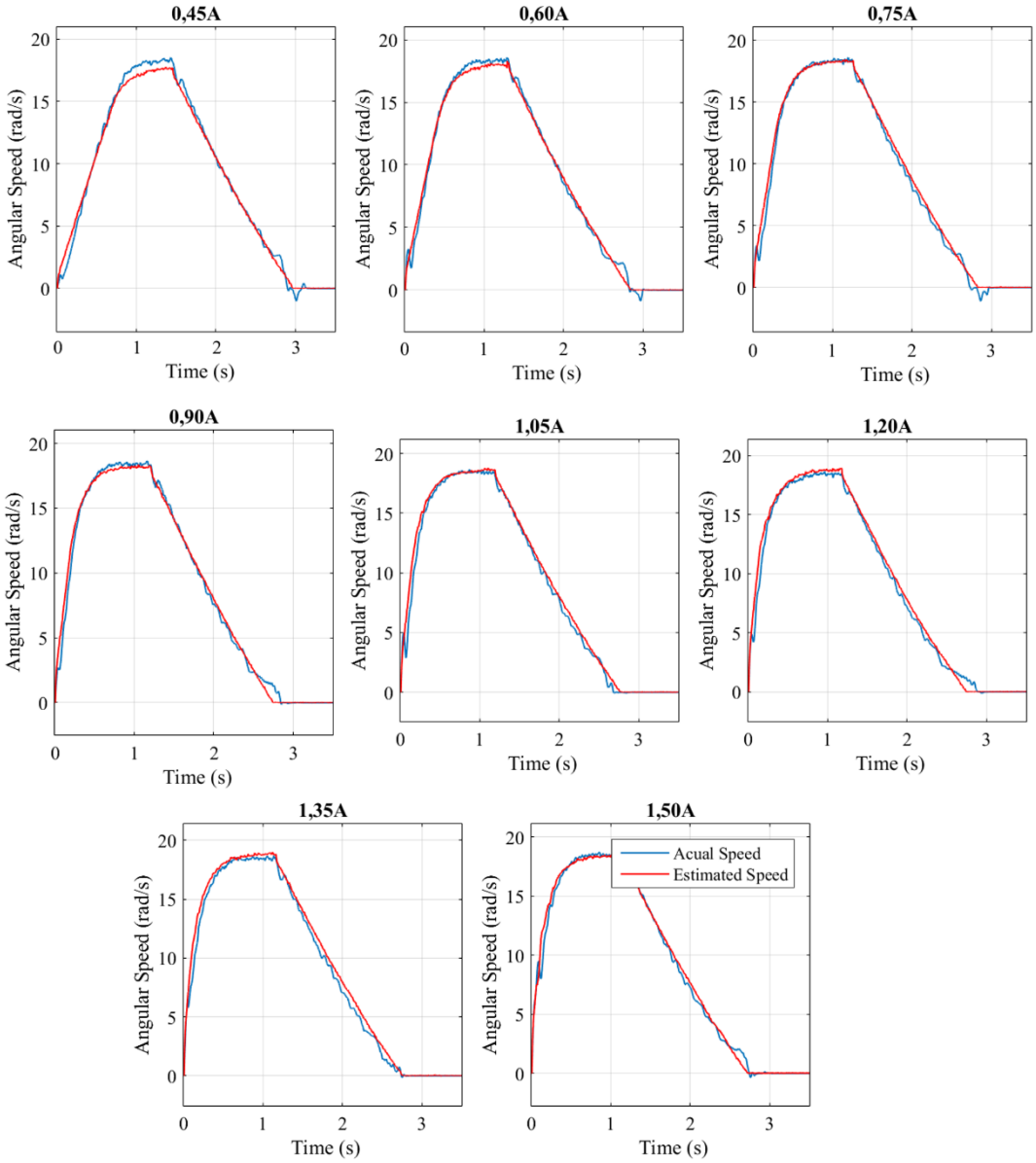

Figure 5.1. Measured and estimated wheel speeds in fault-free tests

During the speed estimation process with the model, the input signal to the model is the current information acquired from the motor driver as an analog signal. Since this signal has measurement noise, the estimated speed is also noisy. To reduce the effect of the noise and system uncertainty, the residual signal is evaluated by taking the root mean square (RMS) of r_1. Consequently, the evaluated residual signal is

$$R_1 = \|r_1\|_{RMS} \tag{5.2}$$

The variation of the evaluated residual signal in each fault-free test is represented in Figure 5.2.

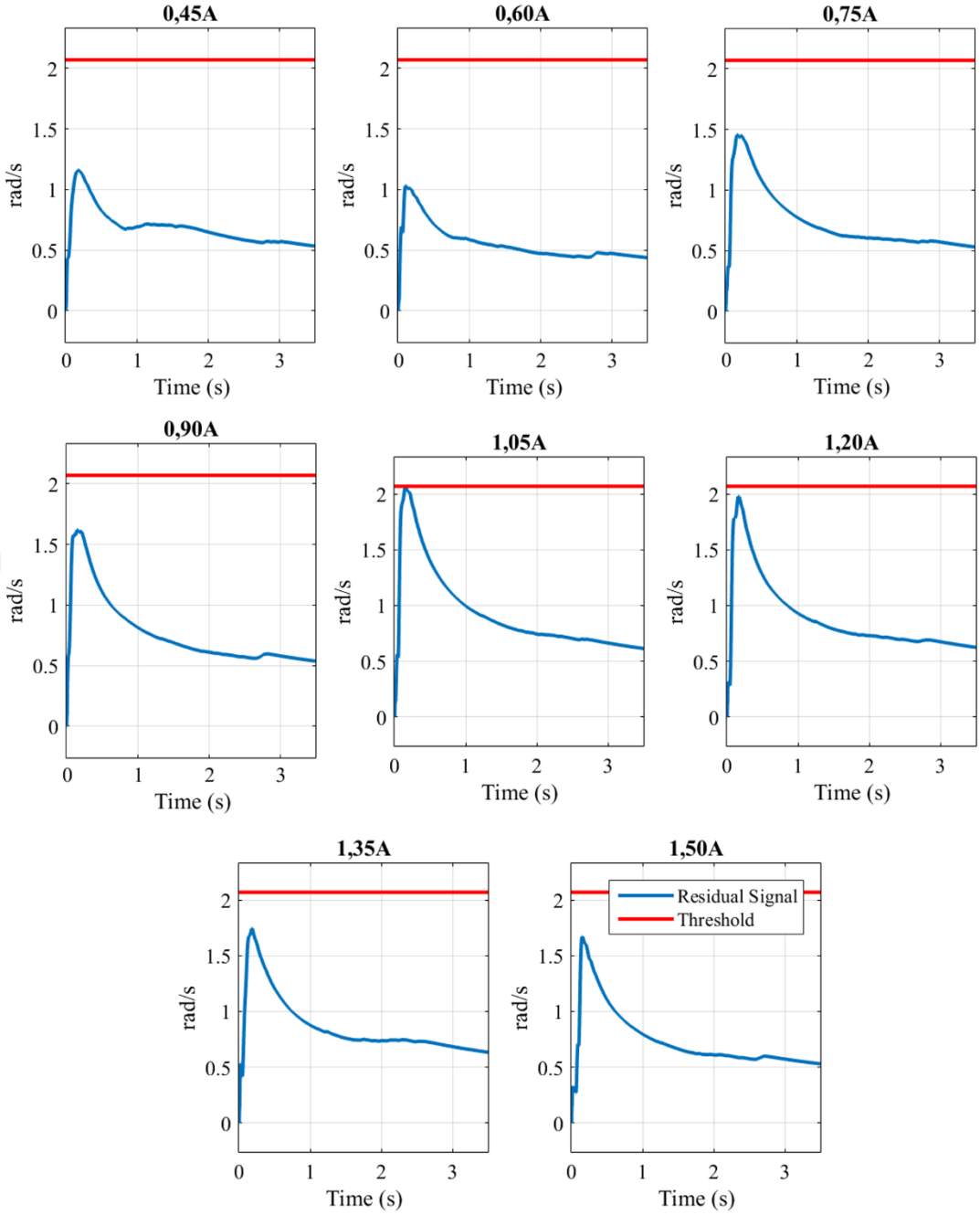

Figure 5.2. Evaluated residual signals in fault-free tests

According to residual signal results in the fault-free case, the threshold value is determined to be 2,07 rad/s via Equation 5.3.

$$Threshold_1 = max\,(R_{1_{fault-free}}) \tag{5.3}$$

This threshold value represents the limit of the residual signal in case of there is no fault in the HMR. If the wheel slippage occurs, the residual signal is expected to exceed

the threshold value. Accordingly, the fault detection procedure is defined and presented in Figure 5.3.

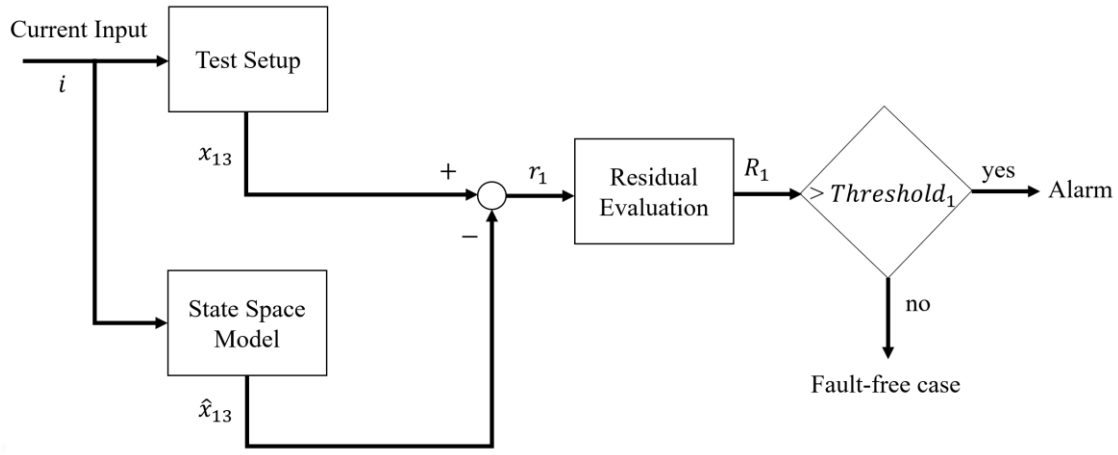

Figure 5.3. Schematic representation of the fault detection

After finding the threshold value, to verify the wheel slippage detection method, various tests are carried out by distorting the friction characteristic between the UTO wheel and ground. In each test, the DC motor that actuates the wheel is driven with a different constant current input. The actual and estimated wheel speeds obtained in each test are presented in Figure 5.4. As can be seen from the results, since the traction force at the moment of acceleration is higher than the traction force while the vehicle moves at a constant speed, the amount of the wheel slippage is higher during the acceleration interval of the motion. Also, because the resultant acceleration is considerably low while the motor is driven with low current inputs, the wheel does not slip, hence, the estimated and actual speed values are close to each other. However, while the robot is driven with higher current inputs, this difference between the estimated and actual speed values increases due to the wheel slippage during the acceleration interval of the motion.

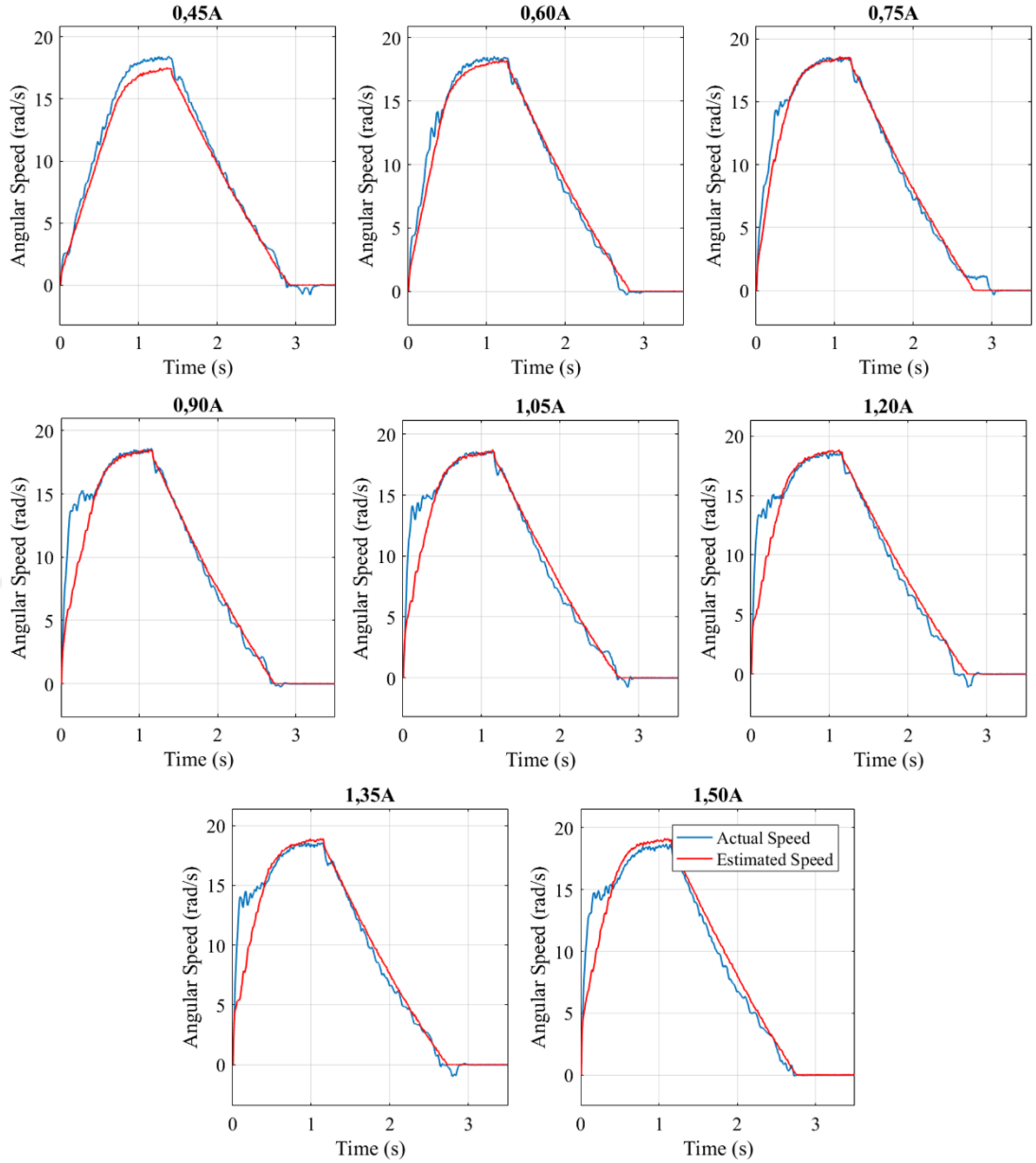

Figure 5.4. Measured and estimated speeds in wheel slippage tests

Figure 5.5 presents the change of the residual signal in each wheel slippage test. As can be seen from the figure, in the tests performed with low current inputs, the residual signal remained below the threshold value. On the other hand, in the tests performed by increasing the current value, after a certain current value, the residual signal dramatically exceeds the threshold. In the tests performed by giving 0.45A and 0.60A current input, because the acceleration of one-quarter of the HMR in the longitudinal axis is low, slippage does not occur, or the amount of slippage is very low level. For this reason, the residual signal, which is directly related to the slippage, remains below the threshold value at these low current inputs. Although low wheel slippage cannot be detected due to the

level of the threshold value, it becomes easier to detect when the wheel slippage increases. As can be seen from the results, the wheel slippage can be detected after a certain level according to the residual signal exceeding the threshold value.

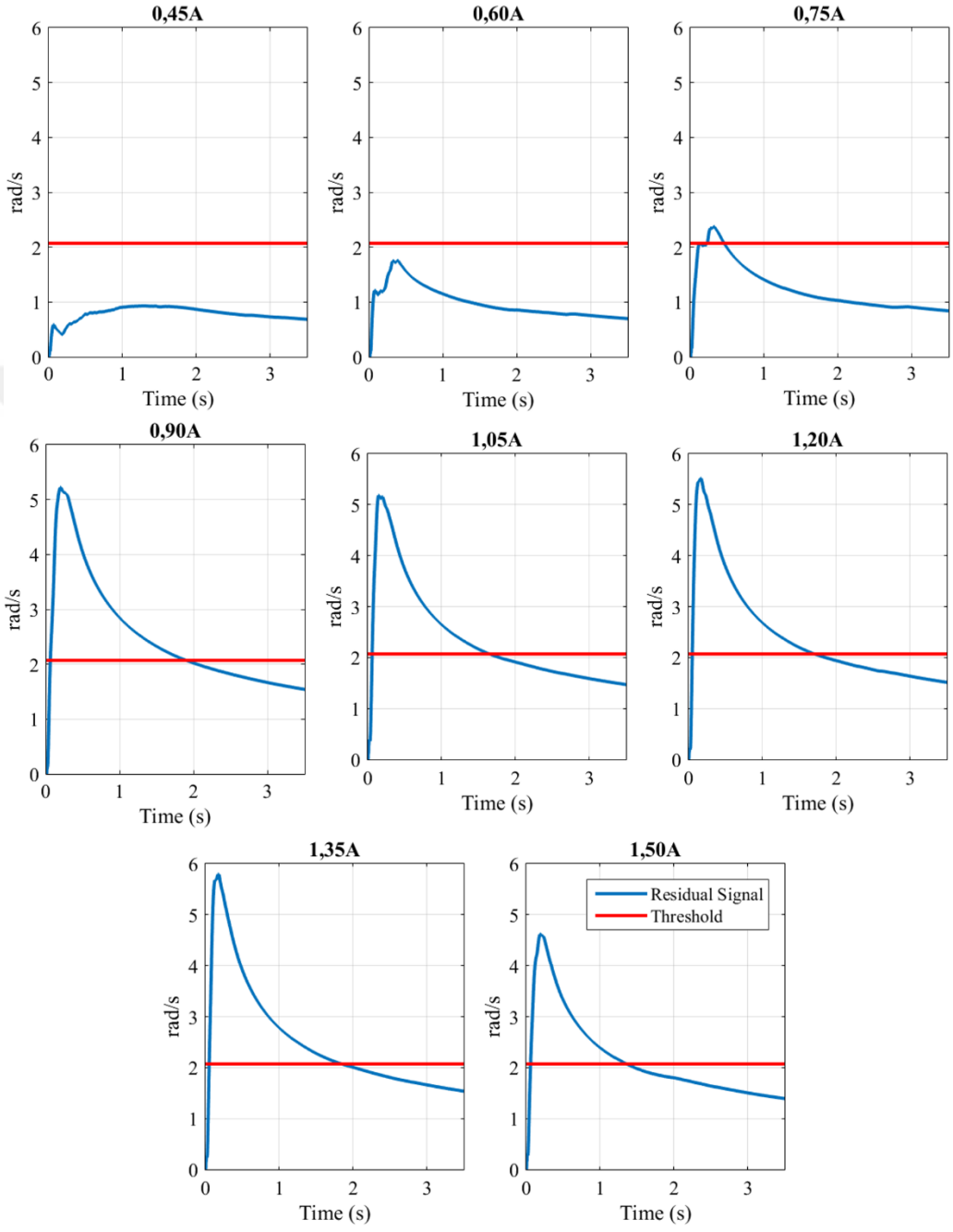

Figure 5.5. Evaluated residual signals in wheel slippage tests

The dynamic model of the robot used in estimating the wheel speed also includes the model of the DC motor. Therefore, if there exists a fault in the motor, it is obvious that this fault influences the obtained residual signal. Therefore, the motor fault can be

detected by the status of the residual signal according to the threshold value. At this point, to be used in the diagnosis studies of motor fault, it is necessary to ensure that the motor used in the system has a fault. As mentioned before, the motor fault that is aimed to be tolerated in this dissertation is the performance degradation. When this fault occurrs in the motor, the motor produces less torque than the torque generated by the fault-free motor for the specified current input. Therefore, in order to generate the motor performance degradation fault for the tests, it should be ensured that the motor produces less torque than expected with the same current input. Also, considering that the same motors are used on the robot after each fault toleration test, the implemented motor fault generation method should not result in a permanent damage to the motor. Therefore, motor performance degradation is provided by including an additional motor that is connected in parallel to the motor that actuates the omnidirectional wheel, as presented in Figure 5.6. In this way, the system with the additional motor consumes more current than the fault-free case.

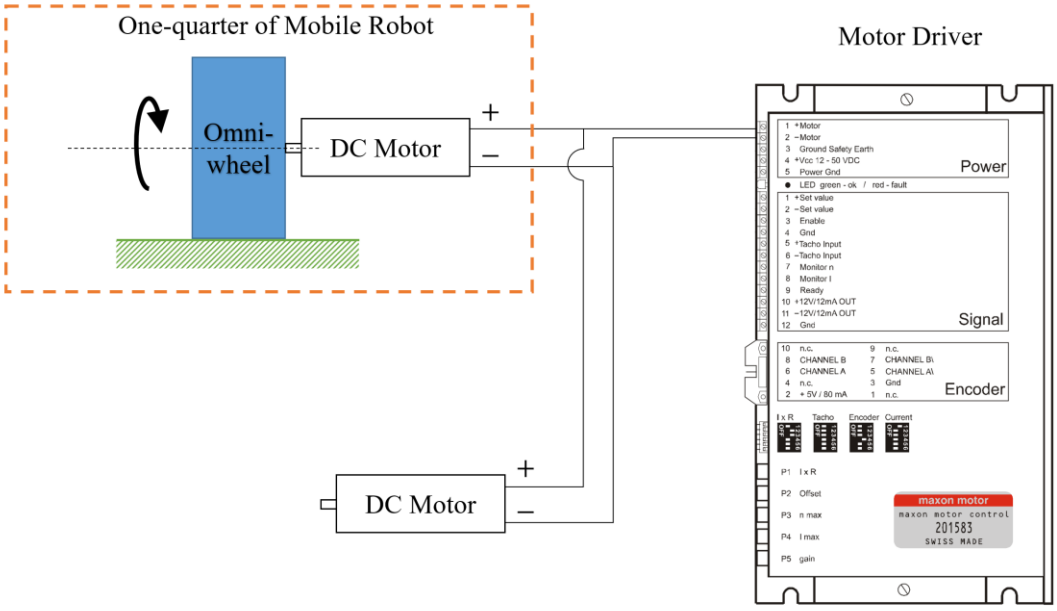

Figure 5.6. Motor fault generation scheme

After the motor in the system is ensured to be faulty, various tests are performed to diagnose this fault. In the tests, one-quarter of the HMR is driven with constant current inputs as in the previous tests. The actual current values drawn by the motor in the tests performed by giving 0.75A of desired current are presented in Figure 5.7.

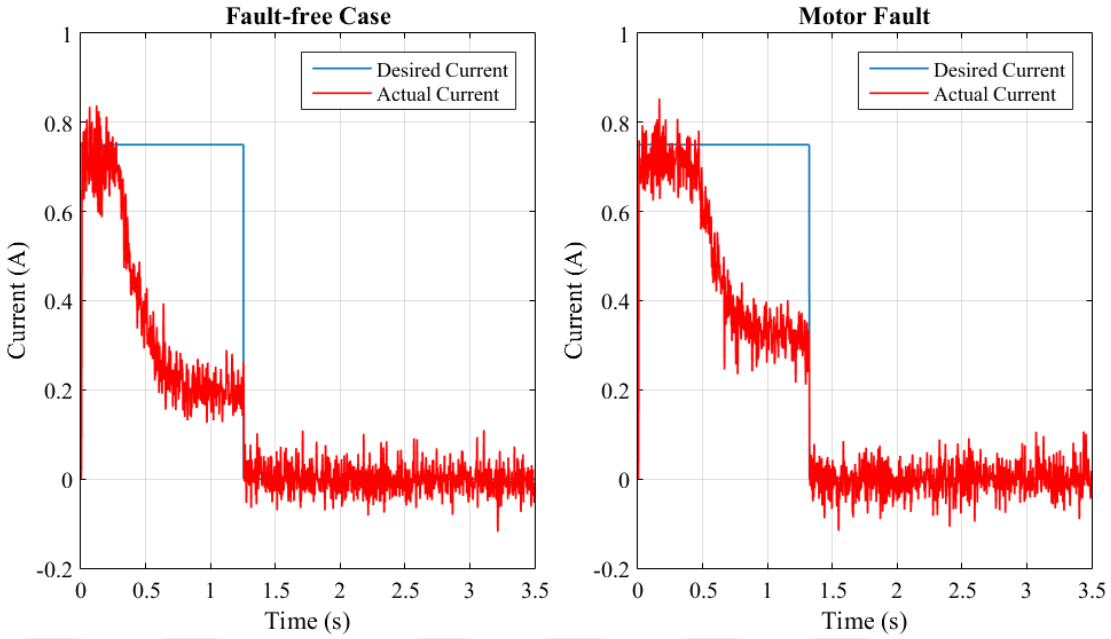

Figure 5.7. Comparison of the current usage of the system in fault-free and motor fault cases

Although a constant current demand is given to the one-quarter of the HMR from the beginning to the end of the motion, the current drawn by the system reaches this value during the acceleration interval of the motion. Then, while the vehicle reaches maximum speed, the drawn current value accordingly decreases. When the results of faulty and fault-free cases are compared, it is observed that the acceleration interval is longer in case of the motor fault. Also, after one-quarter of the HMR reaches the maximum speed, while the drawn current to overcome the friction force at the linear guide and no-load torque for the fault-free case is 0,2A, this value is about 0,35A in motor fault case due to the current drawn by the second motor. In the tests carried out with the motor-fault case, this measured current value is given as the input to the model to calculate the estimated speed, and finally, the actual speed of the wheel and the estimated speed values are compared. Figure 5.8 shows the estimated speed and actual speed values obtained in each test. The residual signals obtained during motor fault tests are presented in Figure 5.9.

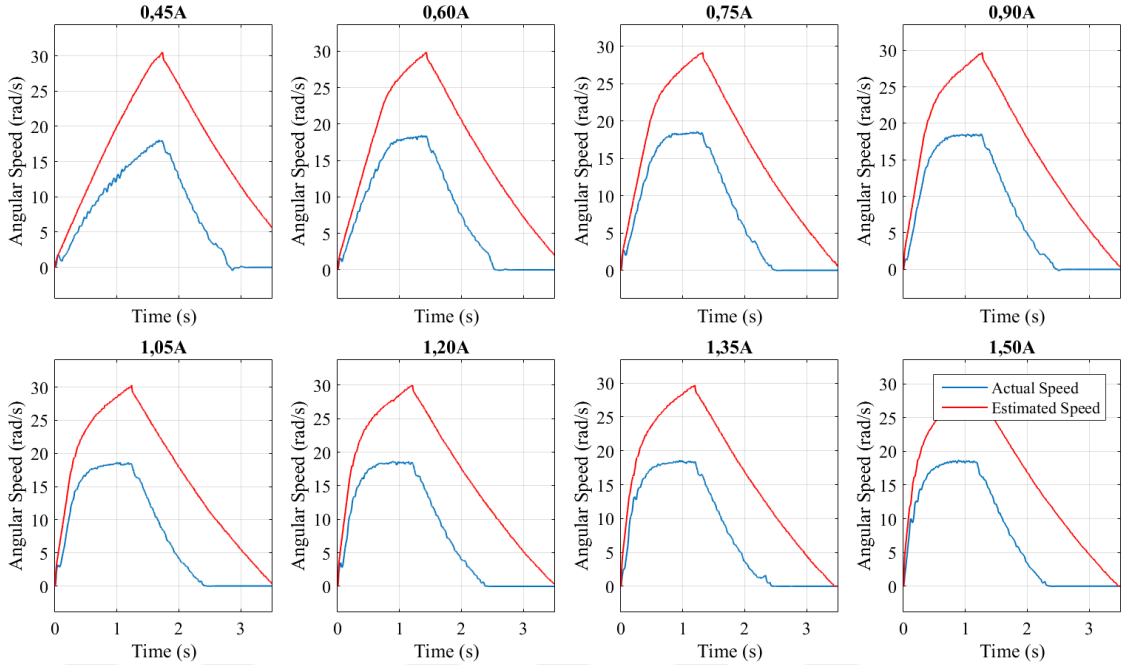

Figure 5.8. Measured and estimated speeds in motor fault tests

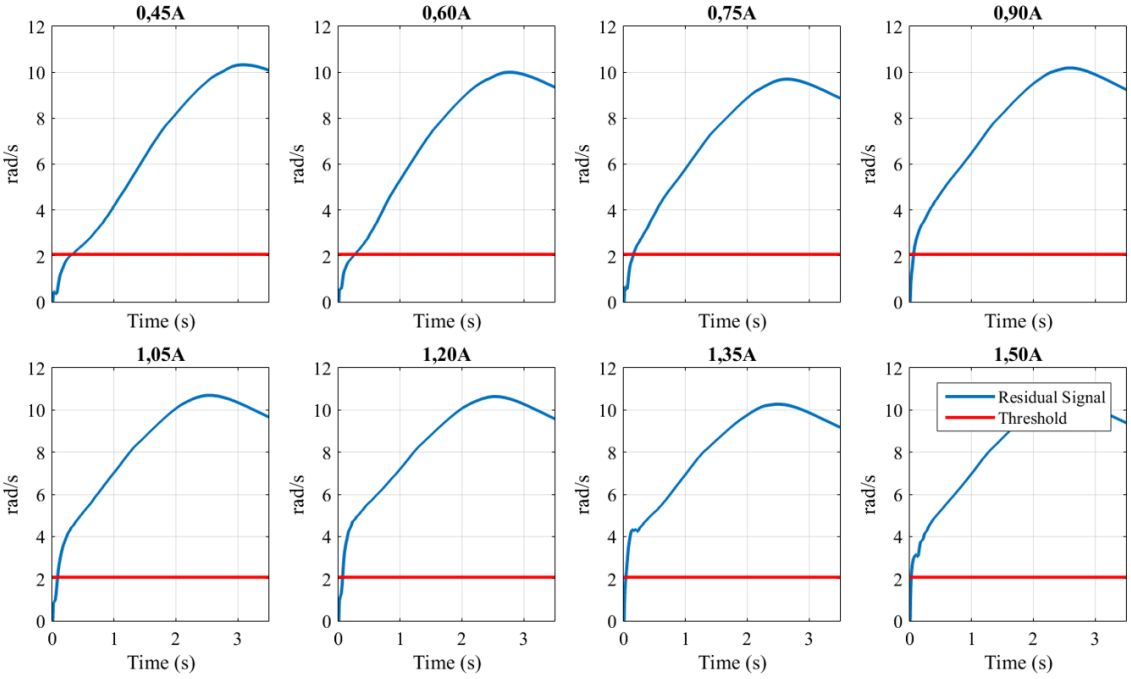

Figure 5.9. Evaluated residual signals in motor fault tests

As a result of the motor fault tests, it is seen that the residual signal exceeds the threshold value. In this way, the motor fault in the system can be detected. As mentioned before, the wheel slippage occurs during the acceleration interval, and the situation (e.g. oil on the ground) that causes the slippage may lose its effectiveness over time. On the other hand, the motor fault is permanent and shows its effect throughout the entire

movement of the robot. Therefore, two separate recovery strategies are needed for both types of faults. To achieve this, the fault that occurs in the system should be isolated. Since the generated residual signal is not indicative of only one of the two faults, a second residual signal that indicates the motor fault or wheel slippage is needed to isolate these two faults. To generate this residual signal, the following equation derived from the test setup dynamics is used.

$$F_{trac_{js\_measure}} = (T_3 - I_3\ddot{\theta}_3)/r \tag{5.4}$$

Since the motor model is known, the traction force can be calculated as a function of the joint space measurements (current and angular acceleration). On the other hand, the traction force can also be calculated in the task space from the following equation. Here, the acceleration value, $\ddot{s}_{1011}$, is measured by an accelerometer that is placed on one-quarter of the HMR.

$$F_{trac_{ts\_measure}} = m_T\ddot{s}_{1011} + (F_{f11}^D + F_{rol}) \tag{5.5}$$

The traction forces that are found by these two equations should be equal when there is no fault in the system or when the wheel slippage occurs. On the other hand, since the applied torque (T_3) on the wheel that is calculated with the measured current is different when there is a fault in the motor, these calculated traction force values are no longer equal to each other. Therefore, the residual signal to be obtained from the difference of these two force values allow the motor fault to be isolated. The second residual signal can be generated as

$$r_2 = F_{trac_{ts\_measure}} - F_{trac_{js\_measure}} \tag{5.6}$$

The second residual signal is evaluated by taking the RMS of r_2. The calculated residual signal is formulated as

$$R_2 = \|r_2\|_{RMS} \tag{5.7}$$

The motor fault can be isolated according to the specified threshold value by the following procedure given in Figure 5.10.

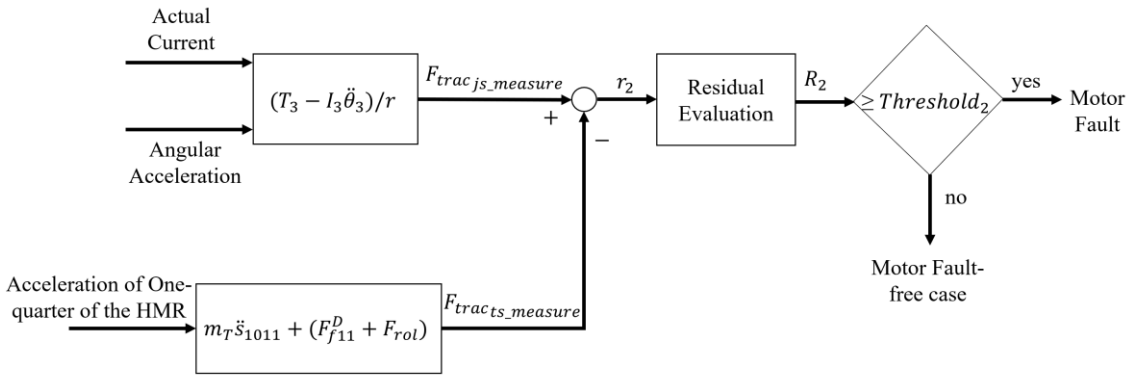

Figure 5.10. Motor fault isolation scheme

To determine the threshold value ($Threshold_2$), it is necessary to find the boundary value of the residual signal when there is no fault in the system and when there is wheel slippage. Accordingly, the one-quarter of the HMR is driven with various current inputs for these two cases. During the tests, the traction force values are calculated in real-time while the robot is in motion. Figure 5.11 shows the variation of the calculated traction forces during these tests.

As can be seen in Figure 5.11, the calculated traction force values in joint space and task space are very close to each other especially in the acceleration interval of the motion and in the interval while the robot moves with a constant speed until the safe location on the linear guide is reached. As mentioned before, there are double rows of rollers in the omnidirectional wheel used in this dissertation. In UTO wheels with double rows of rollers, the outer diameter of the wheel is closer to a full circle than the ones with a single row. Although this double row roller structure decrease vibration despite single row roller, due to the small level differences between the rollers and the joint clearance in the roller's mountings high amplitude vibrations occur while the one-quarter of the HMR decelerates. This is reflected in the traction force value calculated with the acceleration information measured from the accelerometer in the task space. According to the test results in both cases, the threshold value is determined to be 1.32N by using the following equation:

$$Threshold_2 = max\,(R_{2_{fault\ free\ and\ wheel\ slip}}) \tag{5.8}$$

The calculated residual signals obtained during fault-free and wheel slippage cases are represented in Figure 5.12.

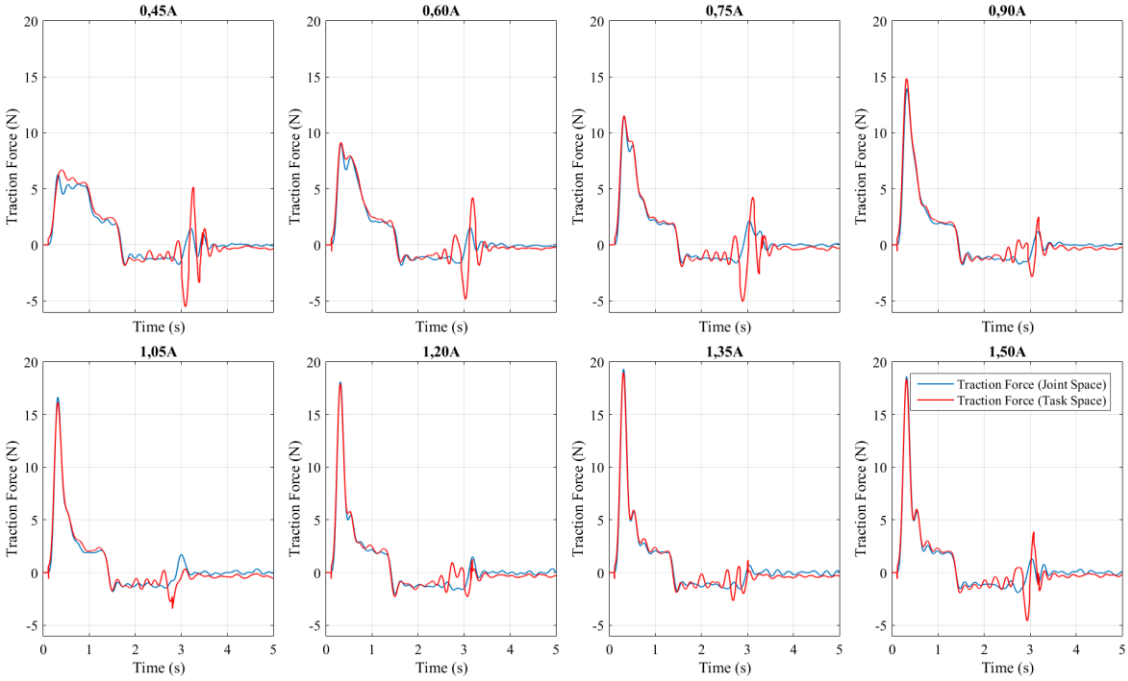

(a)

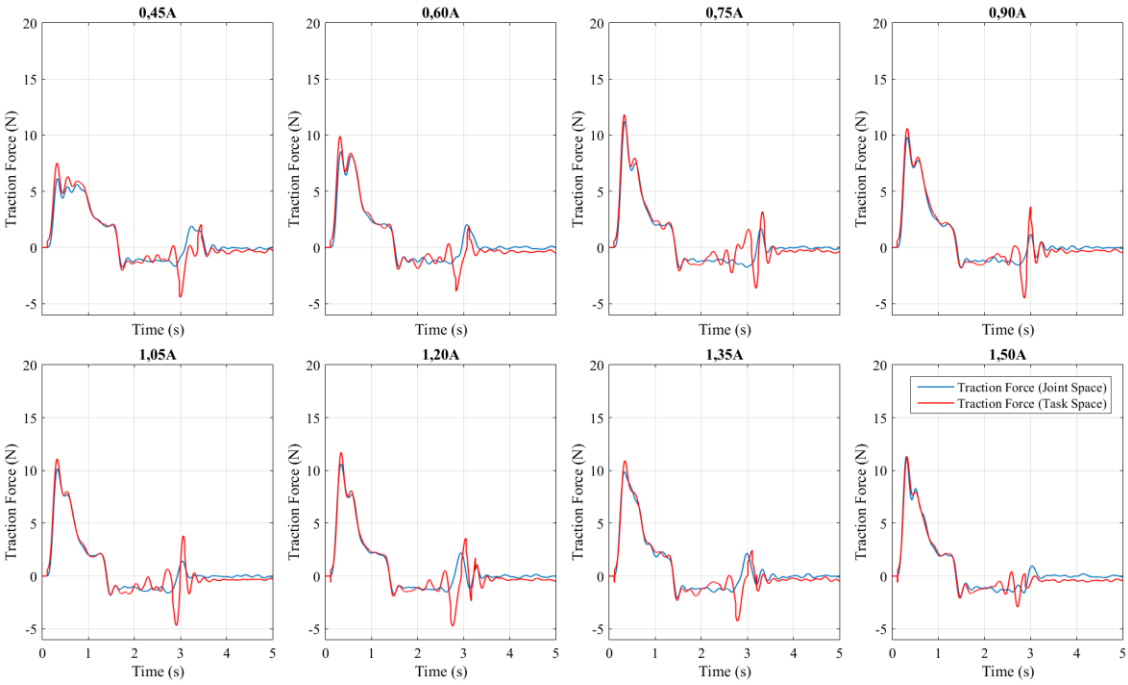

(b)

Figure 5.11. Calculated traction forces with respect to joint space and task space measurements; a) fault-free case, b) wheel slippage case

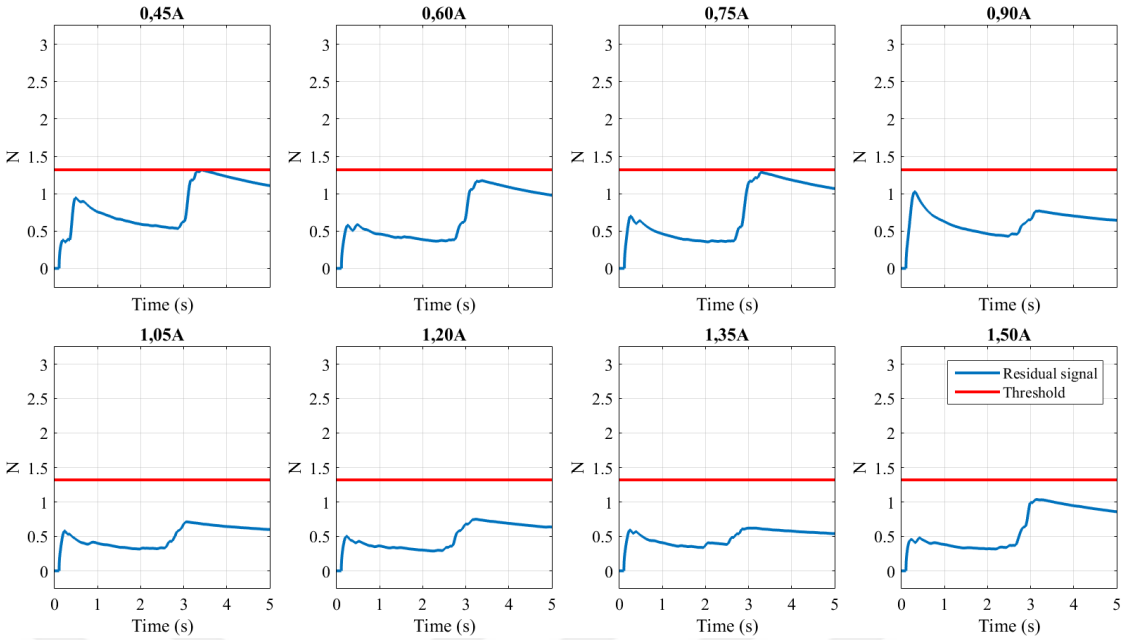

(a)

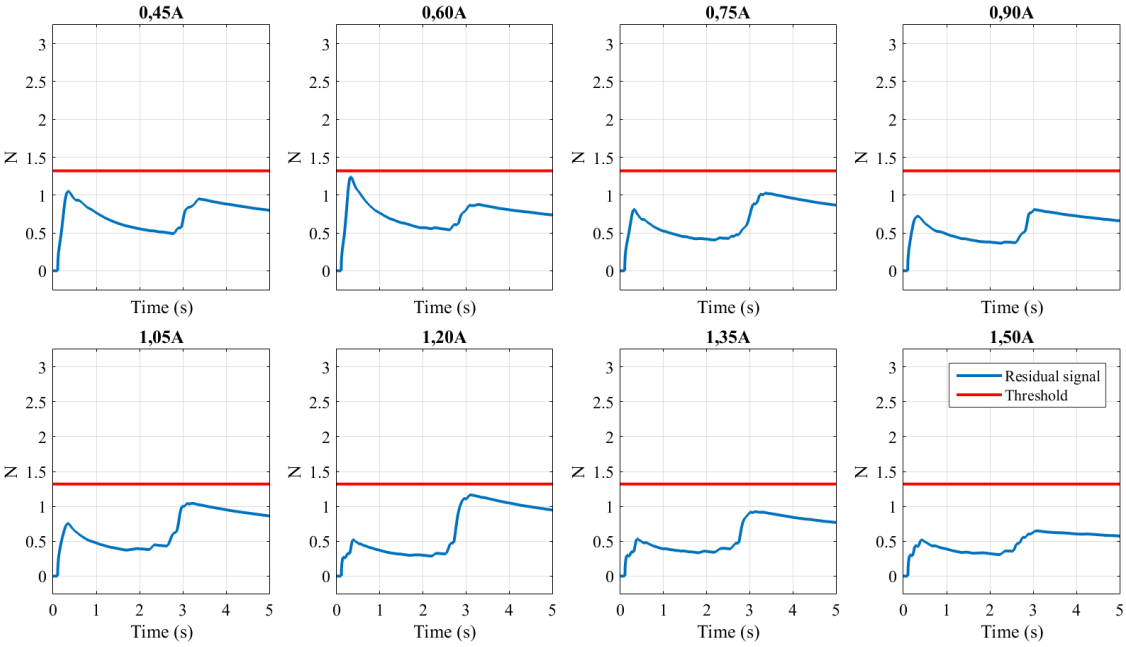

(b)

Figure 5.12. Second residual signal; a) fault-free case, b) wheel slippage case

After determining the threshold value, motor-fault tests are carried out. The calculated traction force values obtained in motor-fault tests are shown in Figure 5.13a. As can be seen clearly in Figure 5.13a, traction force values do not match each other. Consequently, in the case of a motor fault, the residual signal exceeds the threshold value as shown in Figure 5.13b.

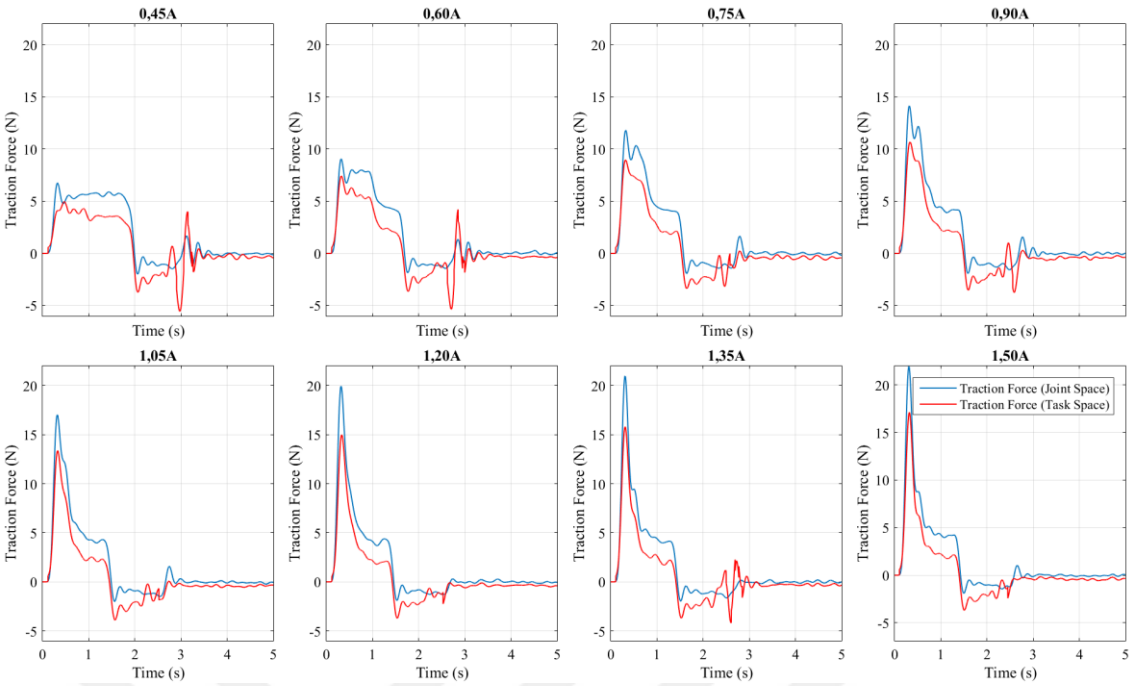

(a)

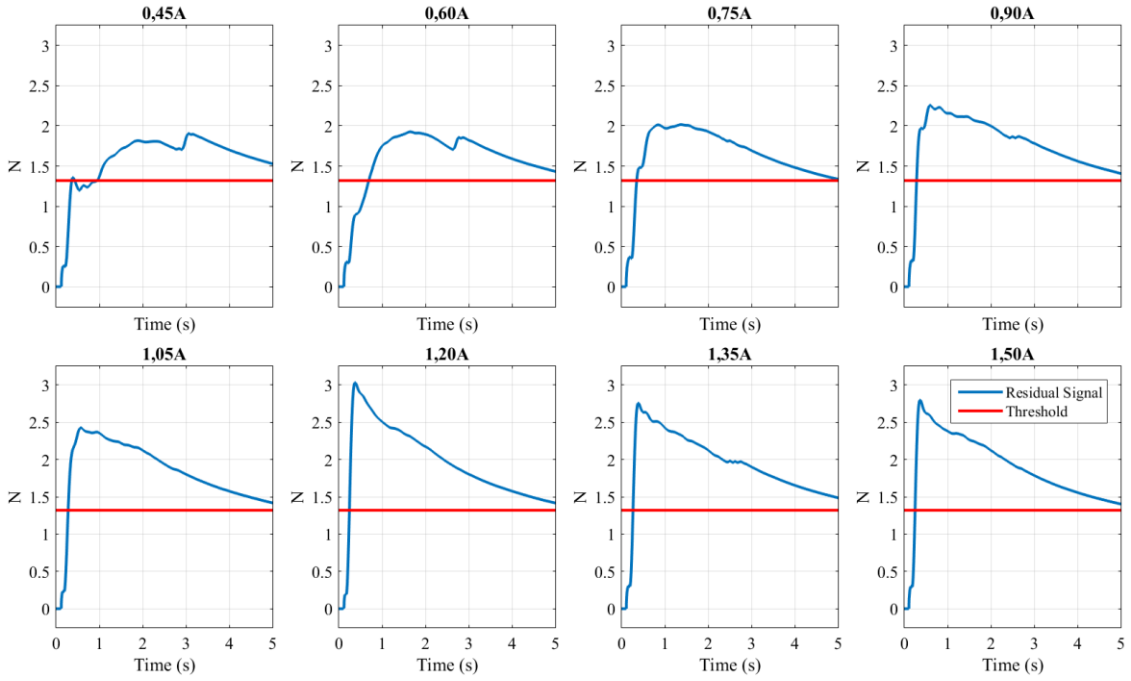

(b)

Figure 5.13. Motor fault test results: a) calculated traction forces, b) second residual signal results

According to the test results, fault isolation can be made with the logic table given in Table 5.1. In this table, “0” means that the residual signal is less than the corresponding threshold value and “1” means that the residual signal is higher than the corresponding

threshold value. If both residual signals are less than the threshold value, this case is the fault-free case. If the first residual signal is higher than the threshold value and the second one less than the threshold, in this case, wheel slippage fault is isolated. If both residual signals are higher than the threshold values, the motor which actuates one-quarter of the HMR is faulty.

Table 5.1. A logic table for isolating faults in the test setup

	R_1	R_2
Fault-free Case	0	0
Wheel Slip	1	0
Motor Fault	1	1

5.3. Fault Diagnosis for the Holonomic Mobile Robot

As can be seen from the results of the tests performed with a single wheel with the test setup, the slippage in the wheel and the performance degradation in the motor can be diagnosed with residual signals obtained using the system model. After the diagnosis method planned to be implemented in the mobile robot is verified with the one-quarter test setup, fault diagnosis studies are carried out for these two faults using the mobile robot. Since there is only one wheel in the test setup, two faults are diagnosed. On the other hand, although there are two types of faults in the mobile robot, considering that there may be slippage in each wheel and degraded performance in the motor that actuates each wheel, eight different faults should be diagnosed. Like the previous diagnosis method applied in the test setup, some residual signals, which are obtained from the differences between the estimated states of the dynamic model of the robot and the measured states, are required. In the mobile robot model whose dynamic equations are given in Chapter 3, the states of the robot's dynamic model can be estimated when the measured currents drawn by the motors are used as inputs to the model during the motion of the robot. Residual signals generated separately for each wheel for the detection of wheel slippage are

$$r_3 = x_5 - \hat{x}_5 \tag{5.9}$$

$$r_4 = x_6 - \hat{x}_6 \tag{5.10}$$

$$r_5 = x_7 - \hat{x}_7 \tag{5.11}$$

$$r_6 = x_8 - \hat{x}_8 \tag{5.12}$$

where, r_i $(i = 3,4,5,6)$ are the residual signals, x_5, x_6, x_7 and x_8 are measured wheel speeds acquired via encoder signals, $\hat{x}_5, \hat{x}_6, \hat{x}_7$ and $\hat{x}_8$ are estimated wheel speeds obtained via the model.

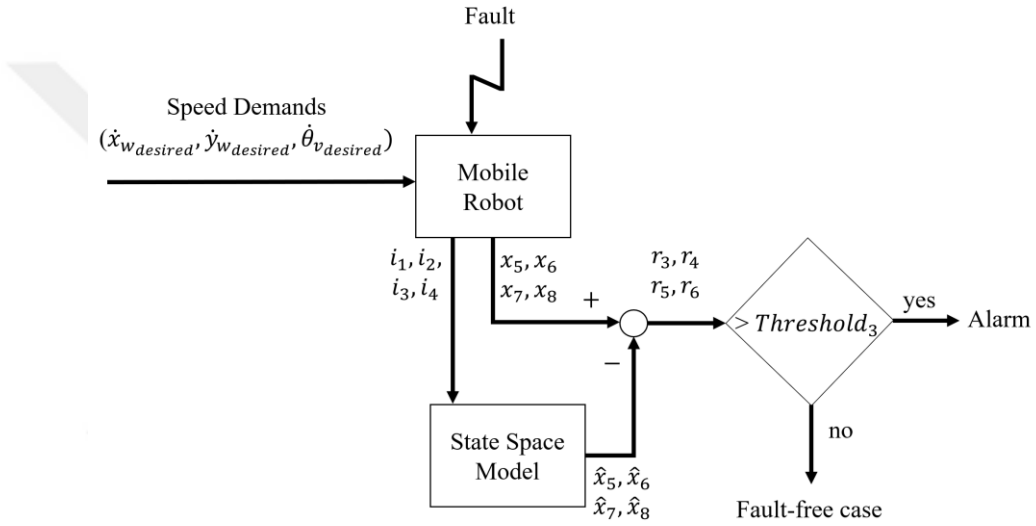

Figure 5.14. Fault detection scheme for HMR

The applied fault detection method for the considered faults in HMR is represented in Figure 5.14. In the tests performed with the test setup, the residual signal obtained from difference between the measured and estimated speed of the wheel is evaluated by taking the RMS of the signal. This evaluation method for the residual signal applied to reduce the effect of measurement noise and uncertainty on the signal. However, this method is not applied for residual signals obtained from the wheel speeds of the mobile robot.The reason for this is that; for the planned recovery strategy, it is necessary to know the instance when the slippage starts as well as the instance when the slippage ends. Based on the results of the tests performed with the one-quarter test setup (Figures 5.4 and 5.5), it can be said that the wheel slippage begins when the residual signal exceeds the threshold value, and the slippage ends before the residual signal goes below the threshold value again. Although in this way wheel slippage can be accurately detected,

the instance when the slippage is over cannot be detected. Therefore, residual signals obtained from wheel speeds are used without evaluating by taking the RMS of them in fault diagnosis.

To find the suitable threshold value, the robot is driven with different speed demands in various directions and the change of residual signals during the motion of the robot is observed. Since the mobile robot used in this dissertation is capable of holonomic motion ability, when the mobile robot's body-fixed frame is parallel to the used world frame, the speed demands issued to the mobile robot are given as the linear speed demands along each the world frame unit vector separately (X_w and Y_w), along both X_w and Y_w axes at the same time, and the angular speed demand about the Z_w axis. In fault-free test that are carried out along different direction motions, high and low-speed profiles for both linear and angular speeds are used as speed demands which are presented in Figure 5.15.

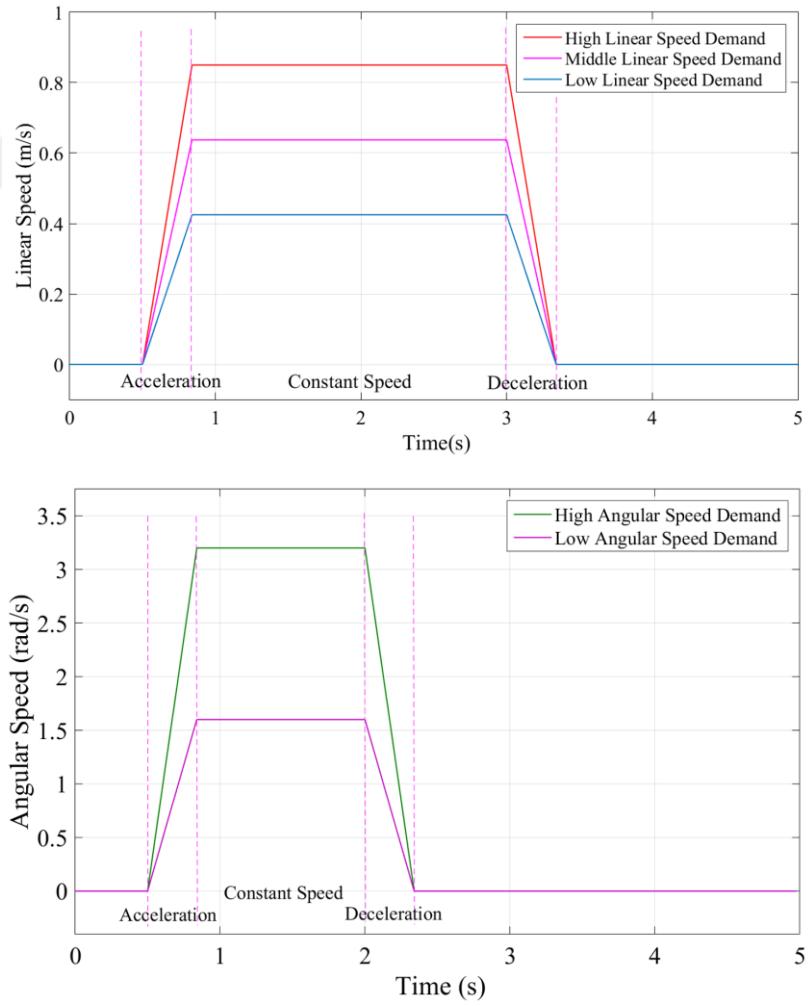

Figure 5.15. Desired speed profiles during the tests

As a result of the tests, the threshold value is determined as follows:

$$Threshold_3 = max\left(r_{3,4,5,6_{fault-free}}\right) = 3{,}9 \text{ rad/s} \tag{5.13}$$

In the wheel slippage tests performed with the mobile robot, the friction characteristic between the wheel and the ground is distorted by a nylon piece placed under the wheel as it is the case in the one-quarter test setup (Figure 5.16).

Figure 5.16. Nylon piece placed between UTO wheel and the ground

The results of wheel slippage tests are shown in Figure 5.17. Tests are carried out separately by placing nylon pieces under each wheel. High-speed demand is given to the robot in the Y_w direction in the tests performed by placing a nylon piece under the first and third wheels, and high-speed demand is given in the X_w direction in the tests performed by placing a nylon piece under the second and fourth wheels. As shown in the result of the test performed by placing a nylon piece under the first wheel, third residual signal corresponding to first wheel exceeds the threshold value during the acceleration interval of the motion. According to this result, it can be deduced that first wheel of the HMR slips. In the other test results achieved with distorting friction characteristic of the second wheel, third wheel, and fourth wheel, similar results are obtained in each test as the faulty wheel's residual signal exceeds the threshold.

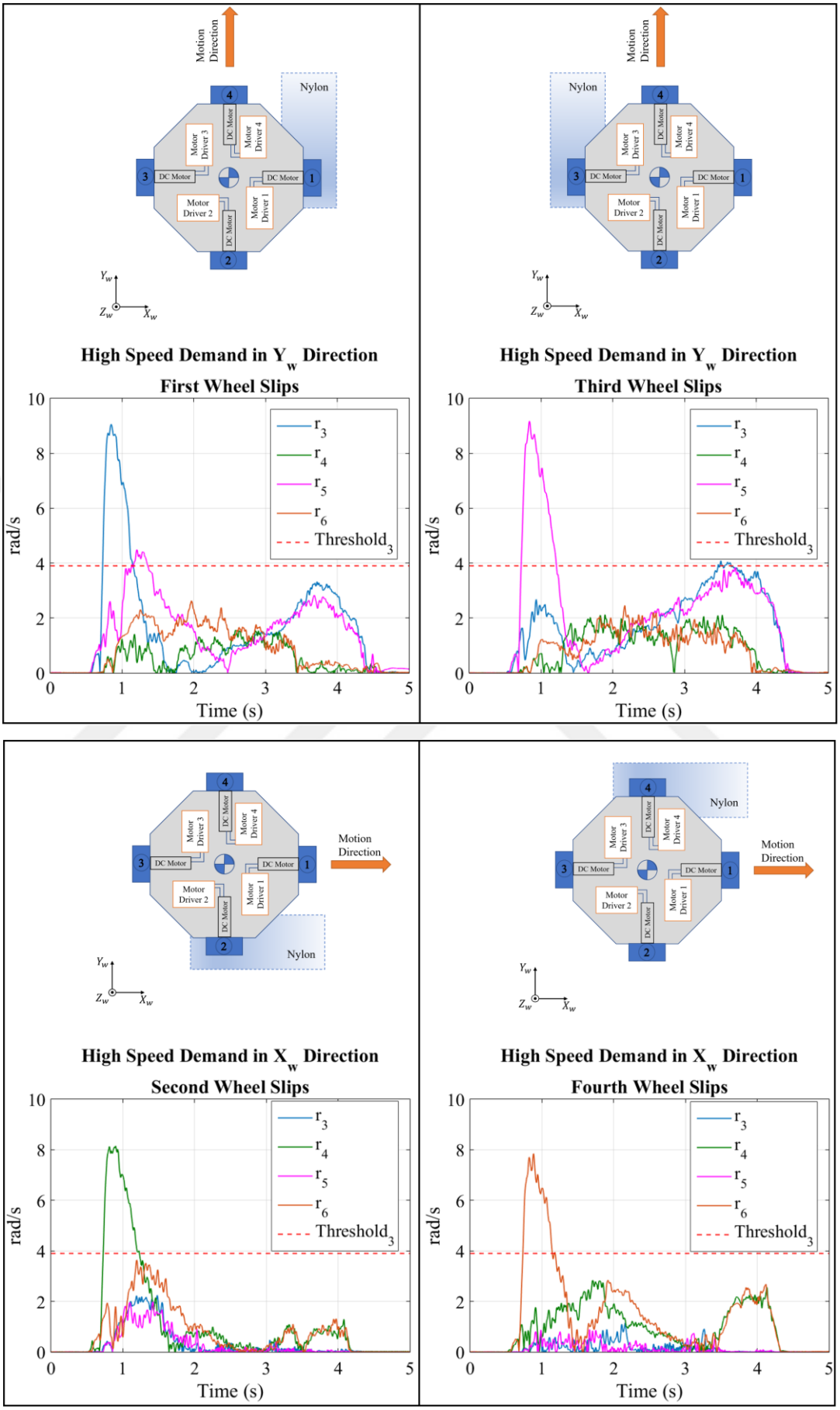

Figure 5.17. Wheel slippage detection tests results

As mentioned before, each wheel of the mobile robot is actuated by a separate DC motor. To reduce the performance of one of these motors, an additional motor is connected in parallel to the motor driver as shown in Figure 5.18. Initially, the output shaft of the additional motor is left free. Since the current usage of this motor is small in this case, a force is applied with the help of a bolt placed perpendicular to the shaft of this motor to increase the amount of current usage and increase the severity of the fault accordingly (Figure 5.18). By changing the intensity of the applied force, different levels of performance degradation are achieved in the motor that actuates the wheel. Here, two different force levels are applied to the shaft of the additional motor and thus, two different levels of performance degradation are created. When the applied force to the additional motor shaft is low, accordingly, performance degradation is low, and this is named as Level 1 fault. When the applied force is increased, in this case, the performance degradation is increased, and this situation is named Level 2 fault. During the tests, the motor whose performance is reduced in this way is the motor that actuates the first wheel of the mobile robot. Motor fault tests are carried out by issuing three different linear speed demands for the mobile robot as represented in Figure 5.15.

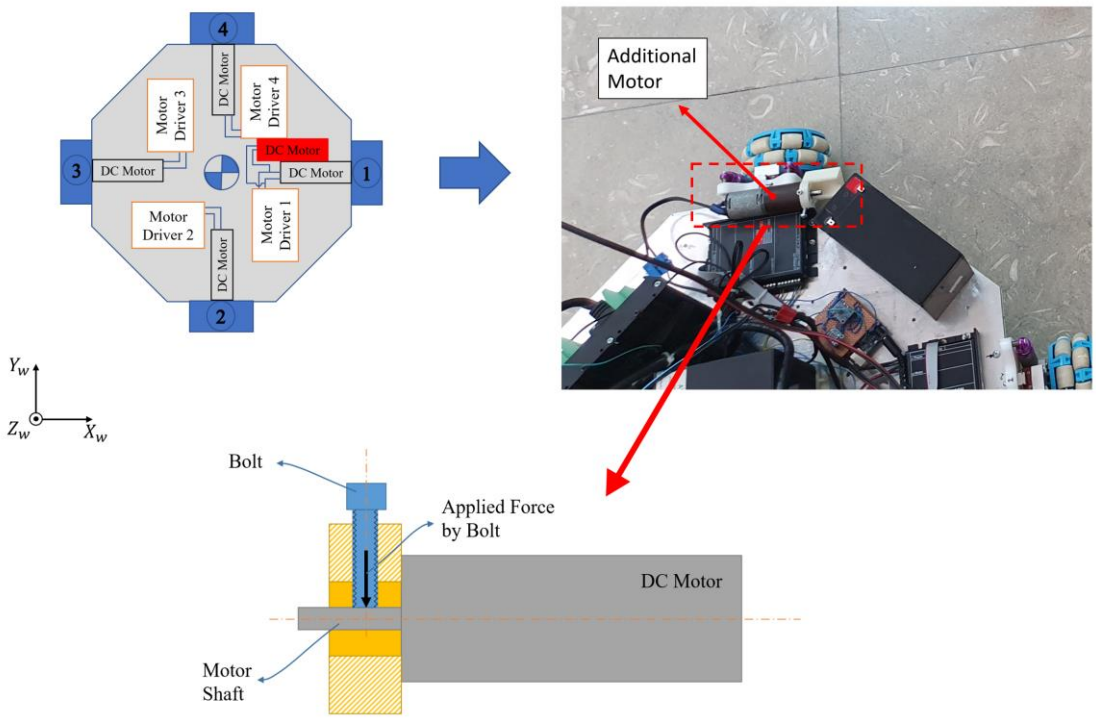

Figure 5.18. The setup which is applied to degrade the performance of the motor that actuates first wheel of the HMR

Since the fault that occurs in one of the motors of the robot means that there is a change in the parameters of the motor, the wheel speeds estimated by the dynamic model do not match the actual values. This means that the residual signals obtained in the case of a motor fault will exceed the threshold value. The results of the first motor performance degradation tests carried out by issuing speed demand along the -Y_w direction is presented in Figure 5.19. When the orientation of the robot is maintained in its initial condition, motion in -Y_w direction is obtained with the first and third wheels of the HMR. Therefore, if there is a fault in one of these motors there is a remarkable change in the residual signals related to these motors. It is observed from all the test results presented in Figure 5.19 that the third residual signal due to faulty motor exceeds the threshold value before the fifth residual signal. Also, as shown in the test results, as the performance degradation level of the motor increases, the residual signals exceed the threshold values in a shorter time. This means that when the performance degradation level of the motor is increased, the difference between the estimated values from the system model and the measured values increase faster. In other tests carried out with the issued desired motion along both -X_w and -Y_w directions, the motion of the robot is provided by all four wheels. Therefore, all residual signals can exceed the threshold values as a result of the distorted system dynamics distorted due to a faulty wheel (Figure 5.20). However, the third residual signal exceeds the threshold value before the other residual signals for this motion scenario as well. Consequently, in all tests, a fault in the motor which actuates the first wheel of the HMR could be detected.

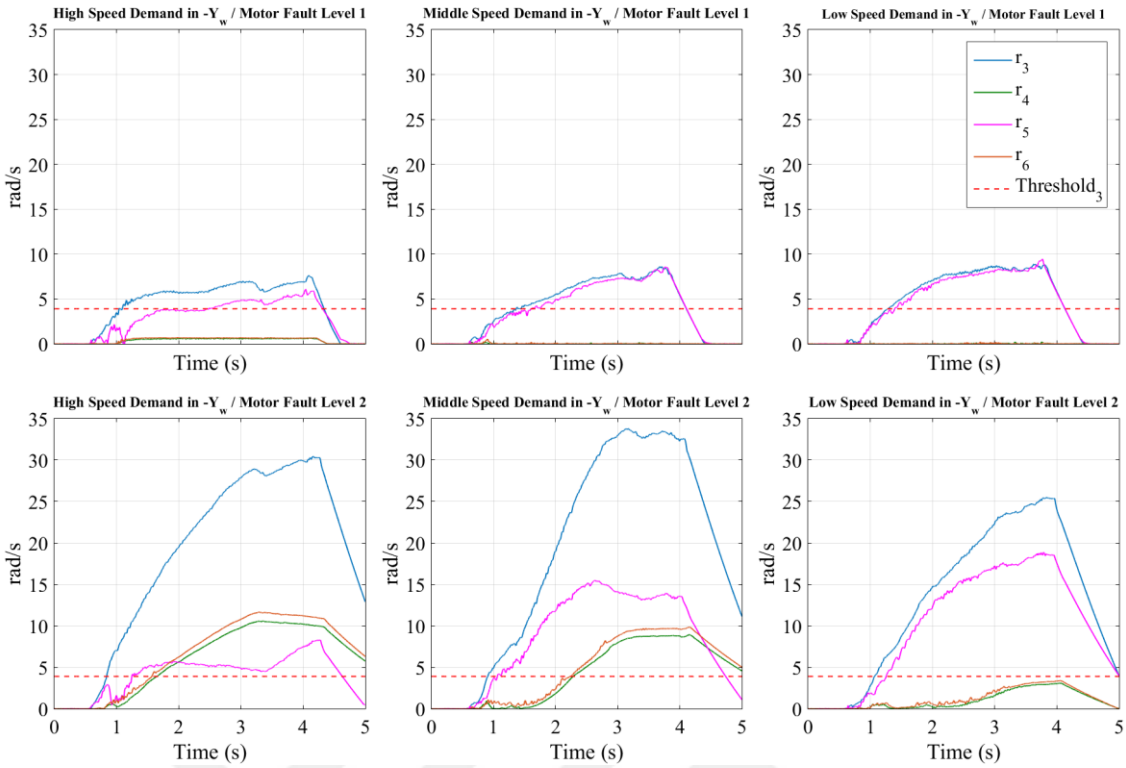

Figure 5.19. Residual signals in motor fault tests achieved with giving motion to the HMR in -Y_w direction

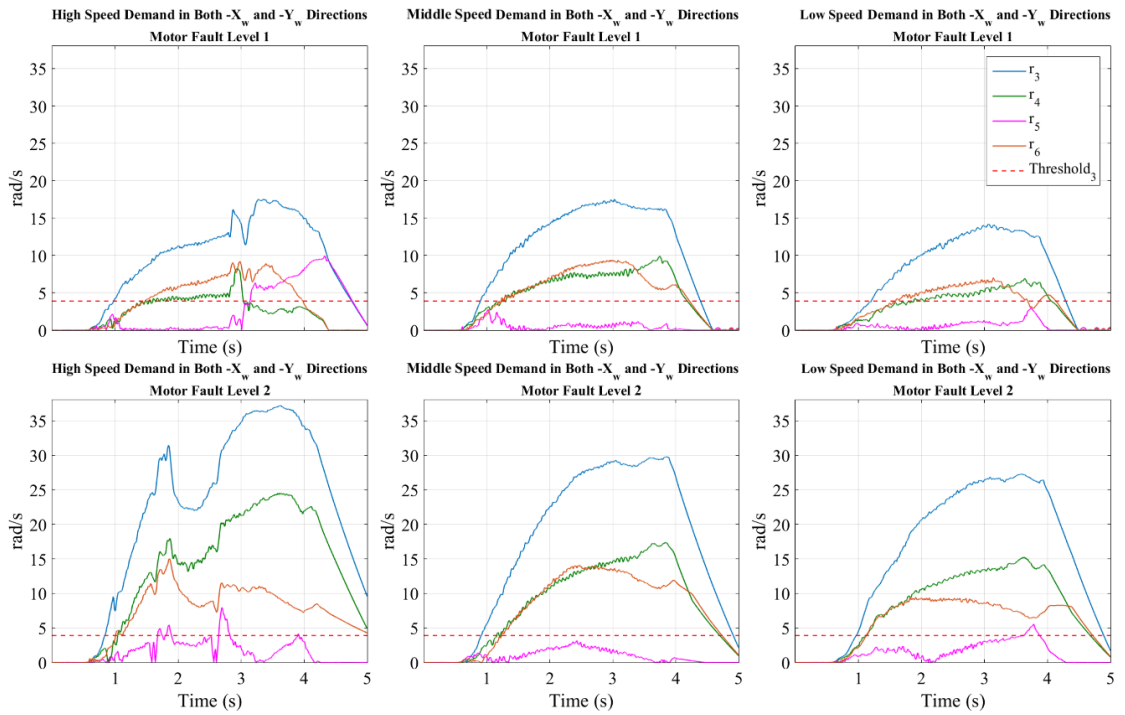

Figure 5.20. Residual signals in motor fault tests achieved with giving motion to the HMR in both -X_w and -Y_w directions

As seen in tests for wheel slippage and performance degradation fault of the motor, detection of both faults can be achieved by four residual signals. However, to isolate the wheel slippage and the performance degradation of a DC motor, additional residual signals that indicate one of these two faults are required. As mentioned before, the acceleration of the mobile robot along both x_L and y_L axes ($\dot{x}_9$ and $\dot{x}_{10}$) are measured with the accelerometer placed on the robot. The total traction forces of the robot produced by the wheels along these directions (F_{trac}^{x} , F_{trac}^{y}) can be calculated from Equations 3.71 to 3.78 by using the measured angular acceleration of the wheels, measured currents of the DC motors, and acceleration measurements in task space. According to joint space measurements, the traction forces in both directions can be found from the following equations:

$$F_{trac_{js}}^{x} = \frac{1}{r}[(K_t(i_4 - i_2) - 2T_{nl})EG_r - \left(T_{friction_4} - T_{friction_2}\right) + \dot{x}_6 I_2 - \dot{x}_8 I_4 - (\dot{x}_8 - \dot{x}_6)\left(J_r + J_g\right)EG_r{}^2] \quad (5.14)$$

$$F_{trac_{js}}^{y} = \frac{1}{r}[(K_t(i_3 - i_1) - 2T_{nl})EG_r - \left(T_{friction_3} - T_{friction_1}\right) + \dot{x}_5 I_1 - \dot{x}_7 I_3 - (\dot{x}_7 - \dot{x}_5)\left(J_r + J_g\right)EG_r{}^2]\,. \quad (5.15)$$

Also, the total traction forces along both x_L and y_L directions can also be calculated from the following equations by using the measured acceleration in the task space:

$$F_{trac_{ts}}^{x} = \dot{x}_9 m_v + \left(F_{f1} + F_{f3}\right) \quad (5.16)$$

$$F_{trac_{ts}}^{y} = \dot{x}_{10} m_v + \left(F_{f2} + F_{f4}\right) \quad (5.17)$$

The traction forces in both directions that are calculated in two different ways should be equal in fault-free and wheel slippage cases. However, if motor fault occurs, these traction force calculations do not match each other. Therefore, the residual signals obtained here can provide information about the motor fault. The motor fault isolation scheme is presented in Figure 5.21. Residual signals obtained from these two traction force calculations are

$$r_7 = F^x_{trac_{js}} - F^x_{trac_{ts}} \tag{5.18}$$

$$r_8 = F^y_{trac_{js}} - F^y_{trac_{ts}} \tag{5.19}$$

Then the evaluated residual signals are

$$R_7 = \|r_7\|_{RMS} \ , \ R_8 = \|r_8\|_{RMS} \tag{5.20}$$

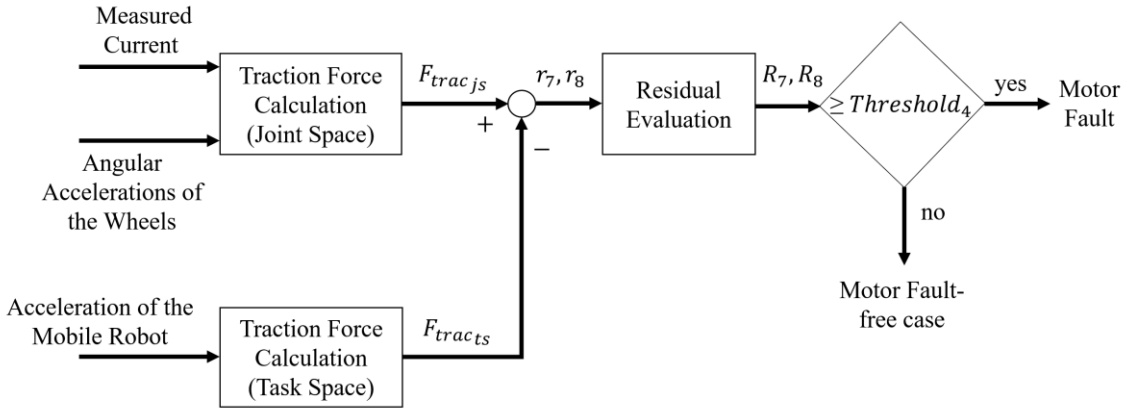

Figure 5.21. Motor fault isolation scheme for the HMR

To find the threshold value for these two residual signals, the limit values of residual signals are measured in cases when there is no fault in the mobile robot and when one of the wheels slip as a result of distorting the friction characteristic between the wheel and the ground. As represented in Figures 5.22, 5.23, and 5.24, both traction force calculations are quite compatible with each other in fault-free and wheel slippage tests achieved by issuing linear speed demands to the HMR along the X_w and Y_w directions.

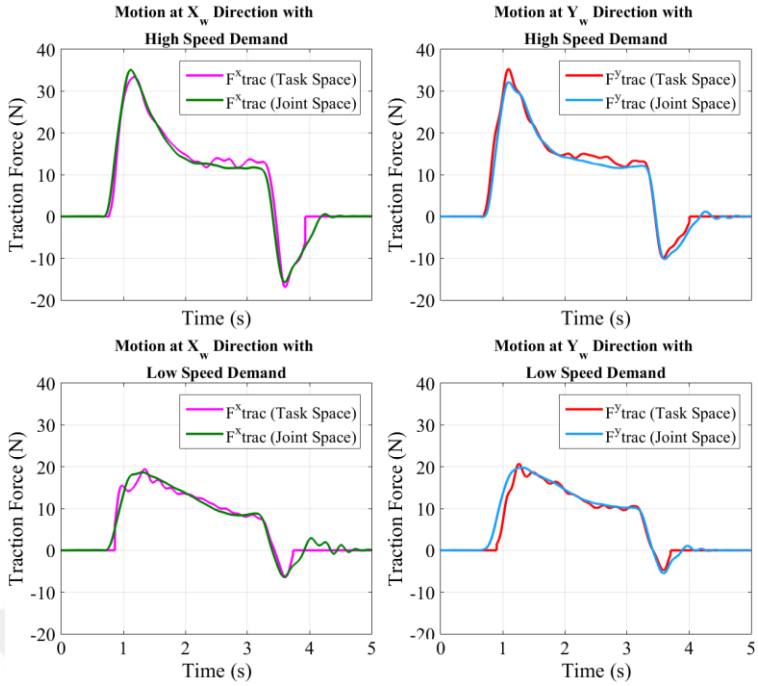

Figure 5.22. Traction force calculations during motion in X_w or Y_w directions in fault-free case

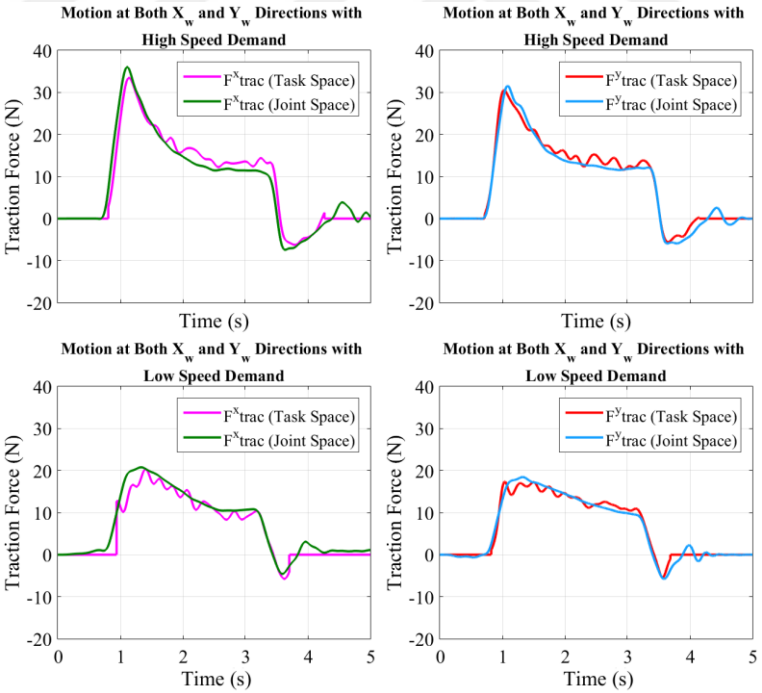

Figure 5.23. Traction force calculations during motion in both X_w and Y_w directions in fault-free case

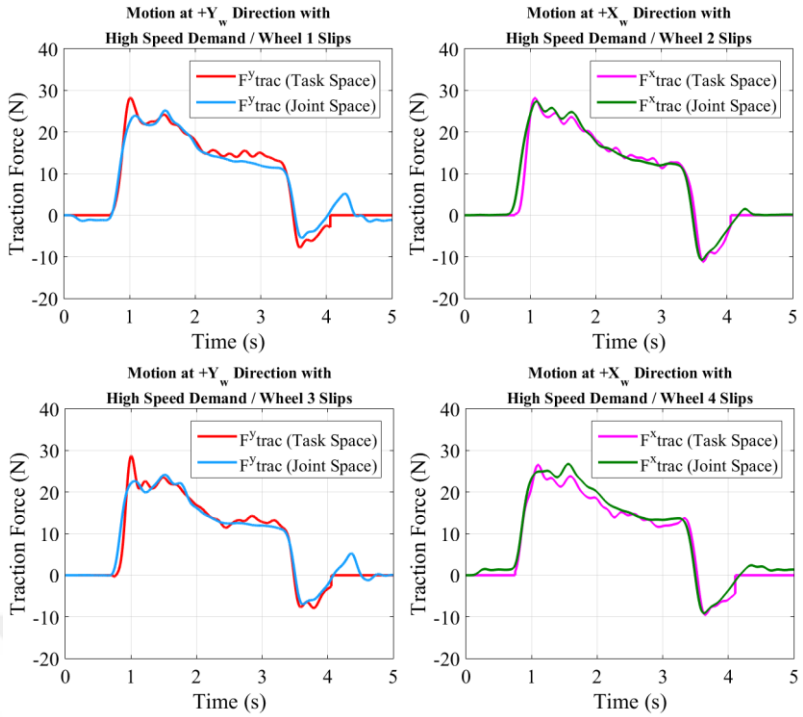

Figure 5.24. Traction force calculation during motion in X_w or Y_w directions in wheel slippage cases

As a result of the tests, the threshold value is determined as follows:

$$Threshold_4 = max\ (R_{7,8_{fault\ free\ and\ wheel\ slippage}}) = 3{,}5\ \text{N} \qquad (5.21)$$

The changes in the traction force calculations during the tests that are carried out with a degraded performance of the motor are represented in Figure 5.25. As seen in the figure, when performance degradation increases, the difference between the two different traction force calculations becomes more easily observable. Figure 5.26 shows the residual signals obtained in the motor performance degradation tests. As sees in this figure, the residual signal exceeds the threshold value in motor performance degradation case. Also, as seen in the test performed by issuing speed demands along both X_w and Y_w directions simultaneously, the R_8 signal exceeds the threshold value due to degraded performance of the first motor, whereas the R_7 signal does not exceed the threshold value. This indicates that the motor which actuates the first or third wheel, one of the wheels that is responsible for motion along the y_L direction, is faulty.

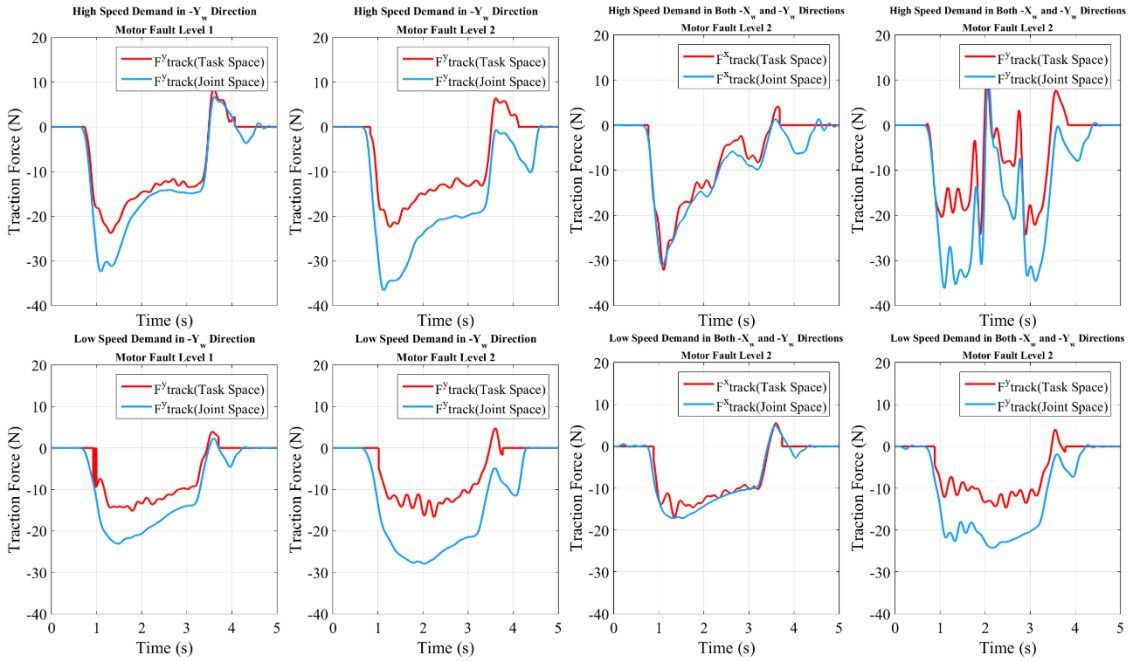

Figure 5.25. Traction force calculations in motor fault case

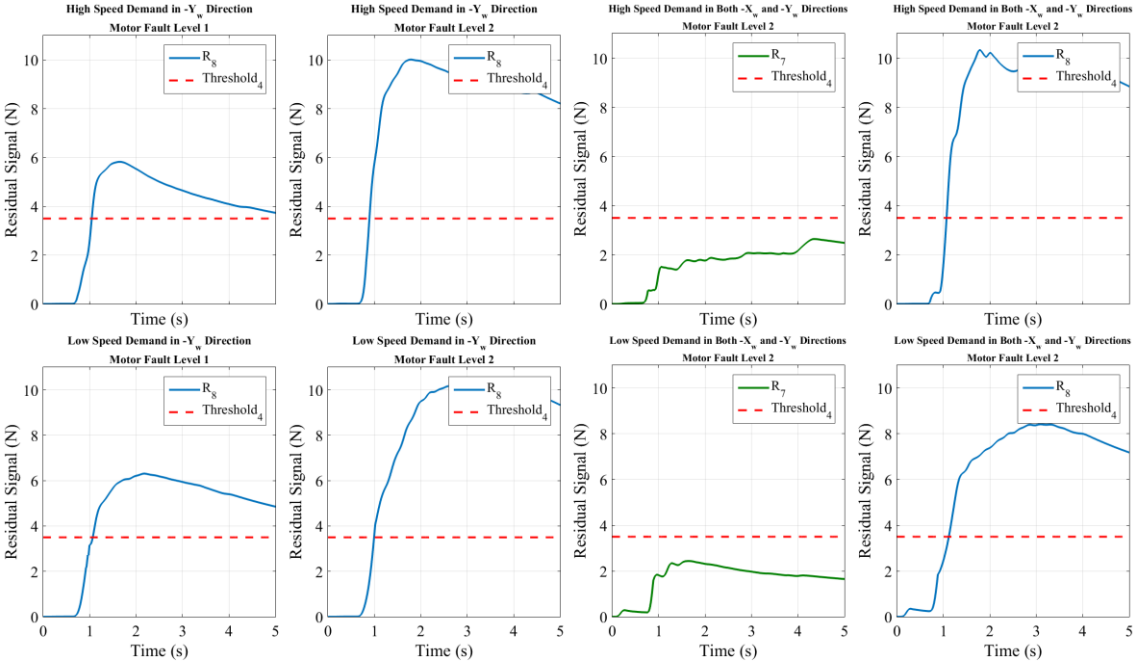

Figure 5.26. Residual signals in motor fault case

According to these test results, the motor performance degradation and the wheel slippage can be isolated with the logic table presented in Table 5.2. In this table, the wheel slippage, and the performance degradations in motors are represented by f_i $(i = 1, \dots, 8)$. The f_i's refer to the following faults:

f_1 : First wheel of the HMR slips

f_2 : Second wheel of the HMR slips

f_3 : Third wheel of the HMR slips

f_4 : Fourth wheel of the HMR slips

f_5 : The degraded performance on the motor which actuates first wheel of the HMR

f_6 : The degraded performance on the motor which actuates second wheel of the HMR

f_7 : The degraded performance on the motor which actuates third wheel of the HMR

f_8 : The degraded performance on the motor which actuates fourth wheel of the HMR.

In Table 5.2, "1" values on the first four columns indicates that the residual signal exceeds the $Threshold_3$ or the residual signal is the first signal within r_3, r_4, r_5 and r_6 that exceeds the $Threshold_3$, "0" indicates that the residual signal does not exceed the $Threshold_3$ or the residual signal is not the first signal that exceeds $Threshold_3$. "1" and "0" values in the fifth and sixth columns indicate if the residual signal exceeds the $Threshold_4$ value or not, respectively.

Table 5.2. A logic table created as a result of the tests for isolating faults of the HMR

	r_3	r_4	r_5	r_6	R_7	R_8
f_1	1	0	0	0	0	0
f_2	0	1	0	0	0	0
f_3	0	0	1	0	0	0
f_4	0	0	0	1	0	0
f_5	1	0	0	0	0	1
f_6	0	1	0	0	1	0
f_7	0	0	1	0	0	1
f_8	0	0	0	1	1	0

5.4. Conclusions

In this dissertation, the slippage of one of the wheels on HMR, and the performance degradation in one of the motors that drive the wheels are aimed to be diagnosed by using a model-based method. In this chapter, the studies performed to diagnose these two types of faults are explained. Initially, the fault diagnosis studies are carried out with the one quarter test setup that is used to modeling the friction between

the wheel and the ground. After the method is verified with the one-quarter test setup, it is adapted to the mobile robot. With the help of the dynamic equations of the robot (explained in Chapters 3 and 4), various states of the robot are estimated. Residual signals that are needed for fault detection, are calculated from the difference between the estimated states and the measured values. As a result of these tests, it is seen that wheel slippage and the performance degradation in one of the DC motors which actuate a wheel can be detected by these residual signals. To isolate these faults, the total traction forces in each axis of the HMR are calculated by the linear acceleration measurements in the task space and by the angular acceleration and measured current values in the joint space. Then, these traction forces that are calculated with respect to joint space and task space measurements are compared and two additional residual signals obtained as a result of these comparisons. Consequently, these two residual signals provide information about motor performance degradation. According to all test results, eight different faults can be isolated by using the developed residual signals.

For wheel slippage, which is a temporary fault, a recovery strategy is needed until the slippage ends. On the other hand, since the performance degradation in the motor is a permanent fault, it should be tolerated by a permanent method. Thanks to the diagnosis strategy presented in this chapter, the type of fault that occurs in the robot can be isolated, so this information allows applying a recovery strategy suitable for the type of fault. In Chapter 6, separate fault recovery strategies that are developed for wheel slippage and motor performance degradation faults are presented and evaluated.

CHAPTER 6

FAULT RECOVERY

As mentioned before, the hardware composition of a mobile robot varies from one to another, and it is important to recover the faults that may arise in those parts that are critical for the robot to complete its task. For this reason, to recover the faults that occur in a mobile robot performing critical tasks, various recovery plans should be made according to the type of fault. However, it may not be necessary to compensate for every fault that occurs in the robot with such a plan. If the severity of the fault and its effect on the robot's motion capability is low, it is possible to tolerate such faults with passive fault-tolerant control. Problems such as the robot's inability to maintain its heading direction during its movement may occur due to manufacturing faults in the mechanical parts of the mobile robot used in this dissertation and the gaps between passive rollers on the wheels used in the mobile robot. To tolerate such faults, a closed-loop control has been implemented to regulate the angular speed of the robot as the robot's top-level control algorithm. This closed-loop control also helps tolerating to some degree the wheel slippage and the motor performance degradation.

Mobile robots work in difficult environments, so the possibility of faults occurred in locomotion systems which are in interaction with the environment is high. One of the preventions to be taken against the faults that may occur in the locomotion systems is to design the locomotion system as a redundant system. For example, in legged mobile robots that are designed to have redundancy, a fault that may occur in one of the legs can be recovered with a new gait strategy to be applied with non-faulty legs. The use of three omnidirectional wheels in the robot used in this dissertation is sufficient to provide holonomic motion. However, in this case, a fault in one of the wheels causes the robot to lose its holonomic motion ability. In this case, if a recovery strategy is developed, the robot can only continue its task as a two-wheeled differential drive type robot. For this reason, the mobile robot used in the dissertation is designed in a four-wheeled structure, so it is proposed that it could continue the task without losing its holonomic motion ability with the recovery strategy to be applied in case of a fault in one of its wheels. However, to achieve this, it is necessary to make changes in the robot's control algorithm. Thanks

to the fault diagnosis algorithm described Chapter 5, wheel slippage in the robot and performance degradation in the motors can be diagnosed. After the fault diagnosis, in order for the robot to carry out the desired motion with the remaining wheels, the fault can be tolerated by adjusting the weight constants of each wheel in the weight matrix of the robot's kinematic equations given in Chapter 3. Initially, the efforts to tolerate the faults in the robot are carried out in the simulation environment. The simulation studies and tests are explained in the following section. After the tests are carried out in the simulation, studies with the mobile robot are carried out to recover wheel slippage and motor performance degradation. In the second section, the fault recovery algorithm implemented in the mobile robot is explained, and then the results of the tests performed by the mobile robot are given.

6.1. Fault Recovery Studies in Simulation

Initial verification of the proposed method for tolerating faults in the mobile robot is carried out through tests conducted in the simulation environment. The simulation model of the mobile robot is developed using Matlab™ Simulink™ Simscape™ blocks. Although the mobile robot contains a suspension system and various electronic components, they are not modelled for the validation tests in the simulation environment for the sake of simplicity. Therefore, the mobile robot is modeled as a chassis and four wheels connected to it in a computer-aided design (CAD) environment, and this model is transferred to Simulink™ as a model consisting of Multibody blocks. The model of the mobile robot developed in the CAD environment is presented in Figure 6.1. The study carried out in the simulation environment focused on tolerating the following fault types:

- Locomotion system fault
- Manufacturing related fault.

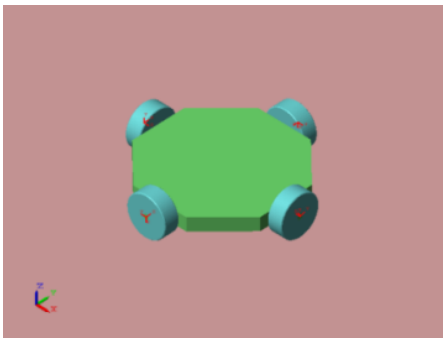

Figure 6.1. The CAD model of the mobile robot used in simulation

6.1.1. Locomotion System Fault

The method to be applied to tolerate the faults that occur in one of the wheels on the mobile robot is to minimize the required efforts from the faulty wheel and give more weight to the remaining three wheels. To accomplish this, the parameters of each wheel in the weight matrix given in Equation 3.11 are adjusted so that the robot performs the desired motion despite the faulty wheel. The studies done in the simulation are carried out in the kinematic level. In the study carried out in the simulation environment, speed demands are issued to the mobile robot on the task space, and wheel speeds are found according to the kinematic equations explained in Chapter 3. The wheels of the robot are controlled in an open-loop manner according to these speed demands. Dynamic effects are not taken into account in the tests performed in the simulation environment. Since it is not possible to simulate the performance degradation that may occur in one of the motors that actuate the wheels in the study performed at the kinematic level, the recovery work performed in the simulation environment has been carried out for the scenario when performance of the one of the wheels is fully degraded.

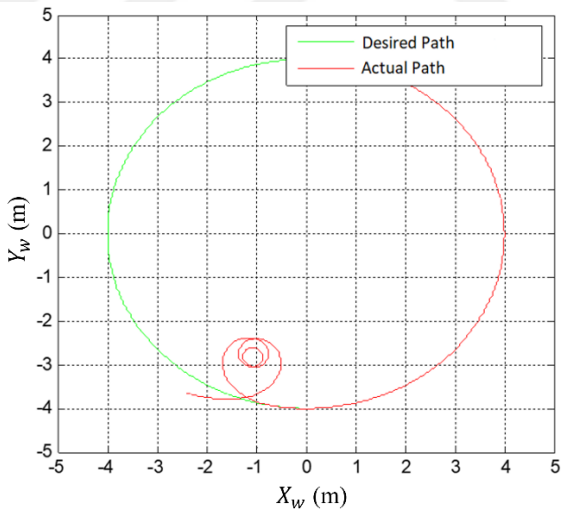

Figure 6.2. Desired and actual path of the mobile robot in the test achieved with equal weight parameters

In the simulation tests the mobile robot's initiation of position is selected as $(X_w, Y_w) = (0m, 4m)$ with respect to the global coordinate frame and its starting orientation is selected as $\theta_v = 0\ rad$. A speed demand is issued to the robot controller so that it completes a circular path of 8 m diameter in the clockwise direction in ten seconds

without changing its orientation. In order to test the recovery procedure, it is assumed that the performance of the first wheel fully degraded in the fifth second of the test, and immediately, this fault is diagnosed. This fault is generated by interrupting the demand signal transfer to the first wheel of the robot in the fifth second of the tests. In the first test, it is assumed that this fault could not be diagnosed, and equal weight values are given to each wheel from the initiation until the termination of the test. The result of the test performed by giving equal weights is presented in Figure 6.2, and the speed demands given to the wheels during the test are presented in Figure 6.3.

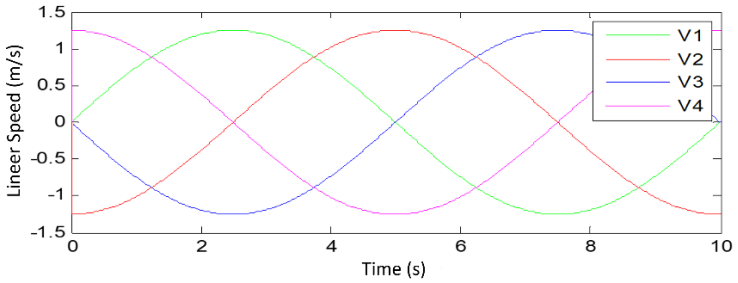

Figure 6.3. Speed demands of the wheels in the test achieved with equal weight parameters

In the second test carried out in the simulation, it is assumed that the fault occurring in the first wheel is diagnosed in the fifth second of the test. After this time, the weights of the wheels are changed, and the desired motion is achieved with the non-faulty wheels. This test for recovering the fault is repeated three times by increasing the weight value given to the first wheel and the position of the mobile robot is monitored. While the weight values of the wheels which do not have faults are assigned as $W_2 = W_3 = W_4 = 1$ during the tests, the weight of the faulty wheel is assigned as $W_1 = 1$ before the fault diagnosed, and after the fault $W_1 = 100,1000, 10000$ weight values are assigned one by one in each repetition. Here, the weight value in the weight matrix is inversely proportional to the effect of the wheel in performing the desired movement. Hence, as the weight value of the corresponding wheel increases, the effect of this wheel on achieving the desired movement decreases. In these tests, the desired path and the actual path of the robot are presented in Figure 6.4. As can be seen from the figure, as the weight value of the faulty wheel is increased after the fault is diagnosed, the desired motion is provided to the other three wheels. Consequently, it is observed that the robot followed a path closer to the desired path as the weight value of the faulty wheel is increased more. Figure 6.5

indicates the change of the linear speed demands of the wheels in the test performed by assigning $W_1 = 10000$ to the faulty wheel after fault is diagnosed. As seen in this figure, while the speed demand of the faulty wheel come closer to zero, speed demands are issued to the non-faulty wheels are increased in order for the robot to follow the desired path.

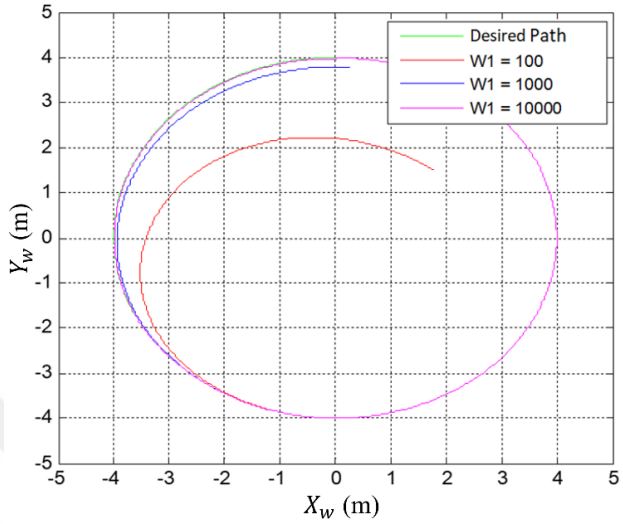

Figure 6.4. Fault recovery simulation results

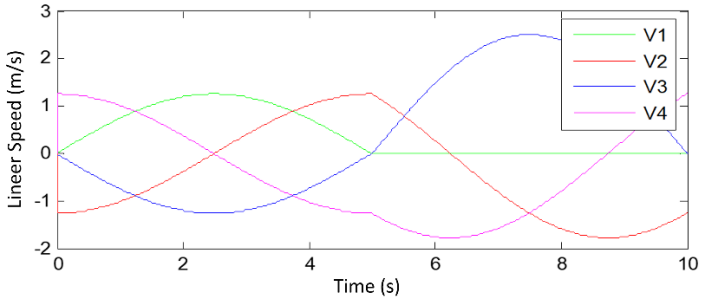

Figure 6.5. Desired wheel speeds in a fault recovery test ($W_1 = 10000$)

6.1.2. Manufacturing Related Fault

Another fault that is focused on this study is the fault that may be caused as a result of manufacturing tolerances of the robot. The mobile robot has a four-wheeled structure, and although the wheel rotation axes are placed relative to each other with 90° orientation change in the kinematic model, this orientation value can be a different value due to manufacturing tolerances. This may cause various control difficulties and the desired motion may not be performed. Therefore, it is proposed to control the angular velocity of the robot with a top-level controller to overcome the problems caused by such

defects. Accordingly, in the study carried out in the simulation environment, the angles between the wheel rotation axes relative to each other are changed to values different than 90° (Figure 6.6), and the top level-control algorithm described in Section 3.2.2 is used to recover this fault.

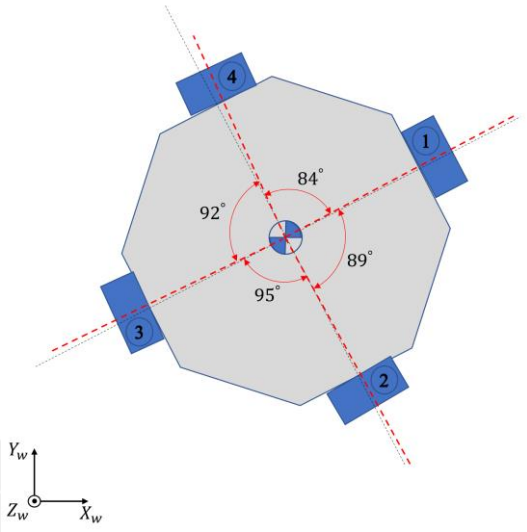

Figure 6.6. Manufacturing fault test configuration

During the verification tests performed in the simulation environment, speed demands are issued to the robot so that it can follow a square-shaped path (6m×6m) in the clockwise direction starting from $(X_w, Y_w) = (3m, -3m)$ position. In the test performed with an open-loop controller, the desired path and the actual path followed by the robot are presented in Figure 6.7.

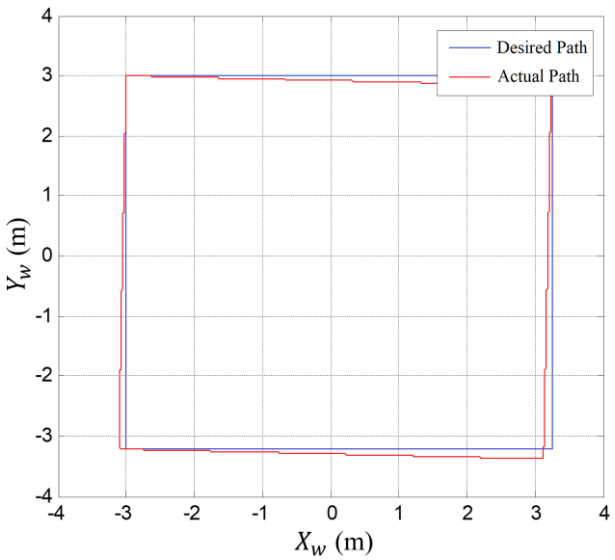

Figure 6.7. Path of the mobile robot in the test achieved with open-loop controller

In the second test performed by giving the same speed demands to the robot, a closed-loop control to regulate the angular speed of the robot is used as the top-level controller. The desired path and the actual path followed by the robot during this simulation test are presented in Figure 6.8. During the simulation of the robot with an open-loop controller, while the biggest position difference between the desired and the actual path is 0.20 m, this difference is 0.03 m for the robot with a closed-loop controller.

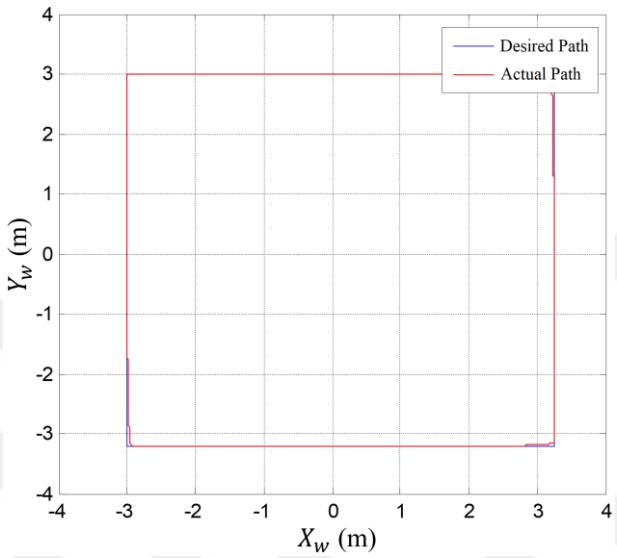

Figure 6.8. Path of the mobile robot in the test achieved with closed-loop controller

6.1.3. Discussions on Simulation Test Results

As can be seen from the results, when the performance of the one of wheels is fully degraded, the desired motion can be achieved with the remaining three wheels by increasing the weight of the faulty wheel which result in issuing minimized demands to the faulty wheel. However, since these tests are carried out in the kinematic level, it is assumed that there is no friction between the faulty wheel and the ground after the wheel stops. In the actual case, there is friction between wheel and ground, so this faulty wheel acts as a pivot point. Therefore, it is foreseen that it becomes difficult for the robot to achieve the desired movement with the remaining three wheels. For this reason, fault toleration should be achieved by taking the pivot point effect into account when the faulty wheel no longer rotates. On the other hand, in cases where the wheel can move freely or there is degradation in the performance of the motor driving the faulty wheel, these faults can be tolerated by adjusting the weights issued to the wheels, as it is the case in the tests

performed in the simulation environment. In the next section, the experimental studies for recovering performance degradation in one of the motors and wheel slippage are explained.

6.2. Fault Recovery Studies with HMR

Wheel slippage due to oil-like materials spread on the ground or object entering between the wheel and the ground is a temporary fault. Since the wheel slippage may disappear by itself during the motion of the robot, the recovery strategy to be developed for this fault should be executed until the fault disappears. However, since the performance degradation in the motor is a permanent fault, the strategy to be developed for this fault should be a permanent one.

The method planned to use for recovery for the abovementioned faults is to issue a higher weight to the faulty wheel with respect to other wheels to minimize the required efforts from faulty wheel and then the desired motion of the mobile robot is achieved with mainly the remaining three non-faulty wheels. The weights of the wheels can be adjusted temporarily or permanently according to the fault type. Two different recovery strategies for these two faults can be developed by adjusting the weight matrix that contains the weights to be issued to the wheels. The fault recovery strategy used in the dissertation is explained in Figure 6.9.

While driving the mobile robot according to the speed demands generated from the operator's demands or a trajectory generation algorithm, when there is no fault, the diagonal elements of the weight matrix expressing the weights to be issued to the wheels are selected to be equal or 1 without the loss of generality. Thanks to the fault detection and isolation (FDI) algorithm that operates in real-time during the motion of the robot, a weight adjustment strategy is developed according to the type of fault as indicated in Figure 6.9: 1) motor performance degradation recovery strategy indicated with red dashed line, 2) wheel slippage recovery strategy indicated green dashed line.

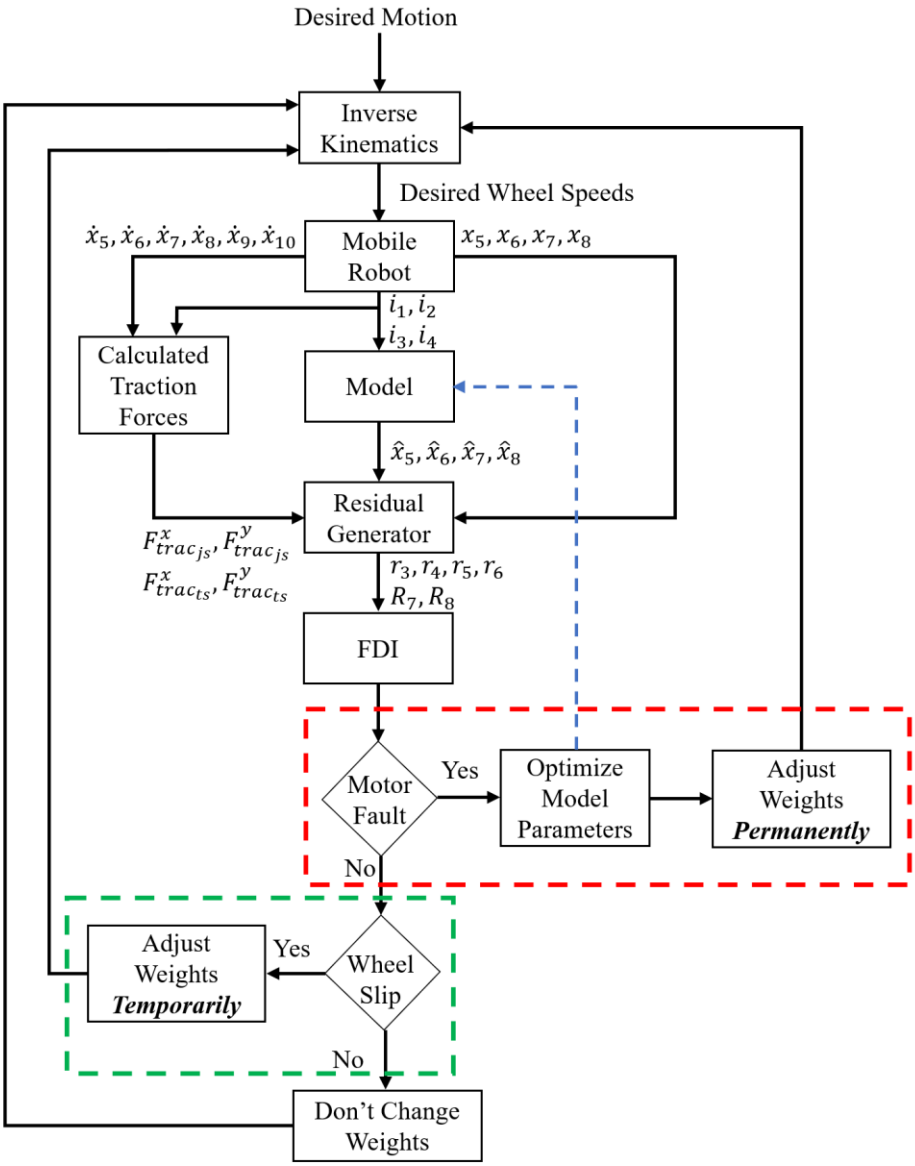

Figure 6.9. Fault recovery algorithm flowchart

6.2.1. Motor Performance Degradation Recovery

If the isolated fault by the FDI algorithm is performance degradation that occurs in one of the motors, the motion of the robot should be continued by adjusting weights of the wheels and the motion can be achieved with the non-faulty wheels. Since the fault is permanent after the fault occurrs in one of the motors, the weight values should be adjusted permanently. Also, the point to be noted here is that the parameters of the faulty motor in the dynamic equations of the robot are changed permanently. This means that the robot that continues the task is now a different robot in terms of how it moves with respect to its initial configuration. For this reason, the parameters in the model of the robot

should be optimized according to the new situation for the robot to continue tolerating fault new faults after motor performance degradation.

6.2.1.1. Model Optimization Algorithm

In the case of performance degradation in a motor, the motor produces less torque when compared to the actual current drawn by the motor. It is assumed that this fault changes the torque constant of the motor after the performance degradation. For this reason, the model of the robot can be optimized according to the new situation after the motor fault by estimating the new torque constant of the faulty motor. Residual signals that directly indicate motor fault (R_7, R_8) can be used to estimate torque constant.

As shown in Figure 5.18, to reduce the performance of one of the motors that actuate the wheels, an additional motor is connected in parallel to the motor driver. Also, two different levels of motor performance degradation (named Level 1 and Level 2) are achieved by applying two different levels of force to the output shaft of this additional motor. In the tests achieved by issuing high-speed demands in -Y_w direction, while the maximum traction force value calculated by using task space measurements is 35 N during the acceleration interval in the fault-free case, it is measured about 25 N in the first performance degradation level (Figure 6.10).

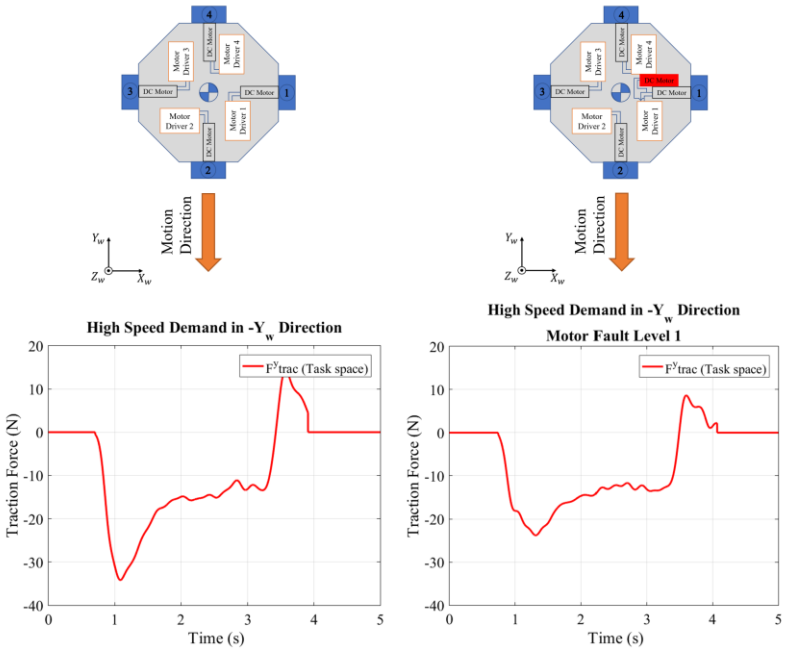

Figure 6.10. Calculated traction forces with respect to task space measurements in tests achieved in -Y_w direction

The traction force drops in -Y_w direction due to a faulty motor during the acceleration interval is approximately 28,5%. As can be seen in Figure 6.10, the motion on this direction is provided by the first and the third wheels of the robot. However, since only one of the motors that actuate the wheels that provide the motion in this direction is faulty, the performance degradation in the faulty motor should be twice of this value. According to this traction force drop, performance degradation in a faulty motor that is responsible for the motion in this direction should be 57%. This value is found 80% in the second performance degradation level.

In the case of a motor fault, the torque constant of the faulty wheel should decrease at the same rate to produce the required traction force. To find the new torque constant, residual signals obtained from traction forces calculated according to joint space and task space measurements obtained in previous tests are used (Figure 6.11).

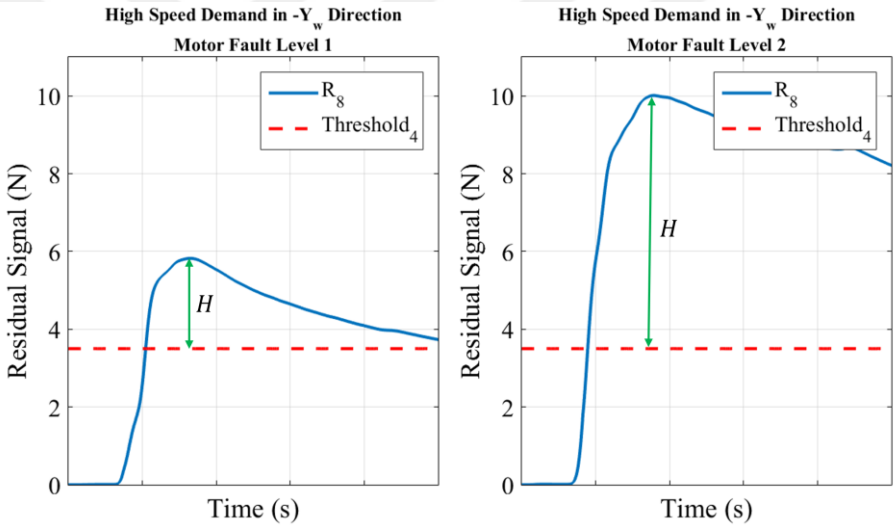

Figure 6.11. Residual signals during motor fault tests

As can be seen in Figure 6.11, the maximum value reached by the residual signal varies according to the different fault levels in the motor in the tests performed with the same speed demands given to the robot in the same direction. When the fault level in the motor increased, the maximum value reached by the residual signal increased accordingly. This maximum value reached by the residual signal includes information regarding the amount of motor fault. However, when estimating the torque constant of the faulty motor from this residual signal, the point to be considered is the threshold value. The motor fault is determined according to whether the residual signal exceeds the threshold value, and it is assumed that there is no fault in any of the motor for values up

to the threshold value of the residual signal. For this reason, for the residual signal, which is equal or less the than threshold value, the motor is considered 0% faulty. Therefore, after the motor fault is diagnosed, while the new torque constant of the faulty motor is estimated, the difference between the threshold value and the maximum value reached by the residual signal (indicated by H in Figure 6.11) is used. While this value is approximately 2.5N in the test performed with first level motor fault, it is found as 6.5N at the second fault level. The 2.5N value indicates 57% performance degradation in the faulty motor and 6.5N indicates an 80% performance degradation. These values are plotted in Microsoft™ Excel™ and the trendline of the obtained graph is found as a 3rd order polynomial (Figure 6.12). Accordingly, new torque constant of the faulty motor formulated as given in Equations 6.1 and 6.2.

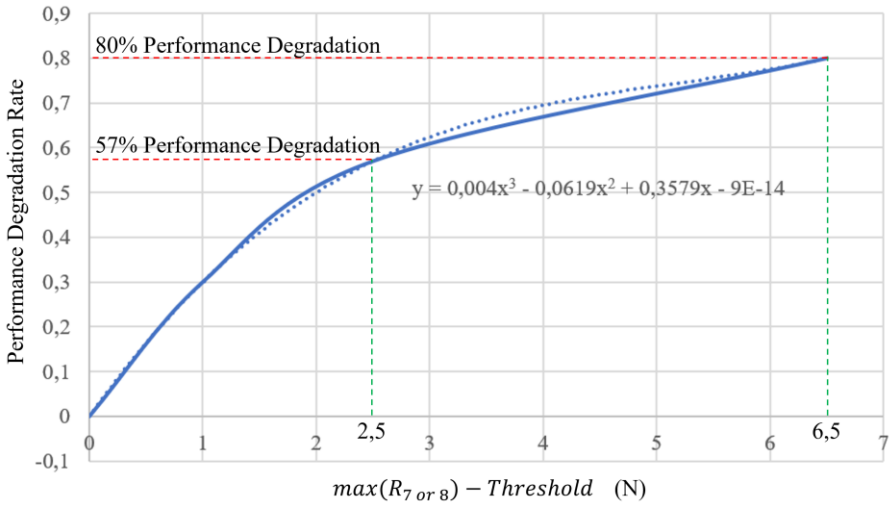

Figure 6.12. Performance degradation rate graph

$$H = max(R_{7\ or\ 8}) - Threshold \tag{6.1}$$

$$K_{t_m} = K_t(1 - (0{,}004H^3 - 0{,}0619H^2 + 0{,}3579\mathrm{H})) \tag{6.2}$$

where K_{t_m} is optimized torque constant of the faulty motor, K_t is torque constant of the motor before the fault.

After the torque constant estimation of the faulty motor is formulated, a real-time model optimization algorithm is developed. The flow chart of the developed optimization algorithm is given in Figure 6.13. In the example given in Figure 6.13, the motor fault is diagnosed according to the residual signal exceeding the threshold value in 1.1s of the

test. After this time, the maximum value of the residual signal is given in Equation 6.2 and the torque constant of the faulty motor is estimated in real time. At the same time, the model is optimized in real time with this estimated torque constant. Thanks to the optimized model, the traction force value calculated in the joint space after a certain amount of time approaches the traction force value calculated in the task space. This ensures that the maximum value of the residual signal remains at a constant value. Therefore, after this time, the torque constant calculated by Equation 6.2 also reaches a constant value. As mentioned before, after the motor fault is diagnosed and the fault is recovered with the recovery algorithm, the robot will be able to continue its task with a different robot configuration. However, in this case, the residual signal should be reset and dropped back below the threshold value in order not to diagnose the same motor fault. For this, the residual signal is reset after the torque constant reaches a constant value.

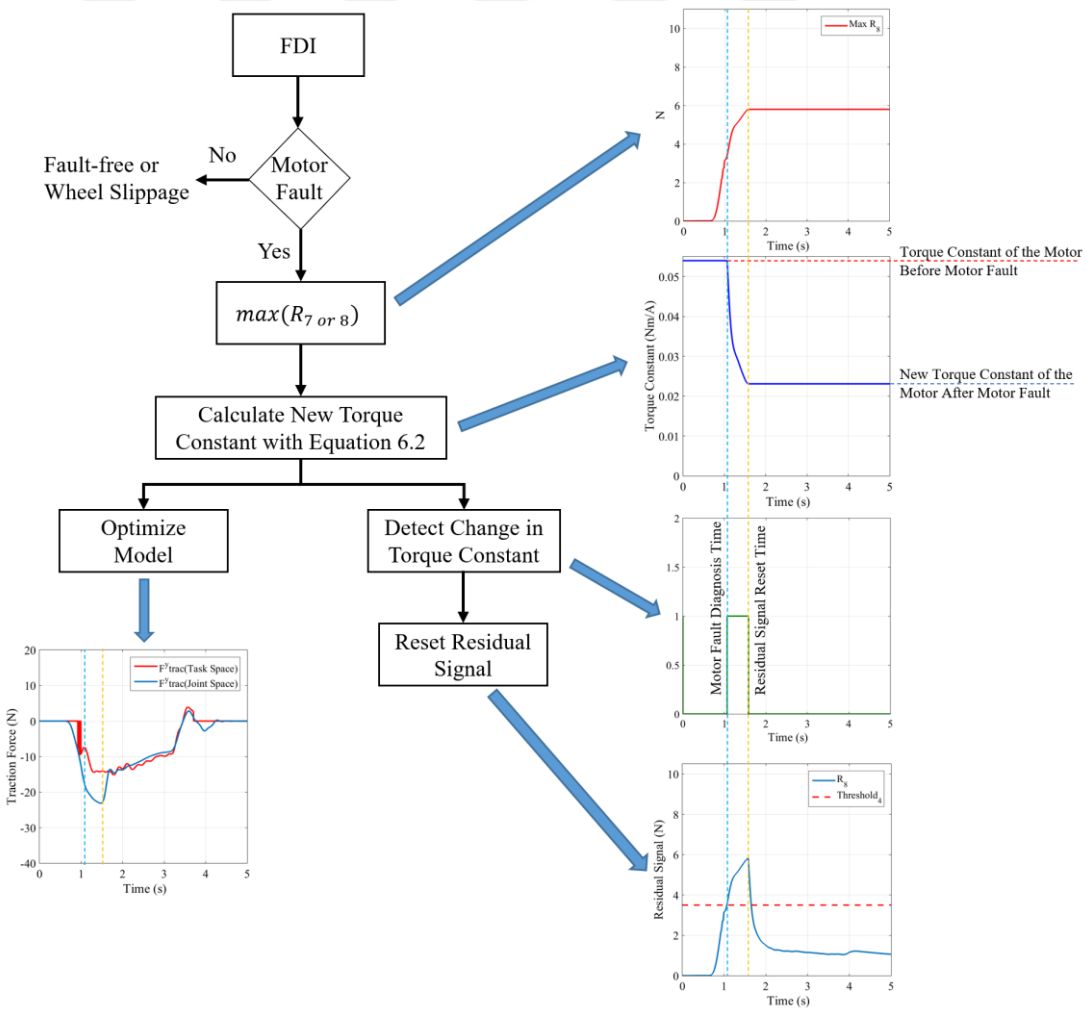

Figure 6.13. Model optimization flow chart

To verify the torque constant optimization algorithm of the faulty motor, the data obtained in motor fault tests presented in Chapter 5 are used. During verification tests, after the motor fault is isolated, the model of the robot is optimized with the new torque constant. Figure 6.14 shows the traction force results obtained when the model optimization algorithm is not functioning, and when the model optimization algorithm is functioning. As can be seen in Figure 6.14, as the model is optimized after the fault is detected, the calculated traction forces value with respect to the measured data in the joint and the task space are close to each other. The residual signal results are represented in Figure 6.15. In the tests achieved when the model optimization algorithm is not functioning, residual signals exceed the threshold value due to faulty motor. On the other hand, when the fault diagnosis and the model optimization algorithms are applied, the residual signal falls below the threshold after a certain amount of time.

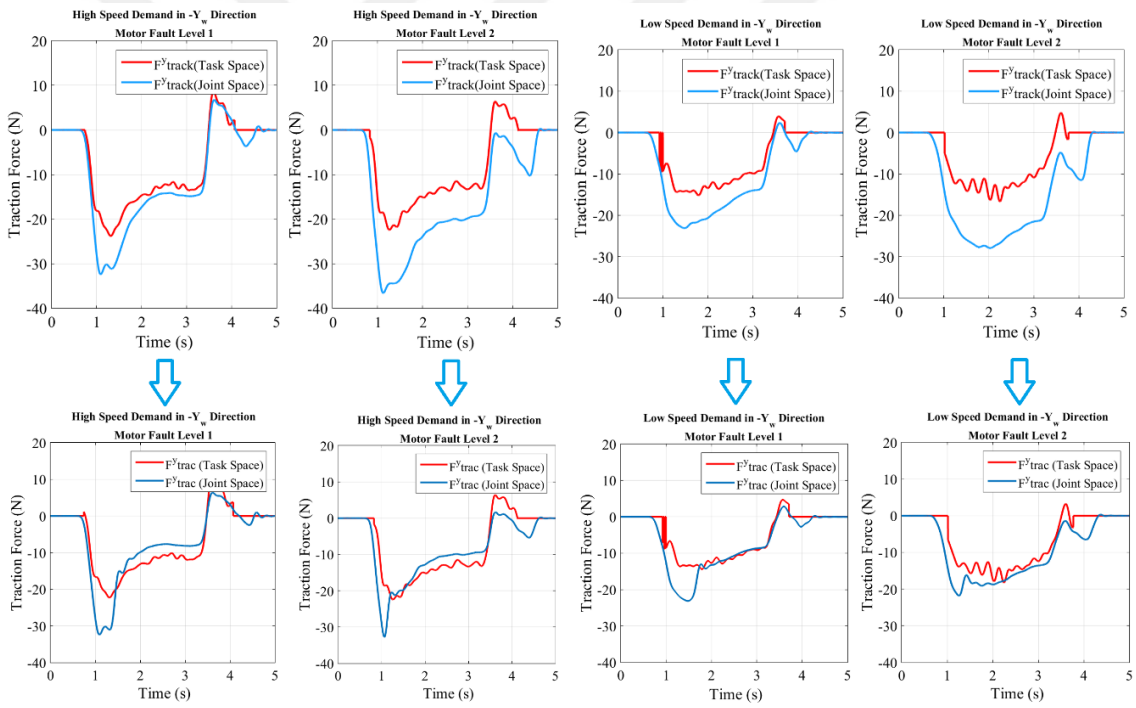

Figure 6.14. Calculated traction force results in optimization tests, upper figures: when optimization closed, buttom figures: when fault diagnosis and optimization open

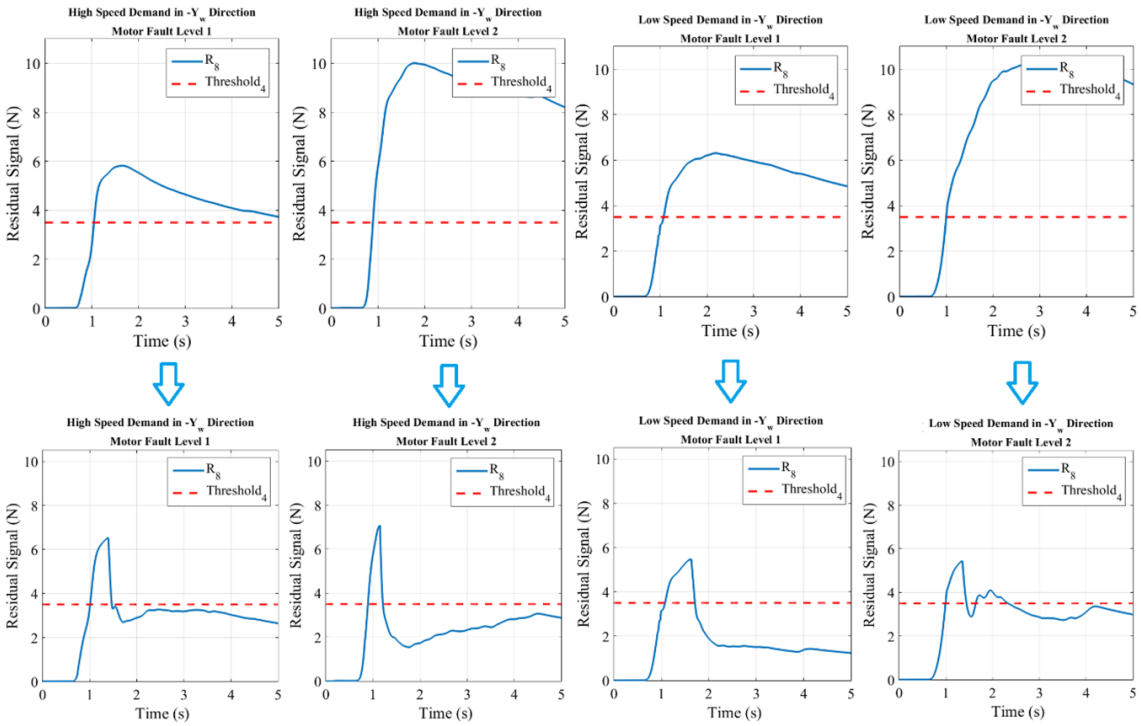

Figure 6.15. Residual signal results in optimization tests, upper figures: when optimization closed, buttom figures: when fault diagnosis and optimization open

6.2.1.2. Motor Performance Degradation Recovery Tests

After the model optimization algorithm is verified, the performance of one of the motors that actuates one of the wheels is reduced and this fault is recovered by applying the motor fault recovery strategy. To recover this fault, the applied method is to adjust the weights given to the wheels permanently according to the optimized torque constants after the fault is diagnosed. While $W_{non-faulty} = 1$ is given to the non-faulty wheels after the fault is diagnosed, the following equation is used for adjusting the weight value of the wheel that has a faulty motor.

$$W_{faulty} = \mathrm{K}_t / K_{t_m} \tag{6.3}$$

In the motor fault recovery tests, an additional motor is connected parallel to the first wheel of the robot as shown in Figure 5.18 and it is checked whether the robot could tolerate this fault when the proposed recovery strategy is applied. The tests are performed by giving high-speed demand in Y_w direction in both cases when the fault recovery

method is functioning and not functioning. The weight values given to the faulty wheel in both cases are represented in Figure 6.16.

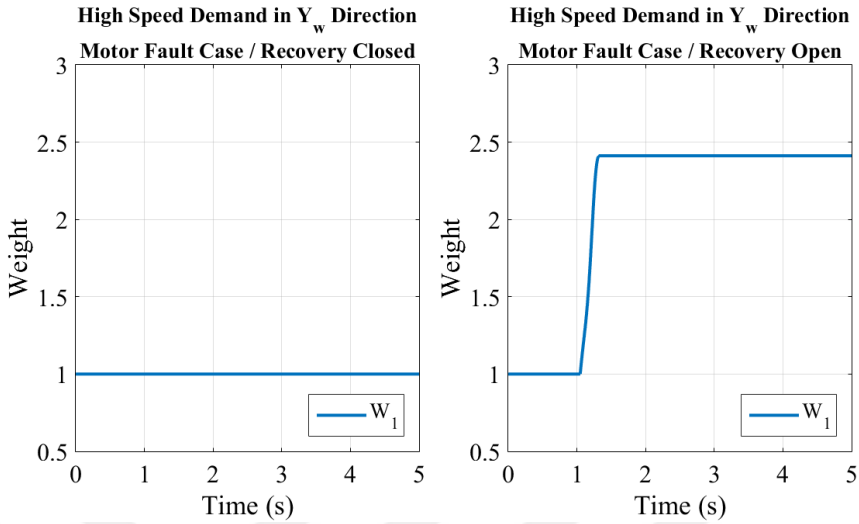

Figure 6.16. Given weights to the faulty wheel in motor fault recovery tests

In the case of the motor fault, the orientation of the robot is changed undesirably during the movement, as the faulty wheel is forced to make the desired motion. Although the top-level control for the angular speed regulation of the robot can tolerate this fault to a certain level, there may be minor orientation variations. With the applied recovery strategy, it is aimed to improve the orientation variations caused by the performance degradation in one of the motors. The orientation variations obtained in the recovery tests performed with motor fault are represented in Figure 6.17. In this test, the aim is to maintain the orientation of the mobile robot at its initial condition. Motion is initiated at 0.5s of the test and the orientation change of the robot is close to each other in both tests, until the performance degradation in the motor is diagnosed. In the test without the recovery algorithm, it is seen that there is a continuous increase in the robot's orientation from the moment the motion starts until the end of motion. On the other hand, in the test performed with the recovery algorithm, the orientation change in negative direction stopped after the recovery algorithm is automatically activated and the weights of the wheels of the robot are adjusted according to the new situation, and the robot started to recover the undesired changes in its orientation. However, as a consequence of the adjusted weights, the orientation of the robot changed in the positive direction (according to the axes of the selected frame) during the acceleration interval of the motion. On the other hand, it is seen that the orientation change of the robot is constant in the part of the

test when the robot moves with zero acceleration demand and moves into to a constant speed phase in time between 2.5s to 3s. After 3s, the robot decelerated and completed its movement around 4.1s. The orientation of the robot is changed in the negative direction in this period of time that the robot decelerates unlike the moment of acceleration. Although the robot moves with the new weights adjusted by the recovery algorithm, the orientation changes occur in the acceleration and deceleration parts of the motion, but the orientation remains constant in the part where the robot moves at a constant speed. In addition, as can be seen from the Figure 6.17, in the test performed with the recovery algorithm is functioning, the greatest orientation change during the robot's movement is lower than the value when the recovery is not functioning.

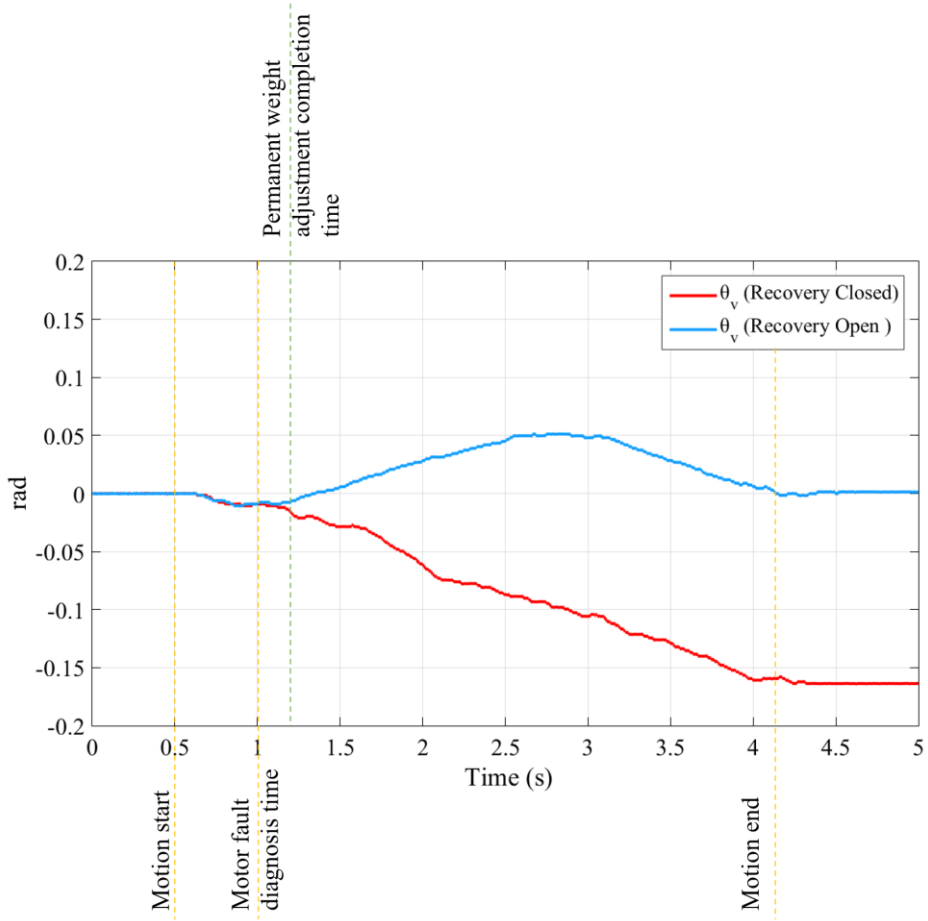

Figure 6.17. Orientation of the mobile robot in motor fault recovery tests

6.2.2. Wheel Slippage Recovery

As mentioned before, slippage in one of the wheels of the robot may cause the robot not be able to follow the desired motion. In traction control systems applied in

automobiles, the wheel slippage is estimated from the measured wheel speeds and road holding of this wheel is ensured by reducing the speed of the slipping wheel by the brake system. In this dissertation, similar to the traction control concept in automobiles, it is aimed to diagnose the wheel slippage by the developed fault diagnosis algorithm and increase the weight of the slipping wheel to reduce the effect of this fault on the motion of the mobile robot. After wheel slippage is diagnosed, the four residual signals obtained from measured and estimated speed differences (r_3, r_4, r_5, r_6) are used to temporarily adjust the weights of each wheel until the slippage condition passes. For this, after the wheel slippage is diagnosed, the weights issued to the wheels are determined according to the following equation.

$$W_i = \frac{r_{i+2}}{r_3 + r_4 + r_5 + r_6} 100 \quad ; \; i = 1,2,3,4 \tag{6.4}$$

Since the residual signal of the slipping wheel is higher than the other residual signals, the weight value calculated by Equation 6.4 is also high for this wheel. In this way, required effort of the slipping wheel in the desired motion of the robot is reduced. This motion is achieved by giving more effort to the other non-faulty wheels. The wheel slippage recovery tests are performed by giving high-speed demand in Y_w direction. In the tests, a nylon piece is placed under the first wheel of the robot. The residual signal changes obtained during the wheel slippage tests are represented in Figure 6.18. Also, the weight values given to the wheels in the test performed with the recovery algorithm are represented in Figure 6.19.

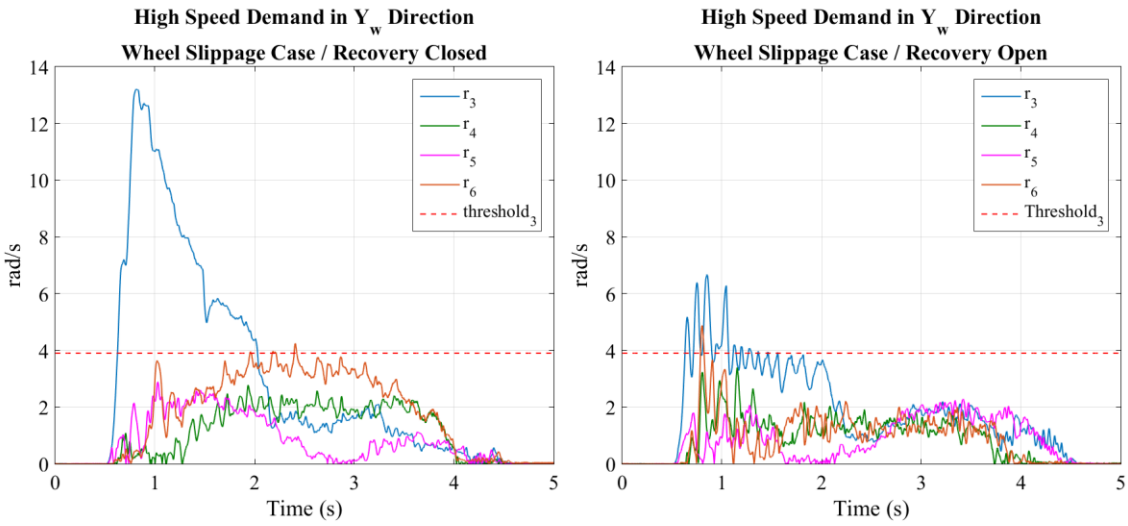

Figure 6.18. Residual signals in wheel slippage recovery tests

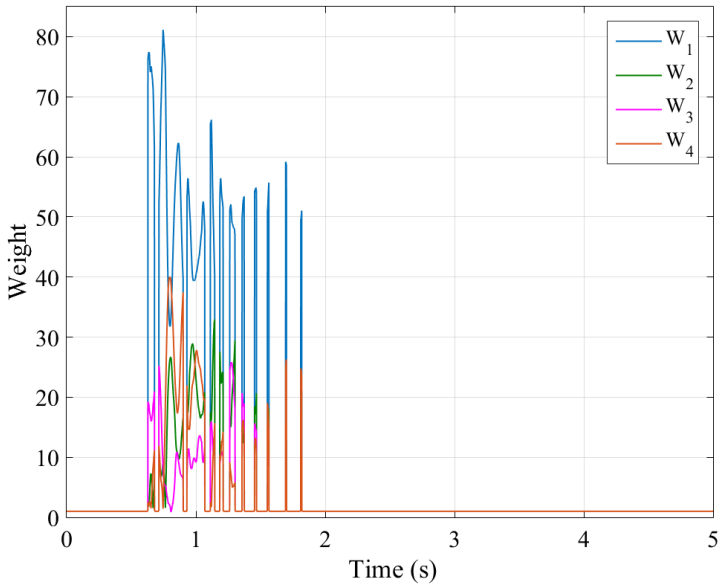

Figure 6.19. Given weights to the wheels during wheel slippage recovery test

In Figure 6.18, it is seen that the first wheel slips less when the recovery algorithm is functioning then it is not functioning. In this way, the robot can follow the desired motion with minimal variation in the orientation trajectory despite the fault. The orientation variations obtained in the tests performed in the case of wheel slippage are represented in Figure 6.20. As can be seen from Figure 6.20, in the test performed when the recovery algorithm is not functioning, the orientation of the robot changed significantly in the negative direction at the acceleration part due to the wheel slippage. As can be seen in the test results obtained when the recovery algorithm is not functioning in Figure 6.18, while the wheel slippage is high due to the high traction force demand at the acceleration part, the wheel slippage is decreased after the robot reaches a constant speed due to the lower traction force demand in this part of the motion. For this reason, in this test, the orientation change is also fixed after 2 s when the robot reaches a constant speed. On the other hand, in the test performed with the recovery algorithm, the weight values are adjusted according to Equation 6.4 and the effort of the slipping wheel on the motion is reduced after the residual signal exceeds the threshold value. This causes the speed of the wheel to decrease, accordingly residual signal of the faulty wheel falls below the threshold value again. Since the residual signal falls below the threshold value, equal weights are given to the wheels and then the wheel slippage increase again. Every time the residual signal exceeds the threshold value, the weights of the wheels are adjusted, and when the residual signal drops below the threshold value, the weights of all wheels are selected to be equal. This situation caused the wheel slippage to remain constant

around the threshold value. In this way, although there is some change in the orientation in the acceleration part of the motion due to the faulty wheel, this change is very small compared to the situation where recovery is not functioning.

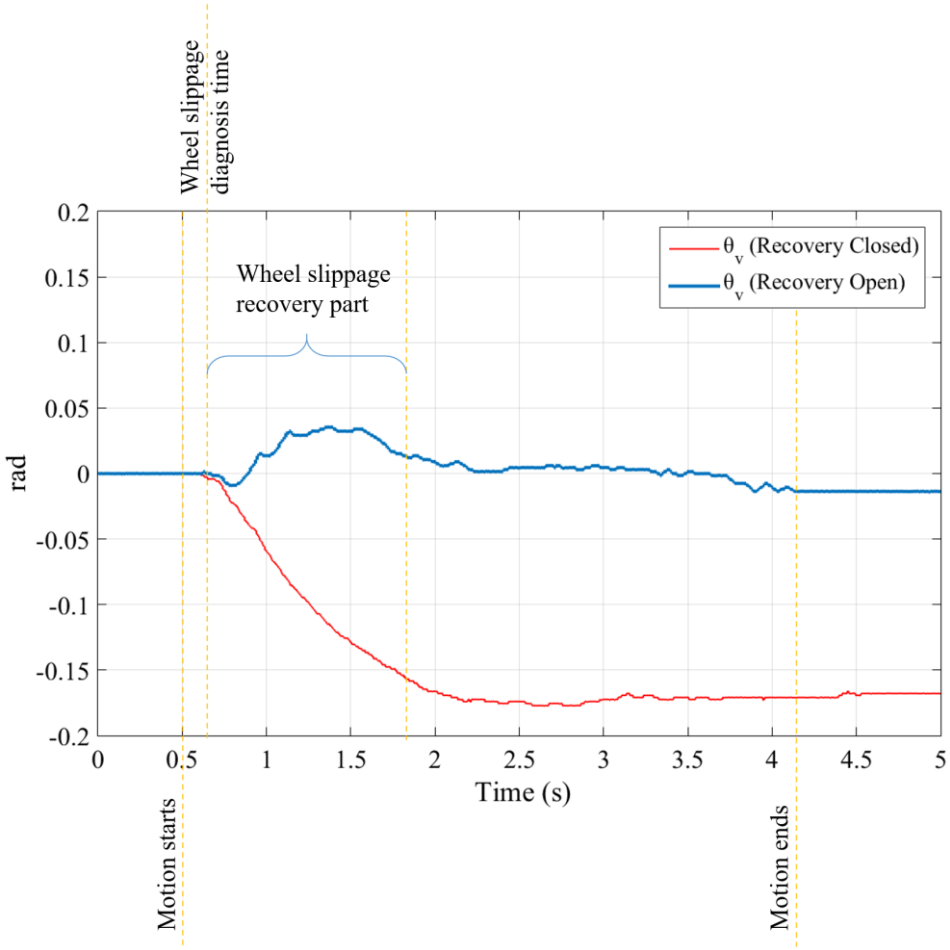

Figure 6.20. Orientation of the mobile robot in wheel slippage recovery tests

6.3. Conclusion

In this chapter, the efforts to recover the faults that may occur in the hardware of the mobile robot used in the dissertation are explained. Recovery studies are first carried out in a simulation environment. The robot has a four-wheeled structure in order to facilitate the recovery of faults. The idea is that if one of the wheels is faulty, the robot is able to perform the task with the remaining three wheels without losing its holonomic motion ability. If there is a fault occurred in the wheels, the desired motion of the robot can be achieved by giving more effort to the non-faulty wheels thanks to the weighted pseudo inverse method applied in the robot's kinematics. In order to verify the method to be applied, the first tests are performed in the simulation environment and the simulation

results are presented in the second section. According to the simulation results, it is seen that the desired motion can be achieved by reducing the weight of the faulty wheel and giving more effort to the non-faulty wheels after fault is diagnosed. Another method tested in the simulation environment is to tolerate the undesired orientation changes of the robot caused by manufacturing defects with a top-level control. As a result of the tests in the simulation environment, it is observed that the robot performs the desired motion better despite manufacturing defects thanks to a top-level control that regulates the angular speed of the robot.

In the second section, firstly, the fault recovery concept for wheel slippage and motor performance degradation is explained. While in case of wheel slippage, the method used for recovery in the dissertation is basically the adjustment of the weights given to the wheels temporarily until the wheel slippage ends, in the case of motor fault, the weights are permanently adjusted due to this permanent fault. In case of motor fault, the model should be optimized according to the new situation in order for the robot to tolerate faults such as wheel slippage again after this fault occurred. Thanks to the algorithm developed for this, the torque constant of the faulty wheel can be estimated, and the model of the robot is optimized with this estimated value. In the verification tests of the optimization method, it is seen that traction force calculations with respect to joint space and task space close to each other after optimization. In addition, the residual signal obtained from these values after optimization also falls below the threshold value again. On the other hand, as seen in Figure 6.14, after the implementation of the residual signal optimization algorithm, the residual signal is very close to the threshold value in some test results or it may move over the threshold value even in a time interval, and this means false alarm. Because the threshold value is chosen according to the behavior of the robot when there is no fault in the robot, this threshold value can also be optimized after a motor fault occurs. Methods of optimizing the threshold value according to the false alarm rate, which are investigated in the literature (Ding, 2008), can be applied in the future algorithm improvement studies. In this way, it is possible to create a more dynamic algorithm. After these tests, the motor fault recovery strategy is tested. As a result of the tests, it has been observed that the problem of orientation change of the robot during the motion due to this fault can be tolerated a certain level thanks to the recovery strategy applied to the robot. In the tests carried out for the recovery of wheel slippage, it is observed that the amount of wheel slippage decreased significantly with the applied recovery method and the orientation change of the robot due to this fault is also reduced.

Since the work carried out in the simulation environment is done at the kinematic level, the pivot point effect caused by the faulty wheel is ignored. After the fault occurred in these tests, it is assumed that there is no friction between the faulty wheel and the ground, and hence, it is seen that the robot could continue its motion with three non-faulty wheels. On the other hand, if there is a fault in one of the wheels, the friction between this wheel and the ground affects the robot's motion. If the wheel becomes free to rotate after the fault, the friction between the wheel and the ground results in the rotation of the faulty wheel. Therefore, one of the important factors that increase the effect of the fault is the back-drivability of the motor that actuates the wheel. Since the motors used on the robot are gearhead motors, their back-drivability is low. For this reason, it becomes difficult for the faulty motor to rotate freely after the fault occurs. While the performance degradation in the motor approaches the full performance degradation, the pivot point effect due to the back-drivability will increase. Therefore, the method applied to recover for motor degradation can be applied up to some level of performance degradation.

CHAPTER 7

CONCLUSIONS

Some mobile robots perform very critical tasks under difficult operating conditions. Faults encountered during their tasks may cause the task to be interrupted or the task to fail completely. For this reason, mobile robots performing critical tasks should be prepared for faults that may arise during the operation. For this purpose, various fault tolerant control methods are used in the literature to tolerate the faults that occur in mobile robots. In AFTC methods, the fault should first be diagnosed with a diagnosis algorithm and recovered with an appropriate recovery strategy. In this dissertation, a four-wheeled holonomic mobile robot is studied to diagnose and recover its faults that occur in its hardware during the operation. For this purpose, initially, the fault-tolerant control methods used in the literature are investigated. FTC is not only a subject of the robotic field, but it is also used for tolerating the effects of the faults on the performance and stability of systems used in various areas. In the second part of the dissertation, the FTC methods are categorized, and the application procedures of these methods are explained. The faults that occur in mobile robots and the methods used in the literature to tolerate these faults are investigated further. Considering the hardware variety of mobile robots, there are also various faults that may occur in these parts. For this reason, it is aimed to apply the AFTC method for the mobile robot considered in the dissertation because of its high fault toleration capacity and the ability to tolerate different types of faults.

The mobile robot used in the dissertation has the holonomic motion ability thanks to its omnidirectional wheels. These wheels provide the mobile robot with allow uncoupled planar motion ability mainly due to the passive rollers around wheels. Although the holonomic motion can be achieved by using three of these wheels, the mobile robot is designed in a four-wheeled structure to increase fault-toleration capability. Thanks to this structure, if one of the wheels of the robot is faulty, the robot can perform the desired motion with three non-faulty wheels. To recover the robot by changing the weight distribution between the wheels in case of a fault, the weighted pseudo-inverse method is used in the robot's kinematics. Various sensors have been used

in the robot to measure speed, acceleration, and current information which are required for the fault diagnosis algorithm.

The AFTC method is divided into two basic parts: diagnosis and recovery. One of the main purposes of the dissertation is to diagnose the slippage occurring in one of the wheels of the holonomic mobile robot and the performance degradation on the motor that actuates one of the wheels with a model-based algorithm. For this, the dynamic model of the mobile robot is needed. One of the important parts of robot dynamics for wheeled mobile robots is the friction characteristic between the wheel and the ground. Many wheels used in mobile robots do not have wheels used in automobiles, and since these wheels are generally designed for use in different applications such as trolley and wheeled lifting equipment, it is not possible to find accurate information about the frictional properties of these wheels. Therefore, the results of the studies performed to find the friction characteristic of the UTO wheels used in the mobile robot is the first contribution of the dissertation to the literature.

To model the longitudinal friction characteristics between the wheel and the ground, the LuGre model is selected from the wheel friction models in the literature and the model parameters are found with the help of the test setup which is built for this purpose. In the Chapter 4, identification studies of longitudinal friction model parameters for three different floor types are explained. The special structures of the omnidirectional wheels used in the holonomic mobile robot allow the motion in the lateral axis. Although the friction between the ground and the wheel during motion in this axis is less than the conventional wheels, it creates force and moment on the various connection elements of the wheel. Another contribution to the literature obtained in the dissertation is the investigation of the effect of lateral friction on the motion along the longitudinal axis.

Model-based fault diagnosis studies are carried out with the dynamic model of the robot, which is completed with the friction characteristic between the wheel and the ground with the help of the test setup. In the fault diagnosis studies of the mobile robot, firstly, the fault detection algorithm planned to be implemented in the robot is verified with the test setup. In cases of wheel slippage and motor fault, even if the source of the fault is different, they can create similar effects such as unwanted orientation changes in the robot. To develop different fault recovery strategies for different fault types, these faults should be detected and then isolated. As seen in the results of the tests performed with the test setup, thanks to the proposed fault diagnosis method, the presence of the fault can be detected, and the type of fault can be isolated. However, unlike the tests

performed with one wheel with the test setup, the mobile robot has four wheels and four motors connected to them. In this case, if it is assumed that there may be slippage in each wheel and performance degradation in each motor, eight separate faults should be diagnosed. Another contribution to the literature of this dissertation work is the development of a method that can isolate which of these eight possible faults is the actual fault occurring in the robot. As a result of the tests performed with the mobile robot, it is seen that the source of the fault in the robot can be isolated. In this way, it has been made possible to create a recovery strategy according to the type of fault in the next step.

The second purpose of the dissertation is to ensure that the fault is recovered so that the robot can continue its operation after this fault is diagnosed. Considering the tasks and working conditions of mobile robots, another issue that is as important as the diagnosis of the fault is the recovery of the fault. Two different strategies have been developed to tolerate the wheel slippage and motor performance degradation that may occur in the mobile robot used in the dissertation. In the case of wheel slippage due to particles contaminating the wheel or parts entering between the wheel and the ground, usually, the wheel returns back to its previous performance after these deteriorating effects are eliminated. Therefore, the recovery strategy applied for this fault has also been a temporary strategy applied until the effect of the fault is over. On the other hand, since the performance degradation in the motor affects the motion of the robot continuously after the fault occurs, the fault recovery strategy applied for this fault is also designed to be permanent. Thanks to the four-wheeled redundant structure of the robot, if a fault occurs in one of the wheels, it can be recovered by giving more weight to the non-faulty wheels without losing the robot's holonomic motion ability.

Since the fault is permanent in case of performance degradation in one of the motors, the model should be optimized to diagnose faults such as wheel slippage that occurs in the robot after this fault. Thanks to the algorithm developed for this, the torque constant of the faulty motor is estimated, and the model is optimized accordingly. The improvement in the motion of the mobile robot that is achieved with the recovery method applied during motor fault tests is observed in the orientation variation of the robot. As seen in Figure 6.17, while the orientation change is constantly increasing in the test performed without the recovery algorithm, it is seen that the orientation remains constant after a while after the fault is diagnosed and the algorithm is activated in the test performed while applying the recovery algorithm. Although there is some change in the orientation during the acceleration and deceleration moments, it is seen that the

orientation change that occurs when the recovery algorithm is turned on remains at a bounded level compared to the situation where recovery is not applied.

The traction control systems are used to increase the safety and driving capabilities of wheeled terrestrial vehicles such as automobiles. In such systems, the slippage of the wheel is predicted, and the speed of the slipping wheel is automatically reduced. In this way, the wheel is held on the road again. Another contribution of the dissertation is to tolerate wheel slippage occurred in the mobile robot similar to the traction control systems applied in the terrestrial vehicles. In the method applied for this, after the slipping wheel is isolated in the diagnosis part, it is aimed to reduce the effort of the slipping wheel on the motion of the robot until the slippage is eliminated. In the part of the motion while there is still wheel slippage fault, the desired motion is achieved by issuing more weight to the non-slipping wheels. In the recovery strategy designed for wheel slippage, residual signals generated from the difference between the estimated wheel speeds by the model and the measured wheel speeds are used to generate the weights of the wheels. These signals contain information about the amount of slippage of the wheels. After the slippage is detected, it is seen that the slippage of the wheel is significantly reduced in the test performed by giving the weights calculated using residual signals. Also, in these tests, it is seen that the change in the orientation of the mobile robot due to the effect of the fault significantly decreased.

The assumption made in this dissertation is that only one fault occurs in the system at a time. However, in practice, it is highly possible that more than one wheel or even all wheels can slip as a result of oil-like substances contaminating the wheels' contact surface. In such a situation, since there is a difference between the system model and the real system, a fault can be detected from the residual signals obtained from the wheel speeds in the developed diagnosis algorithm. However, in case of slippage of more than one wheel, it is not possible to recover this fault by adjusting the weight of the wheels. In this case, the applied method may be adjusted to allow the robot to move with lower acceleration values until the conditions causing the slip are eliminated.

Algorithms developed for the diagnosis and recovery of wheel slippage and performance degradation in one of the motors can also be applied to tolerate such faults in different types of wheeled robots. Although model-based fault diagnosis is applied for a holonomic mobile robot which has UTO wheels, it is possible to diagnose the slippage in mobile robots using conventional wheels with the help of the wheel speeds estimated

with the robot model to be created by similarly modeling the friction between the wheel and the ground.

In this dissertation, the performance degradation in the motor that actuates one of the wheels of the mobile robot is focused on and this fault is recovered to a certain level. However, while the performance degradation in the motor approaches the full performance degradation, the faulty wheel acts as a pivot point and the negative effect of this situation on the motion of the robot increases. In future studies, the faulty wheel can be modeled as a pivot point and the fault recovery method can be developed for the full performance degradation that may occur in one of the motors. In addition, the robot can continue to operation with two non-faulty wheels as two wheeled differential drive robots in case of fault occurred in two wheels. Therefore, this scenario can be handled in future studies.

REFERENCES

Agarwal, R., Grosspietsch, K.-E. (2007). Fault Tolerance for Autonomous Robots by Means of Adaptive Filters. *In 20th International Conference on Architecture of Computing Systems*.

A&D Technology. viewed 27 September 2020, https://aanddtech.com/2018/03/02/fbttr/, https://aanddtech.com/2018/03/05/vms/.

Aghili, F. (2011). Fault-Tolerant Control of Robot Servomotors. *In IEEE International Conference on Robotics and Automation*, 2757-2763.

Al Mamun, M.A., Nasir, M.T., Khayyat, A. (2018). Embedded System for Motion Control of an Omnidirectional Mobile Robot. *IEEE Access 6*, 6722-6739.

Alwi, H., Edwards, C., Pin Tan, C. (2011). Fault Detection and Fault-Tolerant Control Using Sliding Modes. *Advances in Industrial Control Book Series, Springer-Verlag London Limited*.

Amin, A.A., Hasan, K.M. (2019). A review of Fault Tolerant Control Systems: Advancements and applications. *Measurement*, 143, 58–68.

Amory, A., Meyer, B., Osterloh, C., Tosik, T., Maehle, E. (2013). Towards Fault-Tolerant and Energy-Efficient Swarms of Underwater Robots. *In 27th International Symposium on Parallel & Distributed Processing Workshops and PhD Forum*, 1550-1553.

Antonelli, G. (2003). A Survey of Fault Detection/Tolerance Strategies for AUVs and ROVs. *Fault Diagnosis and Fault Tolerance for Mechatronic Systems: Recent Advances*, 109-127.

Arrichiello, F., Marino, A., Pierri, F. (2014). Distributed Fault Detection and Recovery for Networked Robots. *IEEE/RSJ International Conference on Intelligent Robots and Systems*, 3734-3739.

Axenie, C., Cemega, D. (2010). Mobile Robot Fault Tolerant Control Introducing ARTEMIC. *In 2nd International Conference on Education Technology and Computer (ICETC)*, 6-1.

Baghernezhad, F., Khorasani, K. (2016). Computationally Intelligent Strategies for Robust Fault Detection, Isolation, And Identification of Mobile Robots. *Neurocomputing*, 171, 335-346.

Balakrishna, R., Ghosal, A. (1995). Modelling of Slip for Wheeled Mobile Robots. *IEEE Transactions on Robotics and Automation*, 11(1), 126-132.

Blanke, M., Izadi-Zamanabadi, R., Bogh, S.A., Lunau, C.P. (1997). Fault-Tolerant Control Systems - A Holistic View. *Control Engineering Practice*, 5(5), 693-702.

Boskovic, J.D., Mehra, R.K. (2003). Failure Detection, Identification and Reconfiguration in Flight Control. *Fault Diagnosis and Fault Tolerance for Mechatronic Systems: Recent Advances*, 129-167.

Brandstötter, M., Hofbaur, M.W., Steinbauer, G., Wotawa, F. (2007). Model-Based Fault Diagnosis and Reconfiguration of Robot Drives. *In International Conference on Intelligent Robots and Systems*, 1203-1209.

Canudas-de-Wit, C., Tsiotras, P. (1999). Dynamic Tire Friction Models for Vehicle Traction Control. *In Proceedings of the 38th IEEE Conference on Decision and Control*, 3746-3751.

Canudas-de-Wit, C., Tsiotras, P., Velenis, E., Basset, M., Gissinger, G. (2003). Dynamic Friction Models for Road/Tire Longitudinal Interaction. *Vehicle System Dynamics*, 39, 189-226.

Carlson, J., Murphy, R.R. (2003). Reliability Analysis of Mobile Robots. *In International Conference on Robotics & Automation*, 274-281.

Carlson, J., Murphy, R.R. (2005). How UGVs Physically Fail in the Field. *IEEE Transactions on Robotics*, 21(3), 423-437.

Carrasco, R.A., Cipriano, A. (2007). Layered Architecture for Fault Detection and Isolation in Cooperative Mobile Robots. *Proceedings of the European Control Conference*, 2950-2955.

Çelik, O. (2016). Redundant Mobile Robot Control. *M.Sc. Thesis in İzmir Institute of Technology*.

Clover, C.L., Bernard, J.E. (1998). Longitudinal Tire Dynamics. *Vehicle System Dynamics*, 29, 231-259.

Dahl, P.R. (1968). A Solid Friction Model. *The Aerospace Corporation*.

Daigle, M.J., Koutsoukos, X.D., Biswas, G. (2007). Distributed Diagnosis in Formations of Mobile Robots. *IEEE Transactions on Robotics*, 23(2), 353-369.

Dharmaweera, M.N., Khoo, S.Y. (2010). Navigation of Four-Wheel-Steering Mobile Robots Using Robust Fault-Tolerant Sliding Mode Control. *In 11th International Conference on Control, Automation, Robotics and Vision*, 1375-1380.

Ding, S.X. (2008). Model-based Fault Diagnosis Techniques: Design Schemes, Algorithms, and Tools, *Springer-Verlag*.

Duan, Z., Cai, Z. (2009). Particle Filters Based Fault Diagnosis for Internal Sensors of Mobile Robots. *In International Conference on Measuring Technology and Mechatronics Automation*, 47-50.

Duan, Z.-H., Cai, Z.-X. (2006). Fault Diagnosis for Wheeled Mobile Robots Based on Adaptive Particle Filter. *In Fifth International Conference on Machine Learning and Cybernetics*, 370-374.

Erdogan, G., Alexander, L., Rajamani, R. (2011). Estimation of Tire-Road Friction Coefficient Using a Novel Wireless Piezoelectric Tire Sensor. *IEEE Sensors Journal*, 11(2), 267-279.

Eterno, J.S., Weiss, J.L., Looze, D.P., Willsky, A. (1985). Design Issues for Fault Tolerant-Restructurable Aircraft Control. *In Proceedings of 24th Conference on Decision and Control*, 900-905.

Filaretov, V.F., Zuev, A.V., Zhirabok, A.N., Procenko, A.A., Subudhi, B. (2015). Development of synthesis method of fault tolerant systems for autonomous underwater robots with navigation sensors failures. *In 23rd Mediterranean Conference on Control and Automation (MED)*, 335-340.

Filaretov, V.F., Zuev, A.V., Zhirabok, A.N., Procenko, A.A., Subudhi, B. (2015). Development of Synthesis Method of Fault Tolerant Systems for Autonomous Underwater Robots with Navigation Sensors Failures. *In 23rd Mediterranean Conference on Control and Automation (MED)*, 335-340.

Filaretov, V.F., Zuev, A.V., Zhirabok, A.N., Procenko, A.A., Subudhi, B., (2015). Development of Synthesis Method of Fault Tolerant Systems For Autonomous Underwater Robots With Navigation Sensors Failures. *In 23rd Mediterranean Conference on Control and Automation (MED)*, 335-340.

Fourlas, G.K. (2013). Fault Detection Approach for a 4 – Wheel Skid Steering Mobile Robot. *In IEEE International Conference on Industrial Technology*, 64-68.

Fourlas, G.K. (2014). On the Application of Structural Analysis to Fault Diagnosis of a Mobile Robot. *In International Conference on Robotics and Biomimetics*, 259-264.

Frank, P.M. (2004). Trends in Fault-Tolerant Control of Engineering Systems. *In 11th IFAC Symposium on Automation in Mining, Mineral and Metal Processing (MMM'04)*, 37(15), 377-384.

Ganganath, N., Leung, H. (2012). Mobile Robot Localization Using Odometry And Kinect Sensor. *In IEEE International Conference on Emerging Signal Processing Applications*, 91-94.

Gao, Z., Cecati, C., Ding, S.X. (2015). A Survey of Fault Diagnosis and Fault-Tolerant Techniques—Part I: Fault Diagnosis with Model-Based and Signal-Based Approaches. *IEEE Transactions on Industrial Electronics*, 62(6), 3757-3767.

Goel, P., Dedeoglu, G., Roumeliotis, S.I., Sukhatme, G.S. (2000). Fault Detection and Identification in a Mobile Robot Using Multiple Model Estimation and Neural Network. *In International Conference on Robotics & Automation San Francisco*, 2302-2309.

Han, K.-L., Choi, A.-K., Kim, J., Kim, H., Lee, J.S. (2009). Design and Control of Mobile Robot with Mecanum Wheel. *In ICROS-SICE International Joint Conference*, 2932-2937.

Harned, J.L., Johnston, L.E., Scharpf G. (1969). Measurement of Tire Brake Force Characteristics as Related to Wheel Slip (Antilock) Control System Design. *SAE Transactions*, 78, 909-925.

Hoshino, S., Seki, H., Ota, J. (2011). Optimal Maintenance Strategy in Fault-Tolerant Multi-Robot Systems. *In IEEE/RSJ International Conference on Intelligent Robots and Systems*, 2314-2320.

Hoshino, S., Seki, H., Ota, J. (2011). Optimal Maintenance Strategy in Fault-Tolerant Multi-Robot Systems. *In IEEE/RSJ International Conference on Intelligent Robots and Systems*, 2314-2320.

Hrizi, O., Boussaid, B., Abdelkrim, M.N., Aubrun, C. (2013). Fast Adaptive Fault Estimation Algorithm: Application to Unicycle Robot, *In Conference on Control and Fault-Tolerant Systems (SysTol)*, 714-719.

Iagnemma, K., Ward, C.C. (2009). Classification-Based Wheel Slip Detection and Detector Fusion for Mobile Robots on Outdoor Terrain. *Autonomous Robots*, 26(1), 33-46.

Isermann, R. (2005). Model-Based Fault-Detection and Diagnosis – Status and Applications. *Annual Reviews in Control*, 29(1), 71-85.

Isermann, R. (2011). Fault-Diagnosis Applications, Model-Based Condition Monitoring: Actuators, Drives, Machinery, Plants, Sensors, and Fault-tolerant Systems. *Springer-Verlag*.

Isermann, R., Ballé, P. (1997). Trends in The Application of Model-Based Fault Detection and Diagnosis of Technical Processes. *Control Engineering Practice*, 5(5), 709-719.

Ishida, S., Miyamoto, H. (2010). Ball Wheel Drive Mechanism for Holonomic Omnidirectional Vehicle. *In World Automation Congress*.

Jetto, L., Longhi, S., Vitali, D. (1998). Localization of A Wheeled Mobile Robot by Sensor Data Fusion Based on A Fuzzy Logic Adapted Kalman Filter. *In IFAC Intelligent Autonomous Vehicles*, 213-218.

Jiang, J., Yu, X. (2012). Fault-tolerant control systems: A comparative study between active and passive approaches. *Annual Reviews in Control*, 36, 60-72.

Khan, M.T., Silva, C.W. (2009). Autonomous Fault Tolerant Multi-Robot Coordination for Object Transportation Based on Artificial Immune System. *In Second International Conference on Robot Communication and Coordination*, 1-6.

L´opez-Estrada, F.R., Ponsart, J.-C, Theilliol, D., Astorga-Zaragoza, C.M., Zhang, Y.M. (2014). Robust Sensor Fault Diagnosis and Tracking Controller for a UAV Modelled as LPV System. *In International Conference on Unmanned Aircraft Systems (ICUAS)*, 1311-1316.

Li, L., Ding, S.X., Luo, H., Peng, K., Yang, Y. (2020). Performance-Based Fault-Tolerant Control Approaches for Industrial Processes with Multiplicative Faults. *IEEE Transactions on Industrial Informatics*, 16(7), 4759-4768.

Li, L., Wang, F.-Y., Zhou, Q. (2006). Integrated Longitudinal and Lateral Tire/Road Friction Modelling and Monitoring for Vehicle Motion Control. *IEEE Transactions on Intelligent Transportation Systems*, 7(1), 1-19.

Li, Z. (2009). Application of Fault Tolerant Controller Based on RBF Neural Networks for Mobile Robot. *In International Symposium on Intelligent Ubiquitous Computing and Education*, 531- 534.

Li, Z., Jiang, W. (2013). Active Fault-Tolerant Control for Two-wheeled Differential Drive Mobile Robot Based on Fault Compensation method. *Chinese Automation Congress*, 359-363.

Lin, C.-M., Boldbaatar, E.-A. (2015). Fault Accommodation Control for a Biped Robot Using a Recurrent Wavelet Elman Neural Network. *IEEE Systems Journal*, 1-12.

Lin, C.-M., Chen, C.-H. (2007). Robust Fault-Tolerant Control for a Biped Robot Using a Recurrent Cerebellar Model Articulation Controller. *IEEE Transactions on Systems, Man, And Cybernetics—Part B: Cybernetics*, 37(1), 110-123.

Liu, Y.-H., Li, T., Yang, Y.-Y., Ji, X.-W., Wu, J. (2017). Estimation of Tire-Road Friction Coefficient Based on Combined APF-IEKF and Iteration Algorithm. *Mechanical Systems and Signal Processing*, 88, 25-35.

Luprie, J.C. (1995). Dependable Computing and Fault Tolerance: Concepts and Terminology. *In Twenty-Fifth International Symposium on Fault-Tolerant Computing*, 1, 2-11.

Madhusudhanan, A.K., Corno, M., Arat, M.A., Holweg, E. (2016). Load Sensing Bearing Based Road-Tyre Friction Estimation Considering Combined Tyre Slip. *Mechatronics*, 39, 136-146.

Makino, M., Masuta, H., Lim, H.-O. (2013). Fault Diagnosis of Mobile Robot based on Short-Term Prediction using Neural Network. *In SICE Annual Conference*, 1300-1305.

Marin, L., Valles, M., Soriano, A., Valera, A., Albertos, P. (2014). Event-Based Localization in Ackermann Steering Limited Resource Mobile Robots. *IEEE/ASME Transactions on Mechatronics*, 19(4),1171-1182.

Marino, A., Parker, L.E., Antonelli, G., Caccavale, F., Chiaverini, S. (2009). A Fault-Tolerant Modular Control Approach to Multi-Robot Perimeter Patrol. *In International Conference on Robotics and Biomimetics*, 735-740.

Mass, R., Maehle, E. (2012). Fault Tolerant and Adaptive Path Planning in Crowded Environments for Mobile Robots Based on Hazard Estimation via Health Signals. *ARCS Workshops*.

Mösch, F., Litza, M., Auf, A. El S., Jakimovski, B., Maehle, E. (2007). Organic Fault-Tolerant Controller for the Walking Robot OSCAR. *In 20th International Conference on Architecture of Computing Systems.*

Murakami, M. (2006). Task-based Dynamic Fault Tolerance for Humanoid Robots. *In IEEE International Conference on Systems, Man, and Cybernetics*, 2197-2202.

Oftadeh, R., Aref, M.M., Ghabcheloo, R., Mattila, J. (2013). Mechatronic Design of a Four-Wheel Steering Mobile Robot with Fault-Tolerant Odometry Feedback. *In 6th IFAC Symposium on Mechatronic Systems*, 663-669.

Pacejka, H. (2012). Tire and Vehicle Dynamics. *Butterworth-Heinemann*, 3rd Edition.

Patton, R.J. (1997). Fault-Tolerant Control Systems: The 1997 Situation. *In IFAC Fault Detection, Supervision and Safety for Technical Processes*, 1029-1051.

Peela, H., Luo, S., Cohn, A.G., Fuentes, R. (2018). Localisation of a Mobile Robot for Bridge Bearing Inspection. *Automation in Construction*, 94, 244-256.

Portugal, D., Rocha, R.P. (2013). Scalable, Fault-Tolerant and Distributed Multi-Robot Patrol in Real World Environments. *In IEEE/RSJ International Conference on Intelligent Robots and Systems (IROS)*, 4759-4764.

Rath, J.J., Veluvolu, K.C., Defoort, M. (2015). Simultaneous Estimation of Road Profile and Tire Road Friction for Automotive Vehicle. *IEEE Transactions on Vehicular Technology*, 64(10), 4461-4471.

Rotondo, D., Nejjari, F., Puig, V. (2014). Fault Tolerant Control of an Omnidirectional Robot Using a Switched Takagi-Sugeno Approach. *In IEEE International Symposium on Intelligent Control (ISIC) Part of IEEE Multi-conference on Systems and Control*, 2183-2188.

Rotondo, D., Nejjari, F., Puig, V. (2014). Fault Tolerant Control of an Omnidirectional Robot using a Switched Takagi-Sugeno Approach. *In IEEE International Symposium on Intelligent Control (ISIC) Part of IEEE Multi-conference on Systems and Control*, 2183-2188.

Roumeliotis, S.I., Sukhatmet, G.S., Bekey, G.A. (1998a). Fault Detection and Identification in a Mobile Robot using Multiple-Model Estimation. *In International Conference on Robotics & Automation*, 2223- 2228.

Roumeliotis, S.I., Sukhatmet, G.S., Bekey, G.A., (1998b), Sensor Fault Detection and Identification in a Mobile Robot. *In International Conference on Intelligent Robots and Systems*, 1383-1388.

Song, Q., Jiang, Z., Han, J.D. (2006). Active-Model-Based Fault Tolerant Control against Actuator Failures for Mobile Robot. *In 6th World Congress on Intelligent Control and Automation*, 1415-1420.

Song, Q., Jiang, Z., Han, J.D. (2006). Active-Model-Based Fault Tolerant Control against Actuator Failures for Mobile Robot. *In 6th World Congress on Intelligent Control and Automation, Dalian*, 1415-1420.

Sundvall, P., Jensfelt, P. (2006). Fault detection for mobile robots using redundant positioning systems. *In IEEE International Conference on Robotics and Automation*, 3781-3786.

Tadakuma, K., Tadakuma, R. (2007). Mechanical Design of "Omni-Ball": Spherical Wheel for Holonomic Omnidirectional Motion. *In Proceedings of the 3rd Annual IEEE Conference on Automation Science and Engineering*, 788-794.

Tian, Y., Sarkar, N. (2014). Control of a Mobile Robot Subject to Wheel Slip. *Journal of Intelligent & Robotic Systems*, 74(3-4), 915-929.

Tian, Y., Sarkar, N. (2014). Control of a Mobile Robot Subject to Wheel Slip. *Journal of Intelligent & Robotic Systems*, 74(3-4), 915-929.

Valdivieso C., Cipriano A. (2006). Fault Detection and Isolation System Design for Omnidirectional Soccer-Playing Robots. *In Conference on Computer Aided Control Systems Design*, 2641-2646.

Valdivieso, C., Cipriano, A. (2006). Fault Detection and Isolation System Design for Omnidirectional Soccer-Playing Robots. *In Conference on Computer Aided Control Systems Design*, 2641-2646.

Verhaegen, M., Kanev, S., Hallouzi, R, Jones, C., Maciejowski, J., Smail, H. (2010). Fault Tolerant Flight Control - A Survey. *Lecture Notes in Control and Information Sciences, Springer*.

Wang, J., Wu, G., Sun, Y., Wan, L., Jiang, D. (2009). Fault Diagnosis of Underwater Robots Based on Recurrent Neural Network. *In International Conference on Robotics and Biomimetics*, 2497-2502.

Wang, J., Wu, G., Sun, Y., Wan, L., Jiang, D. (2009). Fault Diagnosis of Underwater Robots Based on Recurrent Neural Network. *In International Conference on Robotics and Biomimetics*, 2497-2502.

Wang, M., Deng, J., Pattinson, C., Richardson, S. (2017). A Fuzzy Controller for Fault Tolerant Control of Nuclear Reactor. *In International Conference on Computational Science and Computational Intelligence (CSCI)*, 387-390.

Wang, X., Liang, B., Wu, R. (2008). New Fault Tolerant Robotic Central Controller for Space Robot System Based on ARM Processor. *In International Conference on Industrial Technology*.

Wang, X., Yu, Z., Chen, X. (2010). Controller Design and Real-time Fault Diagnosis for a Humanoid Robot. In International Conference on Automation and Logistics, 480-485.

Washington, R. (2000). On-Board Real-Time State and Fault Identification for Rovers. *In International Conference on Robotics & Automation*, 1175-1181.

Williams, R.L., Carter, B.E., Gallina, P., Rosati, G. (2002). Dynamic Model with Slip for Wheeled Omnidirectional Robots. *IEEE Transactions on Robotics and Automation*, 18(3), 285-293.

Wong, J.Y. (2001). Theory of Ground Vehicles. *John Wiley & Sons*, 3rd Edition.

Yang, B., Fan, S., Shi, M. (2007). Research on Fault-Tolerant Controller for Mobile Robot Based on Artificial Immune Principle. *In Third International Conference on Natural Computation*, Vol. 3.

Yang, J-M., Kim, J-H. (2000). A Fault Tolerant Gait for a Hexapod Robot over Uneven Terrain. *IEEE Transactions on Systems, Man, And Cybernetics - Part B: Cybernetics*, 30(1), 172-180.

Yang, Z., Li, C., Su, C.-Y., Deng, J., Zhang, W. (2016). Vision-Based Model Predictive Control for Steering of a Nonholonomic Mobile Robot. *IEEE Transactions on Control Systems Technology*, 24(2), 553-564.

Yi, J., Wang, H., Zhang, J., Song, D., Jayasuriya, S., Liu, J. (2009). Kinematic Modelling and Analysis of Skid-Steered Mobile Robots with Applications to Low-Cost Inertial-Measurement-Unit-Based Motion Estimation. *IEEE Transactions on Robotics*, 25(5), 1087-1097.

Yong, J., Hongguang, W., Lijin, F., Mingyang, Z. (2006a). A Novel Approach to Fault Detection and Identification in Suction Foot Control of a Climbing Robot. *In International Conference on Intelligent Robots and Systems*, 3423-3428.

Yong, J., Hongguang, W., Lijin, F., Mingyang, Z. (2006b). A Combined Logistic and Model Based Approach for Fault Detection and Identification in a Climbing Robot. *In International Conference on Robotics and Biomimetics*, 1512-1516.

Yu, X., Fu, Y., Li, P., Zhang, Y. (2018). Fault-Tolerant Aircraft Control Based on Self-Constructing Fuzzy Neural Networks and Multivariable SMC Under Actuator Faults. *IEEE Transactions on Fuzzy Systems*, 26(4), 2324-2335.

Zhang Y., Jiang J. (2008). Bibliographical review on reconfigurable fault-tolerant control systems. *Annual Reviews in Control*, 32, 229–252.

VITA

Osman Nuri Şahin

onurisahin@gmail.com

Experience: (1) Project Assistant- "Farklı Kinematik Modellere Sahip Ana ve Bağımlı Robotları Olan Telerobotik Sistemin Geliştirilmesi: Teori ve Uygulamaları", Funded by The Scientific and Technological Research Council of Turkey (TÜBİTAK) -1001 The Support Program for Scientific and Technological Research Projects, (2014-2015). **(2)** Co-founder of Start-up Company: NLFD Tech Co. @ Technopark Izmir, (2015-2017). **(3)** Project Assistant- "Robotic Squid for Underwater Manipulation and Intervention", Founded by TÜBİTAK - 1003 Primary Subjects R&D Funding Program, (2019-2020).

Awards/Grants: (1) 100/2000 CoHE (Council of Higher Education, TURKEY) Doctoral Scholarship. **(2)** İzmir Institute of Technology Department of Mechanical Engineering Graduate Achievement Award

Publications: Thesis: O. N. Şahin "Unlimited workspace teleoperation", M.Sc. Thesis, 2013. **Articles: (1)** O. N. Şahin, E. Uzunoglu, E. Tatlicioglu, and M. I. C. Dede, "Design and development of an educational desktop robot R3D", Computer Applications in Engineering Education, Vol 25/2 (2017): 222-229. (DOI: 10.1002/cae.21792). **(2)** O. N. Şahin and M. I. C. Dede, "Investigation of Longitudinal Friction Characteristics of an Omni-Directional Wheel via LuGre Model", Robotica (Under Review). **Peer-reviewed Conference Papers (First Author): (1)** O. N. Şahin, T. Eriş, and M. İ. C. Dede, "Unlimited-Workspace Teleoperation with Obstacle Avoidance Capability," National Meeting of Turkish National Automatic Control Committee, September 11-12, 2012. **(2)** O. N. Şahin, B. Bağdadioğlu, G. Yaldız, M. İ. C. Dede "Çevrim Oranının Geri Sürülebilirlik Üzerindeki Etkisi (The Effect of Reduction Ratio on Backdrivability)," TOK 2014 Bildiri Kitabı, Kocaeli, Türkiye, 11-13 Eylül, pp. 356-360, 2014. **(3)** O. N. Şahin, M. İ. C. Dede "Dört-Tekerlekli Çok-Yönlü Uzaktan Kontrol Edilen Bir Mobil Robot için Hata Telafisi (Fault Recovery for a Four-Wheeled Remotely-Operated Mobile Robot)," 17. Uluslararası Katılımlı Makine Teorisi Sempozyumu, İzmir, pp. 739-745, Haziran 14-17, 2015. **(4)** O. N. Şahin, O. Çelik, and M. İ. C. Dede "Fault-Tolerance Experiments with a Kinematically Redundant Holonomic Mobile Robot," Mechanisms, Transmissions and Applications. MeTrApp 2017. Dede M., İtik M., Lovasz EC., Kiper G. (eds), Mechanisms and Machine Science, vol 52, pp. 161-170, Springer, Dordrecht, The Netherlands, 2017 (ISBN: 978-3-319-60701-6).